

OPTIMIZATION OF ALLOYING
AND
HEAT TREATMENT PROCESS PARAMETERS
OF
AUSTEMPERED DUCTILE IRON (ADI) CASTINGS



ATILIM UNIVERSITY
THE GRADUATE SCHOOL OF NATURAL
AND
APPLIED SCIENCES

MUSTAFA ALP YALÇIN

DEGREE OF MASTER OF SCIENCE
THE DEPARTMENT OF METALLURGICAL
AND
MATERIALS ENGINEERING

SEPTEMBER 2019

Approval of the Graduate School of Natural and Applied Sciences, Atılım University

Prof. Dr. Ali KARA
Director

I certify that this thesis satisfies all the requirements as a thesis for the degree of Master of Science.

Assoc. Prof. Dr. Ender KESKİNKILIÇ
Head of Department

This is to certify that we have read the thesis “Optimization of Alloying and Heat Treatment Process Parameters of Austempered Ductile Iron (ADI) Castings” submitted by “Mustafa Alp YALÇIN” and that in our opinion it is fully adequate, in scope and quality, as a thesis for the degree of Master of Science.

Asst. Prof. Dr.-Ing. Kemal DAVUT
Supervisor

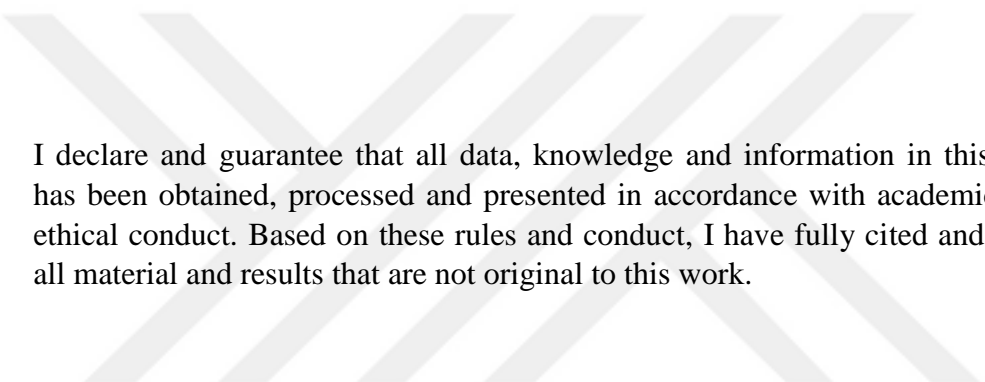
Examining Committee Members

Assoc. Prof. Dr. Ender KESKİNKILIÇ
Department of Metallurgical and Materials Engineering,
Atılım University

Asst. Prof. Dr. Volkan KILIÇLI
Department of Metallurgical and Materials Engineering,
Gazi University

Asst. Prof. Dr.-Ing. Kemal DAVUT
Department of Metallurgical and Materials Engineering,
Atılım University

Date: 17.09.2019



I declare and guarantee that all data, knowledge and information in this document has been obtained, processed and presented in accordance with academic rules and ethical conduct. Based on these rules and conduct, I have fully cited and referenced all material and results that are not original to this work.

Name, Last name: Mustafa Alp YALÇIN

Signature:

ABSTRACT

OPTIMIZATION OF ALLOYING AND HEAT TREATMENT PROCESS PARAMETERS OF AUSTEMPERED DUCTILE IRON (ADI) CASTINGS

YALÇIN, Mustafa Alp

M.Sc., Metallurgical and Materials Engineering Department

Supervisor: Asst. Prof. Dr. Kemal DAVUT

September 2019, 81 pages

Austempered ductile cast iron (ADI) has been extensively used in engineering designs since it offers a good combination of high tensile and fatigue strength, good ductility, toughness, wear resistance and damping characteristics, with light-weighting and low cost. This excellent combination of properties is due to the specific microstructure of ADI; which is composed of spheroidal graphite particles on an ausferritic matrix. The ausferrite consists of carbon free acicular ferrite and carbon enriched retained austenite; which is produced via austempering heat treatment after casting. Problems such as low nodularity level or lower stability of austenite due to inadequate acicular ferrite transformation certainly deteriorate this specific microstructure and hence degrade the mechanical properties of the final product. In the present study the effect of the alloying additions of Cu and Cu + Mo + Ni, heat treatment parameters and sizes and distributions nodular graphite particles on mechanical properties and microstructure of ADI was studied. For that purpose, Y-block specimens having a lean composition and Cu, Cu + high Mo + low Ni and Cu + low Mo + high Ni alloying additions were cast. After austempering treatment, mechanical tests, fractographic and metallographic examinations were performed. The results show that the alloying additions of Cu or Cu + Mo + Ni increased carbon content and stability of austenite in the final microstructure, which means completely homogeneous ausferritic structures can be produced on larger cross-sections without the presence of pearlite or martensite. The Cu + low Mo + high Ni alloyed specimen

proves that since it shows the lowest formation of martensite and has higher strength and elongation than other castings. The lean alloy on the other hand, has the highest nodularity and matrix hardness but the lowest strength and ductility because of the inadequate alloying additions, austempering time and austempering temperature. Lastly, the relation between microstructural parameters and mechanical properties were studied using the Pearson Correlation Coefficient. The results indicate a Petch-like relation between grain size of austenite and yield strength, tensile strength, ductility. EBSD studies also revealed two different austenite: i) film type between acicular ferrite platelets and ii) block type around prior austenite grain (boundaries) that are not transformed during austempering. The grain size of acicular ferrite does not correlate well with the mechanical properties; since its variation among the studied samples is smaller than $0.7\ \mu\text{m}$. For the studied set of samples the nodularity and size of graphite nodules are highly correlated; small differences in nodularity doesn't have significant effect on the mechanical properties. On the other hand smaller nodule size improves both yield and tensile strength values. In addition a Hall-Petch like relation is found between grain size of retained austenite and strength, ductility. Those results should provide a useful basis for further development and improvement of "austempered ductile irons".

Keywords: Austempered ductile iron (ADI), nodularity, ausferrite, retained austenite, microstructure, mechanical properties, correlation

ÖZ

ÖSTEMPERLENMİŞ KÜRESEL GRAFİTLİ DÖKME DEMİRLERDE ALAŞIMLAMA VE ISIL İŞLEM PARAMETRELERİNİN OPTİMİZASYONU

YALÇIN, Mustafa Alp

Yüksek Lisans, Metalurji ve Malzeme Mühendisliği Bölümü

Tez Yöneticisi: Dr. Öğr. Üyesi Kemal DAVUT

Eylül 2019, 81 sayfa

Östemperlenmiş küresel grafitli dökme demir sunduğu yüksek mukavemet, tokluk ve aşınma direncine ek olarak düşük yoğunluk ve maliyet avantajı sayesinde mühendislik tasarımlarında yoğun olarak kullanılmaktadır. Bu malzemelerin güçlü mekanik özelliklerinin nedeni, ösferritik matris üzerinde küresel grafitlerden oluşan özel mikroyapısıdır. Östemperleme ısıl işlemi sonrasında oluşan ösferrit yapısı, iğnemsiz ferrit ve karbonca zengin kararlı östenitten oluşmaktadır. Düşük küresellik değerleri ya da iğnemsiz ferrit dönüşümünün eksik kalması nedeniyle östenit yapısının yeterince kararlı hale gelmemesi gibi sorunlar mikroyapıyı bozmakta ve mekanik özellikleri olumsuz etkilemektedir. Bu çalışmada Cu ve Cu + Mo + Ni alaşım elementlerinin, ısıl işlem parametrelerinin ve küresel grafit parçacıklarının boyutları ve dağılımlarının, östemperlenmiş küresel grafitli dökme demir malzemelerin mikroyapısına ve mekanik özelliklerine etkisi incelenmiştir. Bunun için, düşük alaşımlı ve düşük alaşıma Cu, Cu + yüksek Mo + düşük Ni ve Cu + düşük Mo + yüksek Ni elementleri eklenmiş Y-blok dökümler üretilmiştir. Y-blok parçalardan çıkarılmış numuneler östemperleme ısıl işleminden geçirilmiş; daha sonra mekanik testler yapılmış, kırılma yüzeyi ve metalografik incelemeler gerçekleştirilmiştir. Sonuçlar, Cu + düşük Mo + yüksek Ni ile alaşımlanmış numunenin daha yüksek mukavemet ve uzama değerlerine sahip olduğunu göstermektedir. Bu da, Cu ve Cu +

Mo + Ni alařımları eklenmiř paraların karbonca zengin ve kararlı stenit yapısına sahip olduėunu; ve geniř kesit alana sahip paralarda bile kalınlık boyunca homojen bir sferritik yapı oluřturulabileceėini gstermektedir. Dřk alařımlı numune ise, yetersiz alařımlama ve stemperleme iřlemi nedeni ile en iyi kresellik ve sertlik deėerlerine sahip olmasına raėmen en dřk mukavemet ve uzama deėerlerini vermektedir. Mekanik zelliklerdeki bu deėiřkenliėin, mikroyapıda bulunan kalıntı stenitin yapısı, miktarı ve daėılımı ile doėrudan baėlanıtılı olduėu gzkmektedir. Son olarak, Pearson Korelasyon Katsayısı yntemi kullanılarak malzemenin mekanik zellikleri ve mikroyapısı arasındaki iliřki incelenmiřtir. Sonular, stenit tane boyutu ve akma dayancı, ekme dayancı ve sneklik arasında Hall-Petch benzeri bir iliřki gstermektedir. EBSD alıřmaları sonrasında iki farklı tip stenit yapısı grlmřtir: i) iėnemsiz ferrit yapıları arasında kalmıř ince stenit ve ii) stemperleme iřlemi sırasında dnřmemiř nceki stenit tanelerinden kalan blok tipi stenit. alıřılan numuneler arasında, iėnemsiz ferrit tane boyutu 0.7 μm 'den daha az deėiřkenlik gstermektedir. Bu nedenle iėnemsiz ferrit tane boyutu ile mekanik zellikler arasında iyi bir korelasyon gzkmemektedir. Kresellik ve kresel grafitlerin boyutu arasında ise yksek korelasyon gzkmektedir. Kresellik derecesindeki kk farklar mekanik zellikleri etkilememekle beraber, kk kresel grafit taneleri hem akma hem de ekme dayancı deėerlerini iyileřtirmektedir. Bu sonular stemperlenmiř kresel grafitli dkme demirlerin daha da geliřtirilmesi ve iyileřtirilmesine katkı saėlayabilir.

Anahtar Kelimeler: stemperlenmiř kresel grafitli dkme demir, sferrit, kalıntı stenit, mikroyapı, kresellik, mekanik zellikler, korelasyon



To my Family...

ACKNOWLEDGEMENT

First of all, I would like to express my sincere gratitude to my supervisor Asst. Prof. Dr. –Ing. Kemal DAVUT for his guidance, encouragement, and support throughout my entire postgraduate program.

I would like to express my sincere appreciations to Barış Çetin, Dr. Halim Meço and Managerial Board of FNSS Defence Systems Co. Inc., specifically for supporting this project and giving me the chance of being part of it.

I also would like to thank Akpınar Foundry for casting the samples that used in this study.

I also would like to express my gratitude to director of Metal Forming Center of Excellence where I performed all of the experiments in Dr. Besim Baranođlu. Also a special thanks to Rasim K ksal Ertan and Yasin Demirkol for their technical support on Gleebel Tests.

I am also grateful to the examining committee members of Assoc. Prof. Dr. Ender Keskinlil  and Assst. Prof. Volkan Kılı lı for their valuable comments on this thesis.

Most importantly, I would like to express my deep love to my parents; Mustafa and Nesrin Yal ın for their endless support not only for during this study but my whole life.

TABLE OF CONTENTS

CHAPTER 1	1
INTRODUCTION	1
1.1. Aim of the Study	3
CHAPTER 2	4
LITERATURE SURVEY	4
2.1. History of Austempered Ductile Iron	4
2.2. Production of Austempered Ductile Iron	6
2.3. Heat Treatment Process	7
2.4. Alloying Addition.....	13
2.5. Nodularity.....	17
2.6. Microstructure of Austempered Ductile Iron	19
2.7. Properties and Advantages of Austempered Ductile Iron	21
2.8. Disadvantages of ADI	26
2.9. Applications of ADI	27
CHAPTER 3	29
EXPERIMENTAL	29
3.1. Specimen Preparation.....	29
3.2. Heat Treatment and Mechanical Testing.....	30
3.3. Microstructural Characterization.....	32
3.4. Hardness Measurements.....	35
CHAPTER 4	36
RESULTS AND DISCUSSIONS	36
4.1. Nodularity Analyses	36
4.2. Microstructural Properties	43
4.3. Reliability and Representativeness of EBSD Technique	58
4.4. Correlation between Microstructural Parameters and Mechanical Properties	63
CHAPTER 5	71
CONCLUSIONS.....	71
REFERENCES.....	74

LIST OF TABLES

Table 1.1-1 ASTM A536-84(2019) grades for Ductile Irons and ASTM A897-A897M-16 grades for Austempered Ductile Irons.....	1
Table 2.7-1 Density comparison of several engineering materials	24
Table 3.1-1 Compositions and heat treatment process details of present ADI castings	29
Table 4.1-1 Nodularity analyses of ADI samples before austempering heat treatment process.....	40
Table 4.1-2 Nodularity analyses of ADI samples after austempering heat treatment process.....	40
Table 4.1-3 Comparison of microstructural parameters and nodularity analyses of ADI Samples	42
Table 4.2-1 Mechanical properties of ADI samples.....	48
Table 4.2-2 Comprasion of microstructural parameters and mechanical properties of the ADI samples	55
Table 4.4-1 Correlation between microstructural parameters and mechanical properties.....	65

LIST OF FIGURES

Figure 2.1-1 Number of publications and citations per year related to ADI.....	5
Figure 2.3-1 Time–temperature profile of a typical austempering treatment for ductile irons.....	8
Figure 2.3-2 Developments in the microstructure when austempering ductile iron at (a) high temperatures, (b) low temperatures	10
Figure 2.3-3 UTS vs. %elongation of ADI as a function of austempering duration	11
Figure 2.3-4 (a) Ideal variation of volume fraction austenite with austempering time showing separation of Stage I and II. (b) A schematic of ductility vs. austempering time illustrating the effects of Stage I and Stage II on ductility. Curve A represents an ideal homogeneous structure. Curve B illustrates the effect of alloy segregation. Curve C reflects the presence of intrinsic defects in the structure.	12
Figure 2.4-1 Effect of Mn on the processing window.....	14
Figure 2.4-2 Effect of combinations of Ni, Cu and Mo on the maximum bar diameter that can be austempered without the formation of pearlite	15
Figure 2.6-1 a) Optical microscope and b) SEM images of typical ausferrite structure	19
Figure 2.6-2 The difference between bainite reaction in steel and ADI	20
Figure 2.7-1 The ADI truck trailer hub (left) is 2% lighter and lower in cost than the aluminum hub (right) that it replaced.....	22
Figure 2.7-2 Comparison of Young’s modulus of various materials.....	23
Figure 2.7-3 Comparison of relative weight per unit of yield strength for different material / process combinations	23
Figure 2.7-4 Comparison of relative cost per unit of yield strength for different material / process combinations	24
Figure 2.7-5 Cast ADI end connectors compared to forged steel in a manufacturing sequence	25
Figure 2.9-1 ADI - American market distribution, 2008	28
Figure 3.2-1 The Gleeble 3500 System used for this study	30
Figure 3.2-2 HZT-071 type extensometer used for strain rate and elongations measurements.....	31

Figure 3.2-3 Technical drawing of Gleeble-3500 specimens used in this study.....	31
Figure 3.3-1 Schematic representation of Maximum Feret Diameter (MFD)	32
Figure 3.3-2 Carl Zeiss: Merlin – Field Emission Scanning Electron Microscope ..	34
Figure 3.4-1 The Zwick/ZHV10 hardness tester.....	35
Figure 4.1-1 Optical micrographs of as-polished ADI castings before (left) and after (right) austempering heat treatment process	38
Figure 4.1-2 Comparison of a) Area and b) number fraction of graphite particles' shape factors.....	39
Figure 4.1-3 Nodularity by number and nodularity by area values of ADI castings	40
Figure 4.1-4 Comparison of size distribution of nodular graphite particles with respect to a) area and b) number fractions	41
Figure 4.2-1 Optical micrographs of microstructures of ADI before austempering heat treatment process	44
Figure 4.2-2 Optical micrographs of ADI samples after austempering process	46
Figure 4.2-3 SEM micrographs ADI sample taken at 5000X.....	47
Figure 4.2-4 EBSD phase maps of ADI castings. Large white areas represent nodular graphite particles; green areas represent retained austenite structure; red areas represent ferrite structure	50
Figure 4.2-5 Inverse pole figure with respect to normal direction (IPF-ND) maps of FCC-indexed partition of ADI castings	51
Figure 4.2-6 Inverse pole figure with respect to normal direction (IPF-ND) maps of BCC-indexed partition of ADI castings	52
Figure 4.2-7 SEM images of fracture surfaces of ADI samples taken at 200x (left) and 3500x (right).....	57
Figure 4.3-1 Comparison of effect of hot mounting and cold mounting to the alpha and gamma phase fractions on ADI 1	60
Figure 4.3-2 Comparison of EBSD and XRD results of alpha and gamma phase fractions on ADI 5.....	60
Figure 4.3-3 EBSD phase maps of the ADI 1 (Lean Alloy)	61
Figure 4.3-4 EBSD phase maps of the ADI 5 (Lean + High Ni)	62
Figure 4.4-1 Correlation between nodularity by area and nodule density and nodule size.....	65

Figure 4.4-2 Correlation between retained austenite grain size and yield strength and UTS 67

Figure 4.4-3 Correlation between retained austenite grain size and total elongation 67

Figure 4.4-4 Correlation between nodule size and yield strength..... 69

Figure 4.4-5 Correlation between nodule size and alpha phase fraction 69



CHAPTER 1

INTRODUCTION

Gray cast iron (GCI) is a common engineering alloy since it costs relatively less and has good machinability. However, flake type graphite particles in its structure causes notch effect that limits the tensile strength of the material to 400 MPa and decreases ductility. Ductile Iron (DI) is obtained by turning the flake type graphite particles to nodular type. Tensile strength and ductility of this material are significantly higher than GCI [1]. These mechanical properties can be improved furthermore by a special heat treatment process called “austempering”. Austempering heat treatment process was firstly developed in 1930’s to enhance the mechanical properties of the steel components. Commercially applying this process to ductile irons started in 1970’s [2]. The product obtained after applying the austempering process to ductile iron is called “Austempered Ductile Iron (ADI)”. The differences of mechanical properties between DI and ADI can be seen in Table 1.1-1.

Table 1.1-1 ASTM A536-84(2019) [3] grades for Ductile Irons and ASTM A897-A897M-16 [4] grades for Austempered Ductile Irons

ASTM Standards of Ductile Irons			
Class	Min. Tensile Strength (MPa)	Min. Yield Strength (MPa)	%Elongation
60-40-18	414	276	18
65-25-12	448	310	12
80-55-06	552	379	6
100-70-03	689	483	3
120-90-02	827	621	2
ASTM Standards of Austempered Ductile Irons			
Class	Min. Tensile Strength (MPa)	Min. Yield Strength (MPa)	%Elongation
	750	500	11
1	900	650	9
2	1050	750	7
3	1200	850	4
4	1400	110	2
5	1600	1300	1

ADI is a special class of ductile cast iron that offers a good combination of high tensile and fatigue strength, high toughness and wear resistance. In addition, ADI has good damping characteristics, low cost and low density, the latter of which provides light weighting. Those promising properties of ADI ensures reliable service under heavy conditions of shock, impact and wear; and therefore ADI has been used in many applications including gears, drive wheels, rollers, sliders, suspension parts in automotive, defense, heavy-duty vehicle industries.

This unique combination of improved mechanical properties, low cost and low density is due to ADI's special matrix microstructure, "ausferrite". Ausferrite structure consists of acicular ferrite and carbon enriched stable austenite. Quality of the ADI product highly depends on morphology of ausferrite structure and there are many factors that affect the final microstructure such as size and shape of the nodular graphite particles, composition and quality of the base ductile iron to be austempered, thickness of the part and heat treatment parameters [2], [5]–[7].

Austenitizing at temperatures lower than needed causes presence of proeutectoid ferrites in the final microstructure; insufficient time of austenitizing causes low carbon content in the austenite; carelessly added alloying elements and wrongly applied austempering process cause undesirable structures and phases that ends with undesirable mechanical properties. The shape and amount of nodular graphites affects both austenitizing and austempering times [8].

The enhanced mechanical properties of ADI comes from its unique microstructure. In order to obtain this unique microstructure all of those process parameters should be considered, controlled and adjusted precisely. The influence of each alloying element as well as the influence of heat treatment process parameters on final microstructure and mechanical properties will be explained and discussed in detail in Chapter2.

1.1. Aim of the Study

Austempered ductile iron castings offer a good combination of mechanical properties. This improved properties are due to its unique ausferritic matrix microstructure; as mentioned. The effect of heat treatment parameters, alloying additions on the final microstructure and mechanical properties has been studied extensively. Moreover, the influence of size and morphology of the graphite particles on mechanical properties has also been subject of intense research since the invention of ductile iron. However, the combined effect of all of those mentioned microstructural details on mechanical properties and interrelations between microstructural parameters has yet to be studied. The present study aims at closing this gap.

Within the scope, the following Chapter 2 “Literature Survey” will give detailed information about development of the ADI through the years, production processes that include heat treatment, alloying, nodularity and their effects; and microstructure, properties and applications of ADI. Chapter 2 will be followed by Chapter 3 “Experimental” which will give details about experimental works of this present study. Details of applied heat treatment, castings’ composition and microstructural characterization will be given in 3rd Chapter. Then, all of the results of each experimental work and their relations will be discussed in Chapter 4 “Results and Discussion”. Finally, conclusions will be given in the 5th Chapter “Conclusion”.

CHAPTER 2

LITERATURE SURVEY

2.1. History of Austempered Ductile Iron

Austempered Ductile Iron (ADI) is a special type of ductile iron that is produced by a heat treatment process called “austempering”. Austempering is a type of heat treatment to produce a bainite like metallurgical structure for ductile irons [9]. Austempering heat treatment gives improved strength, ductility and toughness to ductile irons [10]–[12]. Bainite must have been present in steels long before its acknowledged discovery date. However, it could not be identified because of the lack of the advanced metallography techniques and the mixed microstructures formed by the heat treatment practices. The austempering process was first developed in the 1930’s by Edgar C. Bain and Edmund S. Davenport who were working for the United States Steel Corporation during their work about conducting on the isothermal transformation of steel [13]. They discovered a new microstructure consisted of ‘acicular, dark edging aggregate’. This structure was found to be tougher for the same hardness than tempered martensite; however, since heat treatments at the time had no capability of producing fully bainitic microstructures, use of bainitic steel did not become common. Commercial use of bainitic steel came about as the result of new heat treatment methods which involved a step to hold the workpiece at a single fixed temperature for a period long enough to allow the transformation. This process became known as “austempering”.

The production of ductile iron increased rapidly after the announcement of the invention of it by the British Cast Iron Research Association (BCIRA) and the International Nickel Company (INCO) in 1948 [8]. In 1950’s both production of ductile iron and austempering process had been known. Although, companies tried to combine both of them to improve the properties of their product during 1960’s, equipment and knowledge of the process were not enough to produce ADI on an industrial scale until the mid 1970’s [2]. ADI crankshaft produced and used by

Tecumseh Products in 1972 to improve the fatigue strength of the ductile iron compressor crankshafts was the very first commercial application of ADI [14]. This is followed by announcements in a very short range of time from Finland [15] and China [16], respectively, that iron castings could be austempered. At first this new material was called by various names including austempered bainitic nodular iron and austempered SG iron but now it is known as Austempered Ductile Iron (ADI) in the world. As shown in Figure 2.1.1 the announcements of commercial production resulted in a worldwide explosion in research in term of it's strength and ductility [5], [7], [11], [17]–[36], hardness [5], [11], [17], [18], [20]–[23], [26], [29], [32], [34], [36]–[45], wear resistance [5], [18], [21], [36], [41], impact energy [5], [11], [18], [21], [22], [25], [31], [33], [34], [36], [38], [41], [46], fracture toughness [17], [19], [24], [27], [28], [30], [39], machinability [5], [25], [40], [47], transformation kinetics [20], [23]–[25], [28], [29], [38], [41]–[45], and electrical and thermal behaviours [17], which provided a sound foundation for expanding the production of this material in many industrialised countries during the 1990's and beyond [5].

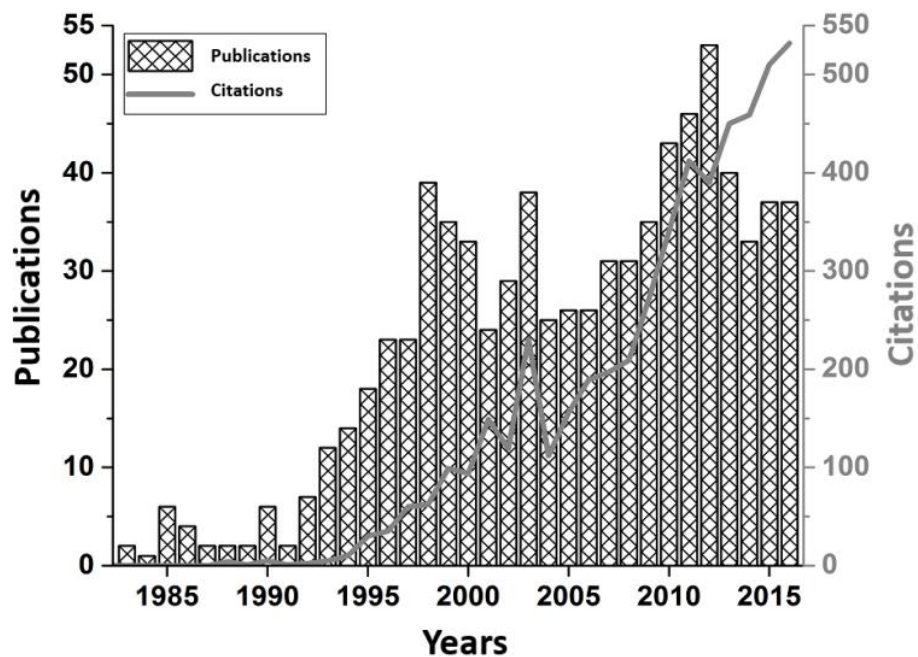


Figure 2.1-1 Number of publications and citations per year related to ADI.

2.2. Production of Austempered Ductile Iron

The quality of Austempered Ductile Iron depends on many factors such as nodularity of graphites and number of nodular graphites [6], [29] , alloying elements [7], [22], [26], [36], [38], [50], [51], [53], cross-sectional area of the part [36], [54], austempering temperature and time [7], [20], [24], [50], [51] but in the end to produce a high quality ADI, firstly and the most importantly, the ductile iron to be austempered should have a high quality [55] and austempering parameters should be adjusted carefully. The austempering process creates a stronger product than conventional ductile iron grades but it doesn't remove defects and heal poor quality iron. On the contrary, austempering magnifies the effects of the smallest defects on the mechanical properties of ductile iron [5], [8]. Thus, the toughness of an ADI component can be severely compromised by the presence of non-metallic inclusions, carbides, shrink and dross even if they remain in between acceptable ranges for conventional ductile iron.

Following chapters include the details of the austempering reaction in ductile irons, followed by a review of the thermal and mechanical stability of the austempered structure and the effects of alloying elements. The effects of composition and processing variables on the development of microstructure and its effect on the development of acceptable mechanical properties in ADI will be examined. Finally, the effect of shape and fraction of graphite particles on microstructure and mechanical properties will be shown.

2.3. Heat Treatment Process

Heat treatment of ADI starts with austenitizing where castings are heated to austenite phase field and held for long enough until the ductile-iron matrix structure is converted to fully austenitic saturated with carbon [5], [7], [8], [50], [55]. To obtain desired properties in ADI, the casting should be fully austenitized.

Typically holding the material between 850 °C - 900 °C for 1 - 2 hours is enough for austenitizing. On the contrary of steels, time and temperature of austenitization process is highly important because of the C content and the homogeneity of the matrix [56]. There are 3 main variables that the austenitizing time depends on:

- The section thickness: Section that are much thicker will require more time to be quenched [5];
- The nodule count: High nodule counts causes small spaces between graphite particles which leads to reduction in the distance that carbon needs to diffuse to obtain a uniform carbon content[6], [29]. Some elements such as Sb, Sn and Cu segregate between the graphite and the matrix and work as a diffusion barrier that causes longer time carbon to saturate. Effect of nodularity will be discussed in coming chapters.
- The initial microstructure: The microstructure before the austenitizing doesn't affect the final microstructure. However, it affects the austenitization time. If the matrix of the casting is mostly ferritic, austenitization time will be longer than the pearlitic matrix since the pearlitic matrix already has about 0.7% carbon in it [5], [55].

Austenitization of the casting is followed by quenching into an intermediate-temperature salt or oil bath maintained at a temperature within the bainitic temperature range (between 250 °C – 450 °C), holding for a period of time (1 – 4 hours), followed by cooling to room temperature. This heat treatment process is called “austempering”. Typical austempering heat treatment cycle is shown in Figure 2.3.1.

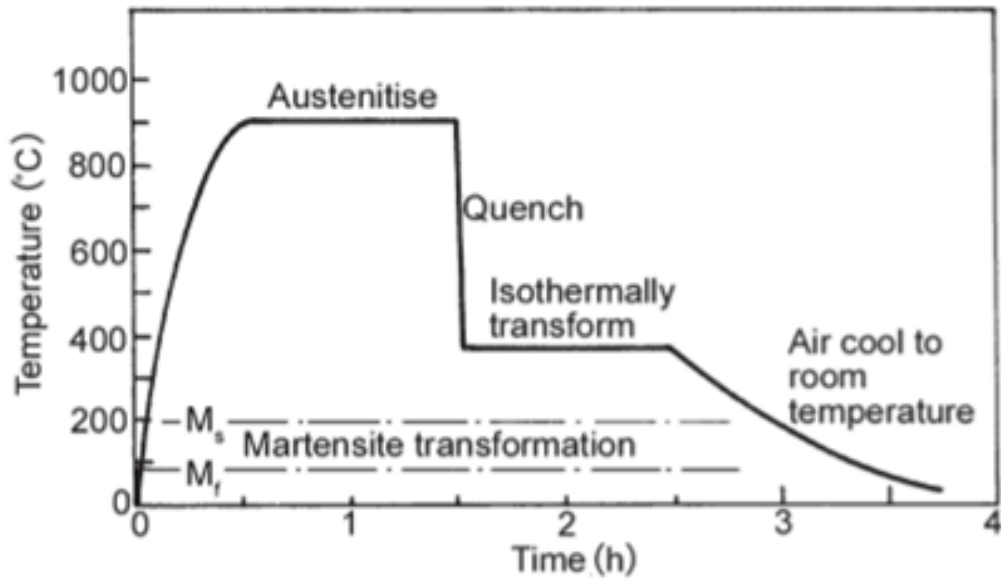


Figure 2.3-1 Time–temperature profile of a typical austempering treatment for ductile irons [5]

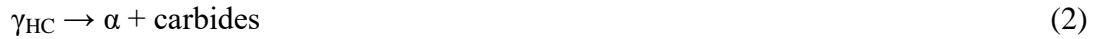
Austempering in conventional steels result in the formation of classic upper and lower bainite microstructures, composed of acicular ferrite along with the carbides. However, the austempering reaction in ductile irons is different than the bainite reaction in steels since austempering of ductile iron is a two-stage reaction [7], [55]. At the end of a successful austempering the acicular ferrite and carbon enriched stabilised austenite microstructures are obtained. Two stage austempering reaction of ductile irons is shown in Figure 2.3.2. for both high and low austempering temperatures [7].

Formation of ferrite platelets start during isothermal holding at the austempering temperature. The high silicon content of the ductile iron inhibits the carbide formation that normally results as bainite structure, allowing the carbon rejected by the formation of ferrite to enrich the carbon content of the remaining austenite. After sufficient time at the austempering temperature, the austenite surrounding the ferrite platelets becomes thermally stable to well below room temperature since carbon content in it reduces the M_s temperature [7]. In the end of the process a structure consists of ferrite platelets set in a matrix of stabilized retained austenite is obtained. This special microstructure is known as “ausferrite” and the reaction is called as the Stage I reaction which is shown in Fig. 2.3.2.:



There are no martensites present in the final structure of ADIs in the room temperature at the end of Stage I.

Longer austempering time leads to a Stage II reaction to occur in which more ferrite is formed and carbides are precipitated:



This affects mechanical properties negatively. Low austempering temperature causes more ferrite formation which makes carbon diffusion harder and slower. This can result large amount of carbon stuck in the ferrite and the precipitation of silico-carbides in the microstructure and eventually having ADI with low ductility and toughness. Also, since carbon diffusion rate is low martensite can be seen in the final microstructure at low austempering temperature [5], [7], [50], [51]. If the austempering temperature is increased, coarser ferrites and increased amount of retained austenite, which is the typical ausferrite structure, are obtained. This type of structure results in the increase in ductility and the decrease in strength and hardness [23].

The period between the end of Stage I (t_1) and the start of Stage II (t_2) is known as the 'processing window' [7], [50]. Between the end of the Stage I and beginning of the Stage II small changes happen in the morphology of the structure. The optimum combination of mechanical properties is obtained when the austempering time is between these two values. Thus, it is important to arrange the process carefully to keep it in the range of process window.

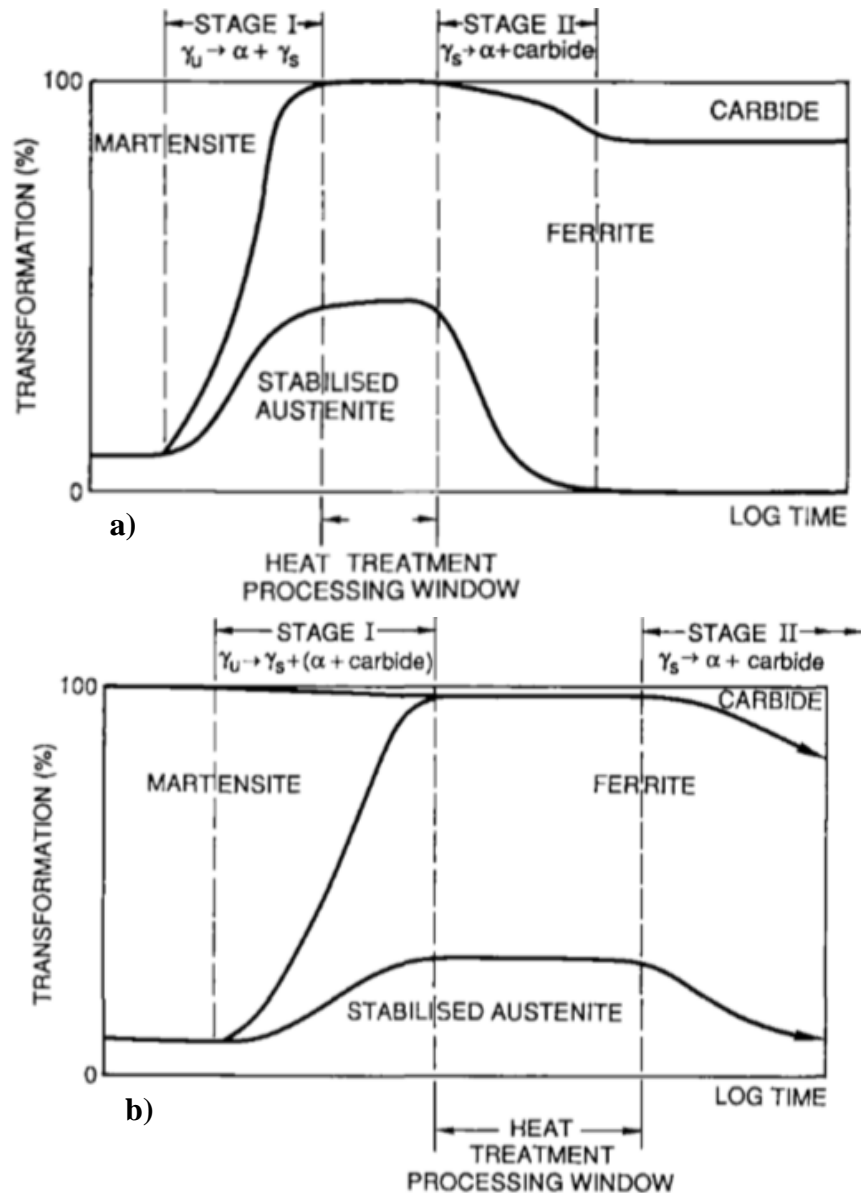


Figure 2.3-2 Developments in the microstructure when austempering ductile iron at (a) high temperatures, (b) low temperatures [7]

There are ways to delay the Stage II reaction to occur and widen the process window. Austempering kinetics are mainly depends on alloy composition, segregation of alloying elements and temperature. Rundman et al, shows that Stage I reaction mainly depends on the carbon content difference between the austenite in the product and the austenite in the matrix and the Stage II depends on mostly the alloying elements [50].

To obtain an optimum combination of strength and ductility, austempering time and temperature should be selected to get maximum ductility [7], [50], [51]. Tensile data

gathered by Moore et al, and Dorazil et al, is shown in Figure 2.3.3. [51]. It shows during austempering process the strength changed a small amount compared to elongation. Elongation shows increase at first then decreases drastically with the formation of bainite.

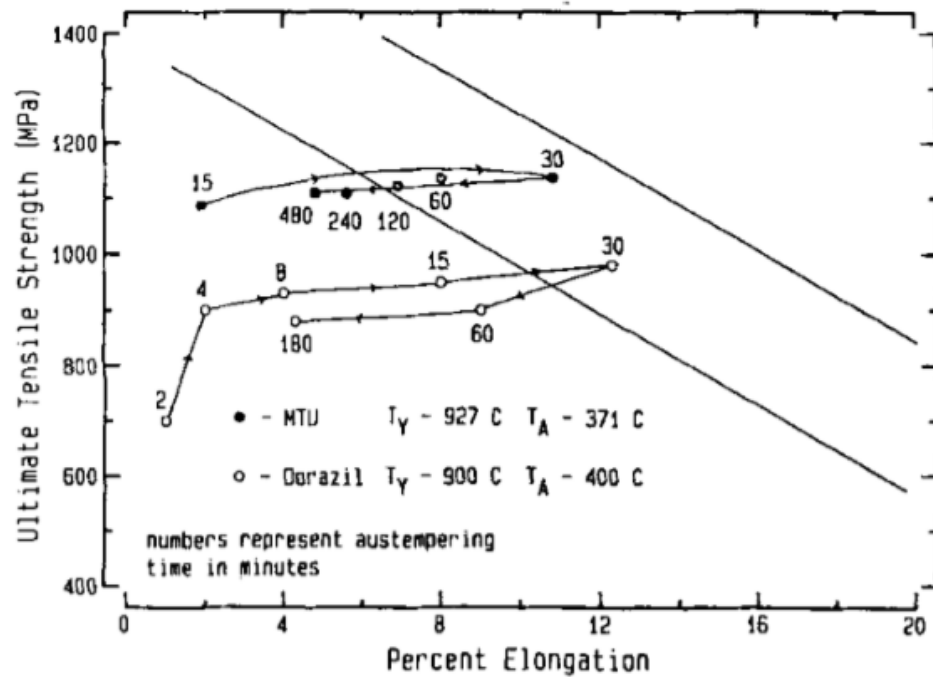


Figure 2.3-3 UTS vs. %elongation of ADI as a function of austempering duration [50]

In an ideal austempering process Stage I and Stage II process would be separated and shows no change in ductility between the end of Stage I and the beginning of Stage II as shown in Figure 2.3.4. However, in most cases scenario is not like that. One of the reasons is both Stage I and Stage II reactions are nucleation and growth events where Stage II nucleation starts as soon as high carbon austenite presents in Stage I. This means, Stage I and Stage II are not separated, on the contrary both of the reactions occur at the same time but with different rates. Stage II reaction takes place at slower rate. Second reason is segregation of certain alloying elements. The segregation changes the reaction rates since alloy content is not homogeneous through the matrix. This makes unclear where Stage I ends and Stage II starts. Additionally, defects comes from casting process such as slag, interdendritic carbides or porosity could decrease ductility of the product [7], [50], [51].

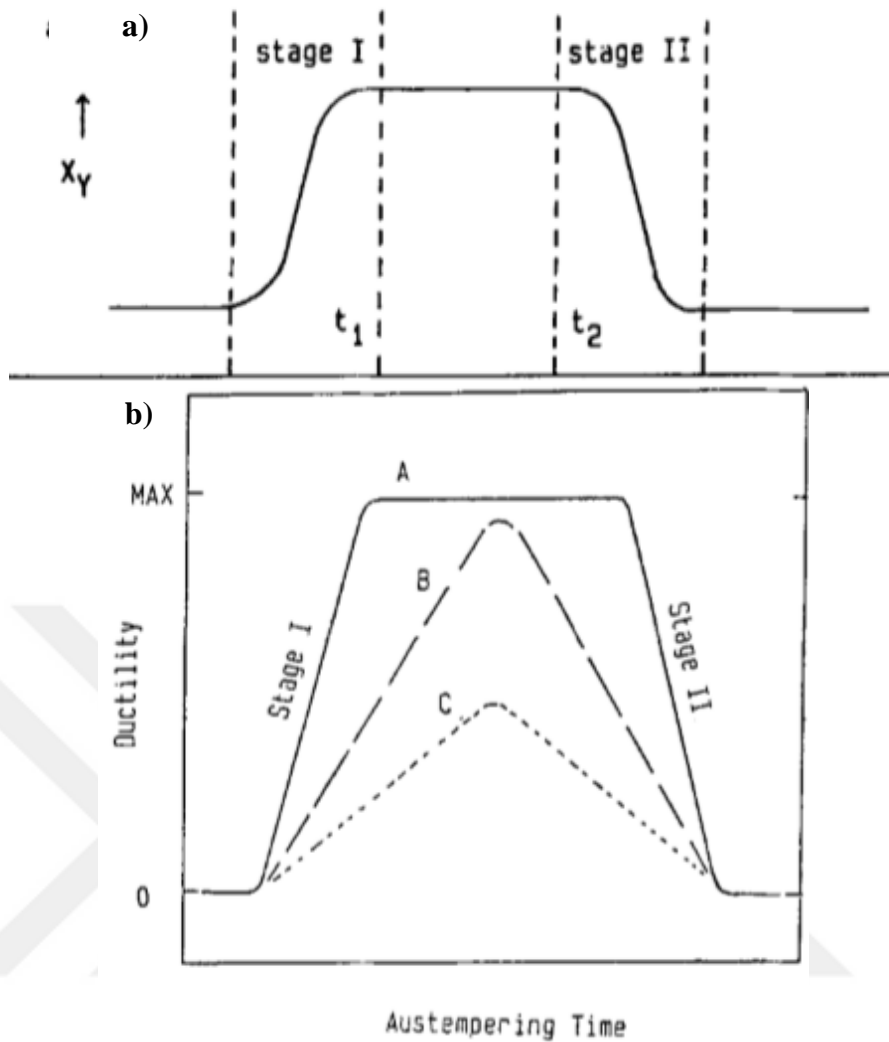


Figure 2.3-4 (a) Ideal variation of volume fraction austenite with austempering time showing separation of Stage I and II. (b) A schematic of ductility vs. austempering time illustrating the effects of Stage I and Stage II on ductility. Curve A represents an ideal homogeneous structure. Curve B illustrates the effect of alloy segregation. Curve C reflects the presence of intrinsic defects in the structure.[50]

As mentioned before, austempering alone is not enough to improve mechanical properties of poor quality castings. But for good quality castings austempering process is the most important process that determines the final properties.

2.4. Alloying Addition

It is very important that the ductile iron is correctly alloyed to obtain the required microstructure during the austempering heat treatment process. Before deciding the chemical composition of the material, elements which affect the production of non-nodular graphites, formation of carbides and inclusions or promotion of shrinkage should be kept in mind [8]. Then, to improve the hardenability, austemperability in this case, elements like carbon, silicon, manganese, copper and molybdenum should be considered. Elements and amount of the elements depend on materials thickness and austempering parameters.

A ductile iron with size up to about 20 mm can be successfully austempered without need of any alloying elements. For thicker section size, selective alloying is required to austemper the parts entirely and avoid pearlite in the heat treated microstructure [5], [7], [8], [57]. Some major elements to increase the hardenability of ADI are:

Carbon: Having 3-4% carbon in the material improves the tensile strength without a significant difference in elongation and hardness. Carbon should be kept between 3.6-3.8% unless deviations are required to provide a defect free casting [57].

Silicon: As mentioned in the heat treatment chapter, silicon acts as ferrite stabilizer and carbon rejected by the formation of ferrite enriches the carbon content of the austenite. Silicon increases Stage I reaction rate and delays Stage II reaction to start. Increasing the silicon content increases the impact strength of ADI and lowers the ductile-brittle transition temperature. Silicon should be between within the range 2.4-2.8% [7], [56], [57].

Manganese: Manganese strongly increases hardenability and it also delays the beginning of the Stage I and Stage II reactions. However, it also segregates to grain boundaries and forms carbides. This acts as a retarding factor to austempering process and delays the end of the Stage I reaction. If the ductile iron to be austempered has poor nodule count or large thickness, manganese segregation can be high and produce shrinkage, carbides and unstable austenite. These faults decrease machinability and reduce mechanical properties. It is suggested to keep manganese

level less than %0.3 in ADI to avoid these defects and improve mechanical properties [7], [50], [51], [56], [57].

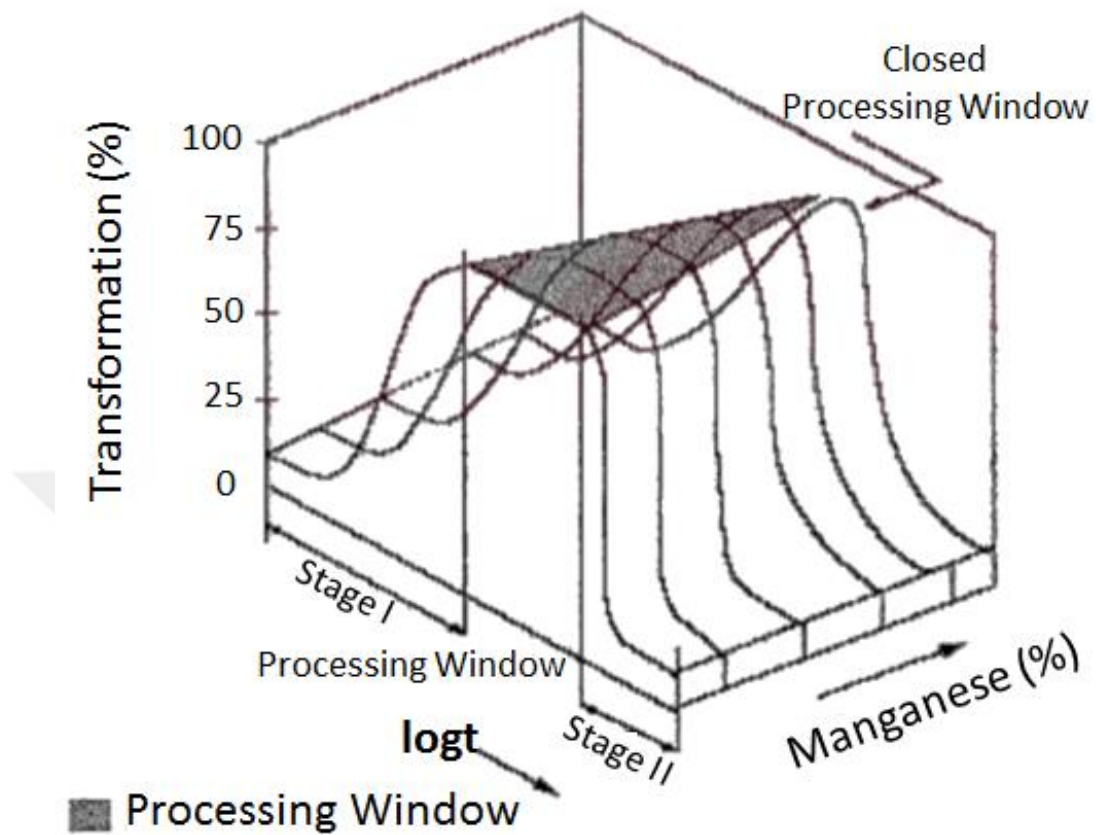


Figure 2.4-1 Effect of Mn on the processing window [56]

Molybdenum: Molybdenum is the most effective element to increase hardenability of the material and required to avoid formation of pearlite in large sections. Like manganese, molybdenum also delays the Stage I and Stage II reactions. The level of molybdenum shouldn't exceed 0.2% since, again like manganese, it can segregate to grain boundaries and form carbide. This causes decrease in both tensile strength and ductility [7], [50]. Especially at high austempering temperatures, delaying effect of Mo addition causes martensite at room temperature [22], [58]–[60].

Copper: Copper is the first element to be considered to increase the hardenability of ADI because of its price. It has no notable effect on tensile properties but increases ductility at austempering temperatures below 350°C [57]. It is suggested not to exceed 0.8% copper in ADI since it can create barriers around graphite nodules that

inhibits carbon diffusion during austenitizing [8]. Shelton and Bonner (2006) shows excess amount of Cu causes decrease in the strength of the material [19].

Nickel: If 0.8% Cu is not enough to obtain a homogeneous microstructure for the existing section size, nickel additions of up to 2% are typically made to increase hardenability of ADI. For austempering temperatures below 350°C nickel reduces tensile strength slightly but increases ductility and fracture toughness [8], [57].

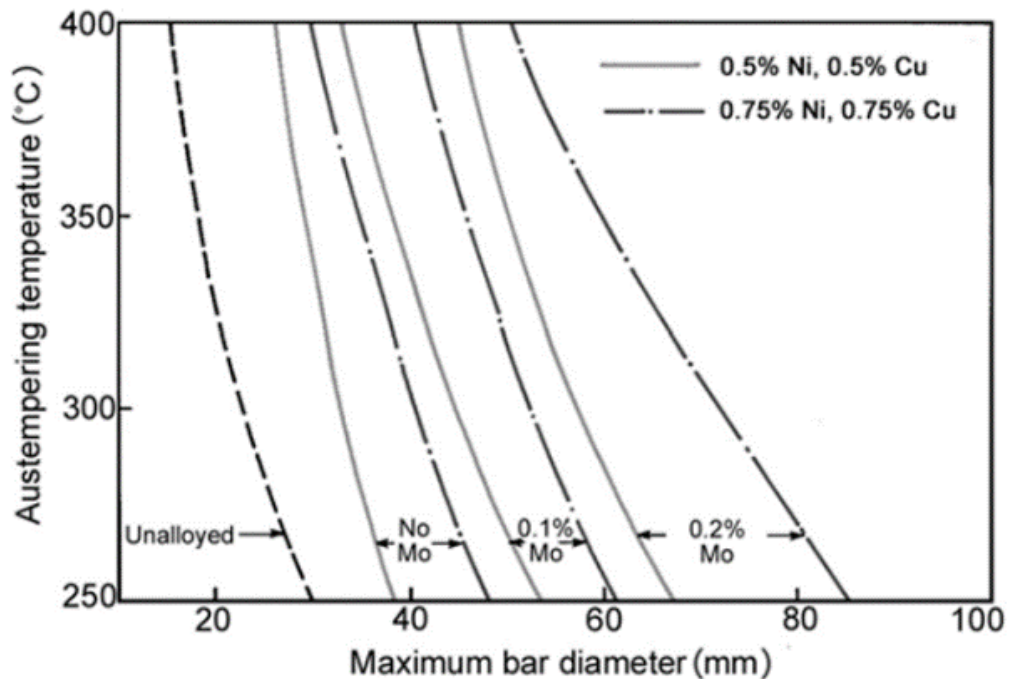


Figure 2.4-2 Effect of combinations of Ni, Cu and Mo on the maximum bar diameter that can be austempered without the formation of pearlite [5]

Harding (2007) shows the effect of different amounts of Ni, Cu and Mo on the hardenability of casting in Figure 1-3 [5]. This figure was obtained by quenching simple shapes into a well-agitated salt bath where the volume of salt greatly exceeded the volume of castings being quenched. In industrial production, the metal:salt ratio will be considerably higher and components may be more complex; both factors will result in a reduced quench rate which may necessitate higher alloy additions [5].

Voigt and Loper (1984) had determined a formula to find appropriate alloying addition which includes Mo, Ni, Cu and Mn, and austempering temperature depending on the section size of the part [25].

$$pct C_{\gamma} = \frac{T_A}{420} - 0.17(pct Si) - 0.95 \quad (3)$$

$$CD = 124C_{\gamma} + 27(\%Si) + 22(\%Mn) + 16(\%Ni) - 25(\%Mo) - 1.68 \times 10^{-4}(T_a)^2 + 12(\%Cu)(\%Ni) + 62(\%Cu)(\%Mo) + 88(\%Ni)(\%Mo) + 11(\%Mn)(\%Cu) + 127(\%Mn)(\%Mo) - 20(\%Mn)(\%Ni) - 137 \quad (4)$$

In equation 2;

CD = the critical diameter in mm

C_{γ} = austenite carbon content comes from equation 1

T_a = the austempering temperature in °C

There are studies on the effect of alloying elements to the austemperability of the material. Both A. R. Mattar, etal (2011) and B. Bosnjak, etal (2001) confirm Voigt-Loper equation in their works and show how alloying additions delay pearlite formation through the thickness [36], [45]. In addition to Cu, Ni, Mo, and Mn, Padan (2012) shows the elements of vanadium and niobium also enhance austemperability of the material [26].

2.5. Nodularity

Nodularity has a direct effect on mechanical properties of ADI [6], [29]. Presence of nodular graphites is the main reason why ductile iron is ductile at the first place. High nodularity increases the ductility of the material and on the contrary low nodularity decreases the ductility. It is expected that base ductile iron have at least %85 nodularity [8].

$$\%Nodularity \text{ by Area} = 100 \times \frac{\text{Total Area of Nodular Graphite Particles}}{\text{Total Area of Graphite Particles}} \quad (5)$$

Shape of graphite particles determine the nodularity of ductile iron. To say a graphite particle above the minimum size qualifies as a nodule, its shape must be quantified. Roundness or circularity will be assessed by use of a shape factor. For each particle, the area of a reference circle is calculated using the following equation:

$$\text{Area of Reference Circle} = \frac{\pi(\text{Max. Feret})^2}{4} \quad (6)$$

The shape factor for each graphite particle is calculated from:

$$\text{Shape Factor (SF)} = \frac{\text{Area of Graphite Particle}}{\text{Area of Reference Particle}} \quad (7)$$

According to ASTM E2567 [61] the minimum required shape factor value chosen to qualify a particle as being a nodule is suggested to be 0.60.

Nodule count is also important when it comes to alloying. Jincheng Liu and R. Elliot (1999) shows that increasing the number of nodular graphites in mm^2 causes a finer and more homogeneous ausferrite structure that increases the strength, ductility and impact energy of the ADI [6]. Low number of nodular graphites means large spaces

between graphites which increases the chance of segregation of alloying elements to this spaces. It is discussed earlier, how segregation of certain elements effects austempering kinetics and mechanical properties negatively.

If the segregation becomes too dense, it inhibits the transformation of austenite during the austempering process and low carbon austenite or martensite is obtained. High number of nodular graphites in mm^2 (min. 100 per mm^2) is suggested to avoid martensite formation [6], [8], [29].

$$\text{Area Frac. of Nodular Graphite Particles} = 100 \times \frac{\text{Total Area of Nodular Graphite Particles}}{\text{Total Area of Matrix}} \quad (8)$$

Another factor that affects nodularity of the material is “Carbon Flotation”. During the solidification of thick sections, the nodules have lower density than the matrix come up to the surface. Decreasing the carbon equivalent, pouring temperature or increasing the cooling rate of the casting will help avoiding graphite floatation [62].

2.6. Microstructure of Austempered Ductile Iron

Austempered Ductile Iron has a unique microstructure among cast irons. Its exceptional mechanical properties come from this microstructure consists of acicular ferrite and high-carbon stable retained austenite which is called “ausferrite” [55].

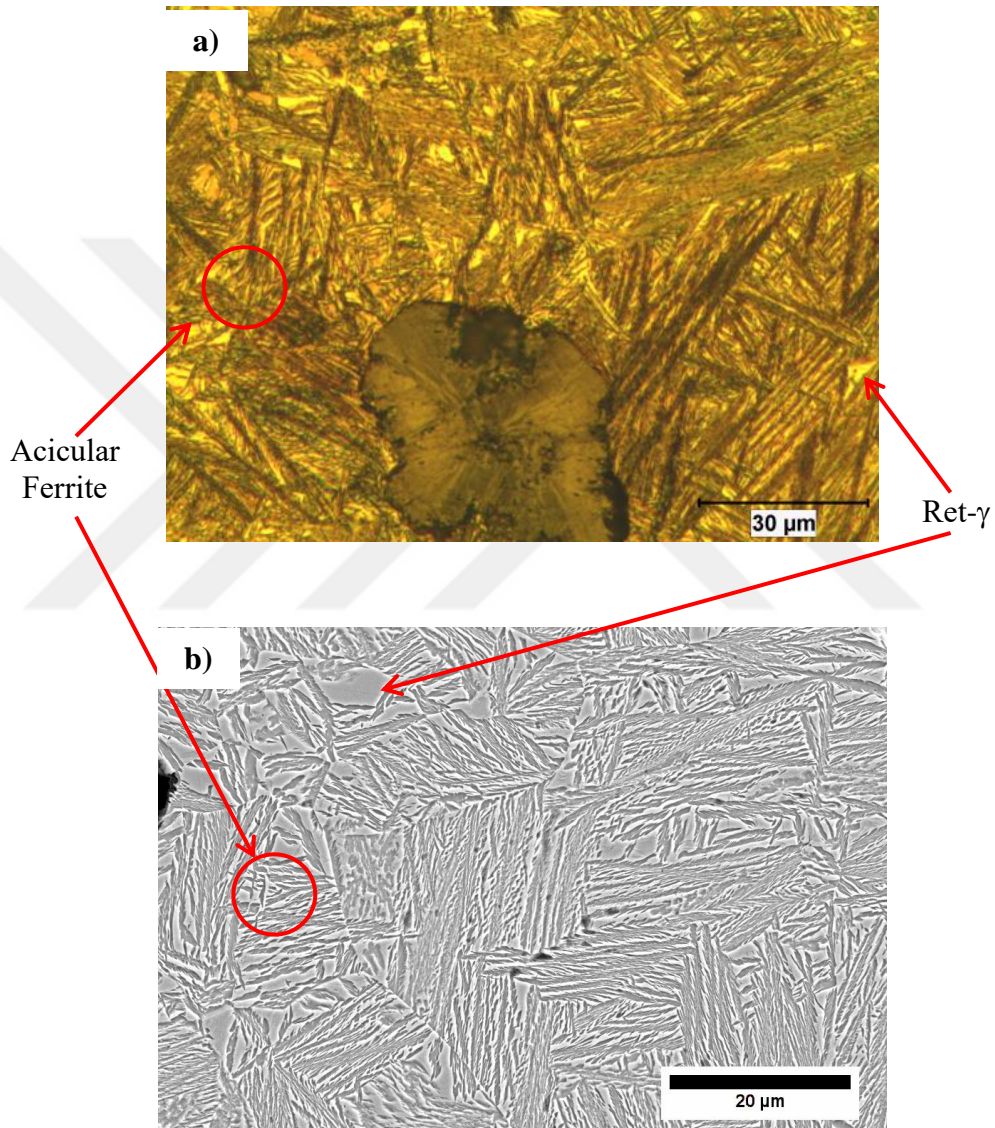


Figure 2.6-1 a) Optical microscope and b) SEM images of typical ausferrite structure

Sometimes microstructure of ADI is called bainite, but it actually is not. On the contrary, as mentioned above bainite formation takes place at Stage II and is undesirable in ADI [5], [7], [55]. There are reasons of this misunderstanding.

Ausferrite structure forms at the bainitic transformation temperature and it seems similar to bainite structure under microscopy. However, bainite consists of acicular ferrite and carbide. On the other hand, ausferrite consists of acicular ferrite and high-carbon stable retained austenite. Bainite transformation in steel occurs in one step process that is transformation of austenite directly to ferrite and carbide. Bainite is obtained in ADI only if it is austempered longer than needed. The ausferrite structure is what makes ADI special so bainite in ADI is not wanted [55].

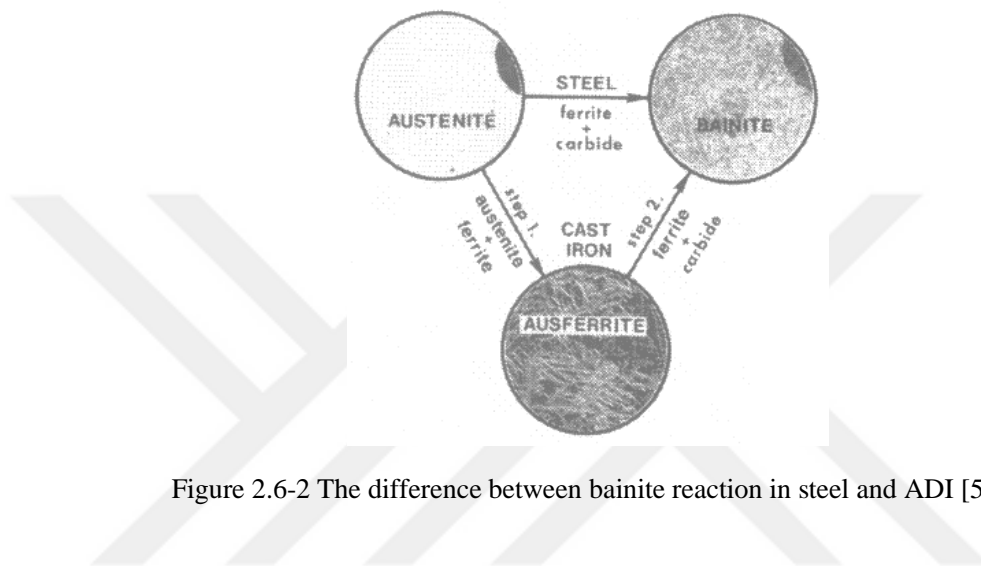


Figure 2.6-2 The difference between bainite reaction in steel and ADI [55]

There is also a confusion with the term “retained austenite” in ADI. When it is compared to steel, retained austenite in steel is undesirable. It is not the case when it comes to ADI. Two types of austenite can occur in ADI. These are stable austenite and metastable austenite. Stable austenite means, it is stabilized with carbon during heat treatment and do not transform to martensite at low temperatures. This type of austenite is very important and beneficial for ADI to obtain good properties. In most cases, “retained austenite” refers to metastable austenite which is undesirable and may cause problems. High-carbon stabilized austenite in ADI is stable thermodynamically, but it can undergo a strain-induced transformation under stresses and transform to martensite. This transformation gives ADI remarkable wear resistance [55].

2.7. Properties and Advantages of Austempered Ductile Iron

Properties of ADI depend on a many interlinked factors. As mentioned before, alloying element [7], [22], [26], [36], [38], [50], [51], [53], section thickness [36], [54] and the nodularity of the casting [6], [29], austenitizing and austempering times and temperatures [7], [20], [24], [50], [51] affect the final property of the casting. Among them heat treatment parameters are the most important. Various types of ADI can be produced by changing the ausferritic matrix with different amounts and distributions of ferrite and retained austenite with different austempering times and temperatures.

ADI shows improved mechanical properties and fatigue strength, has a high strength-to-weight ratio, good dynamic properties and wear resistance for a given hardness, and offers good toughness when compared to other castings [2], [63]. These advantages make ADI more superior to other castings. Also makes it a great alternative for certain steel grades and even aluminum alloys [64]–[66]. Moreover, like all other metal castings, production of ADI requires fewer steps, has less waste of material and consumes less energy than hot and cold rolling, extruding and welding [63]. In addition, as can be seen in Table 2, ADI is 8-10% lighter than wrought steels because of the graphite particles inside it [2], [63], [65], [66]. Stiffness and strength-to-weight comparisons can be seen in Figure 2.7.1 and Figure 2.7.2., respectively. It means if a part produced by ADI can meet the requirements in terms of mechanical properties and shape that is produced by steel, an important advantage will be gained in terms of weight [2]. Works of Vidyarthee, et al, and Frás, et al, aluminum castings can be successfully replaced by austempered ductile iron castings [65], [66].

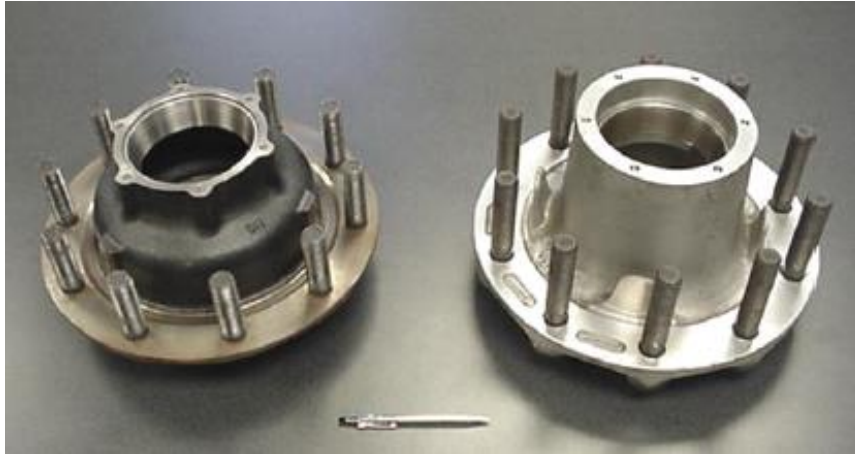


Figure 2.7-1 The ADI truck trailer hub (left) is 2% lighter and lower in cost than the aluminum hub (right) that it replaced [63]

Figure 2.7.1. shows an ADI wheel hub for a Class 8 truck trailer. The ADI hub was designed to take maximum advantage of ADI's high strength-to-weight ratio. It is 2% lighter than the aluminum hub that it replaced and lower in cost. For a given annual production volume, ADI is typically 20% lower in cost than a comparable steel component and over 30% lower in cost than an aluminum component. In addition, the lowest strength grade of ADI is about three times stronger than the highest strength aluminum and ADI's density is only 2.4 times that of aluminum. This means, by replacing steel or aluminum with ADI which has same configuration, less material (mass) will be needed and less will be paid for the material (per unit of mass [63]). Figure 2.7.3 shows the comparison of cost per unit of yield strength for various engineering materials.

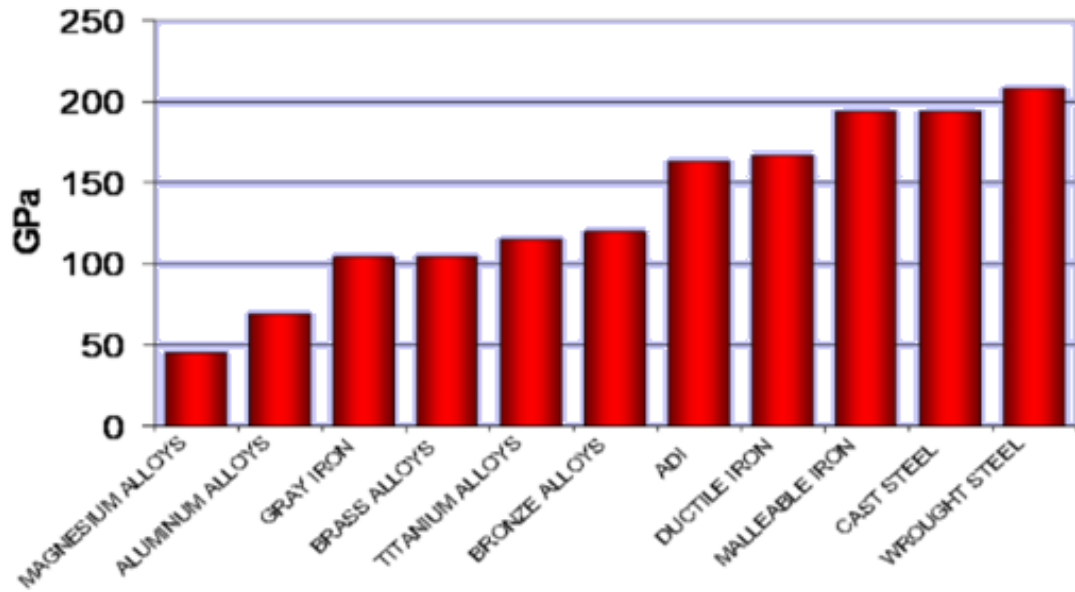


Figure 2.7-2 Comparison of Young's modulus of various materials [63]

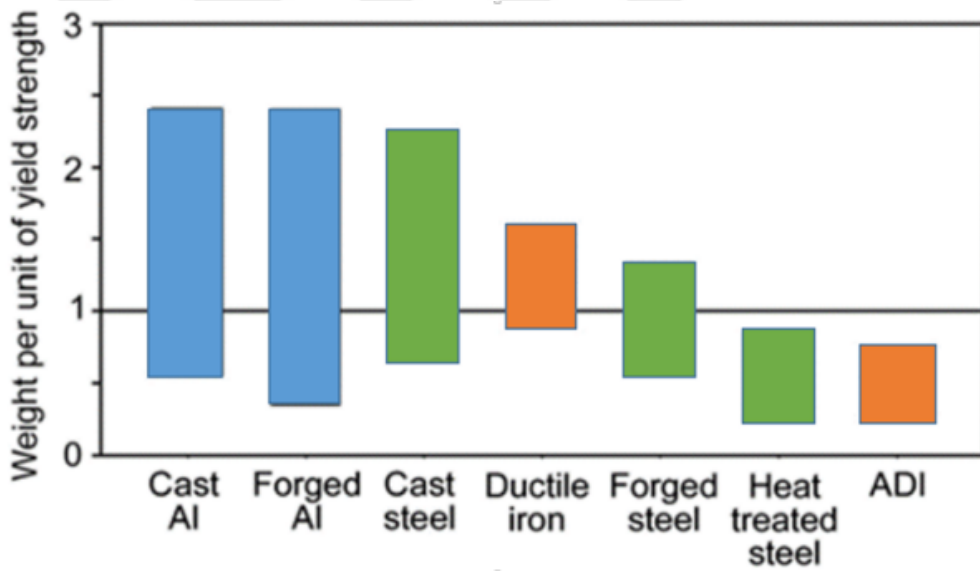


Figure 2.7-3 Comparison of relative weight per unit of yield strength for different material / process combinations [2], [63]

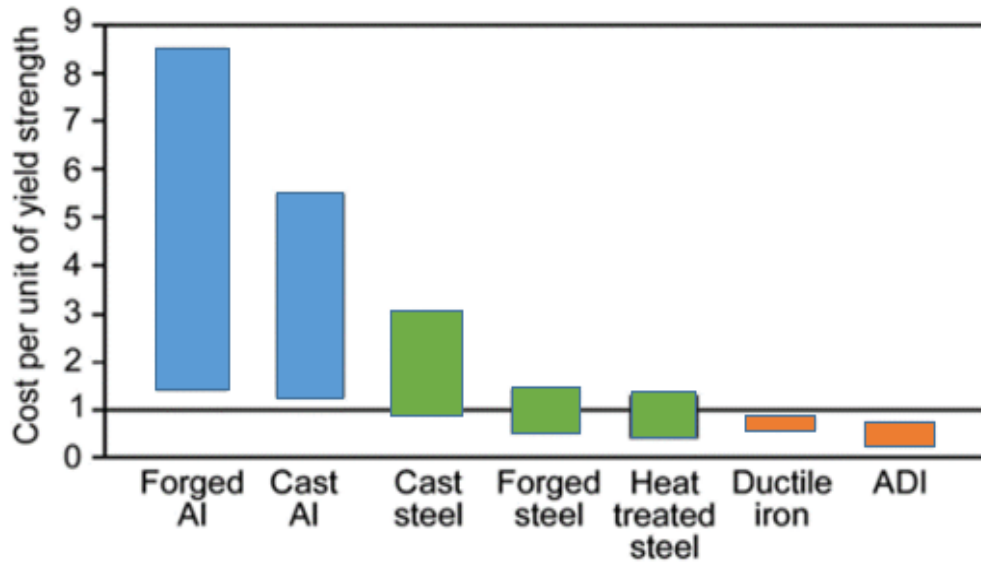


Figure 2.7-4 Comparison of relative cost per unit of yield strength for different material / process combinations [2], [63]

Table 2.7-1 Density comparison of several engineering materials [65]

Material	Specific Gravity (gm/cm ³)
Carbon Steel	7.8
Ductile Iron / ADI	7.2
Titanium Alloys	4.5
Aluminum Alloys	3.0
Carbon Fiber Composite	2.3
Magnesium Alloys	1.7
Polymers	0.95-2.0

Ductile iron has many casting methods such as green sand, bonded sand, lost foam, lost wax, continuous casting, centrifugal casting and permanent mold casting to production [63]. This high fluidity that enables the near-net-shape production of complex parts and good machinability before the heat treatment causes reduction in the cost of production process and increases the life of tools. Sum of all above makes ADI a very attractive material for the various sectors of industry such as automotive, rail transportation and agriculture [14].



Figure 2.7-5 Cast ADI end connectors compared to forged steel in a manufacturing sequence [63]

Figure 2.7.5. shows the comparison of ADI casting and forged steel end connector. ADI is the winner of this comparison. First of all, since ductile iron 10% less dense and the holes have been cored into the casting, less material is needed. Secondly, near-net-shape production cause less machining and waste which make ADI cost effective over forged steel.

2.8. Disadvantages of ADI

Despite having lots of advantages ADI also has disadvantages. As mentioned above ADI has the best cost per unit of yield strength ratio. However, austempering heat treatment equipment requires high capital investment; and small scale production of austempered components is, therefore, not profitable. Many metallurgical defects such as shrinkage, low nodule count, distorted graphite nodules, graphite floatation and carbides can occur during casting process because of poor inoculation, high carbon equivalent, long pouring time etc. These defects in ductile iron can be very costly to the foundry, not only because the part has to be remade or rectified, but due to the unfortunate fact that many defects are not revealed until after the expensive machining stage. Care in the selection of raw materials, good process control in the melting stage and proper metal handling procedures will go a long way to the prevention of defects [60].

Like most of the cast irons ADI also has poor weldability, thereby it is necessary to preclude the use of welding as part of the assembly process or for in-service repair. One of the other limitations of ADI is its service temperature. The service temperature range of ADI is limited to about -40° to $+200^{\circ}$ C because of the risk of microstructural changes, which in turn can cause changes in mechanical properties.

2.9. Applications of ADI

The application of ADI differs on considering different grades of ADI [67]. Since the grade 900 and grade 1050 have high ductility, they are mostly used in suspension components and many other dynamic applications; because of their high hardness, grade 1200 and grade 1400 are used when wear resistance is the main criteria for material selection [68]. ADI is also a proper material for chassis application because of its unique combination of high strength and toughness combined with material design flexibility [69]. Crankshafts of TVR Tuscan Speed Six's inline six cylinder engine is produced by ADI because of its low production costs and weight saving [70].

ADI is good choice for the cases where the damping capacity and lubrication are under consideration such as rail wheels. Austempered ductile iron is also used in the production of lock cases since its strain hardening property makes it resistant to penetration even under the very harsh conditions [67]. Gear materials can be produced by ADI because of its bending strength, surface durability and the pitting strength [71]. Gears produced by ADI are used in diesel engines for their strength, noise reduction and ease of production. Steel wheel axles are replaced by ADI for agricultural applications [67]. ADI is currently used in ground engagement components-digger bucket teeth and dozer blades, truck suspension brackets, differential spiders, tow hooks, cylinder liners, engine con rods and crankshafts [67]. ADI can be easily shaped to different formations which is an advantage for thin products that cannot be fabricated by common casting techniques and also for components used under severe conditions [71].

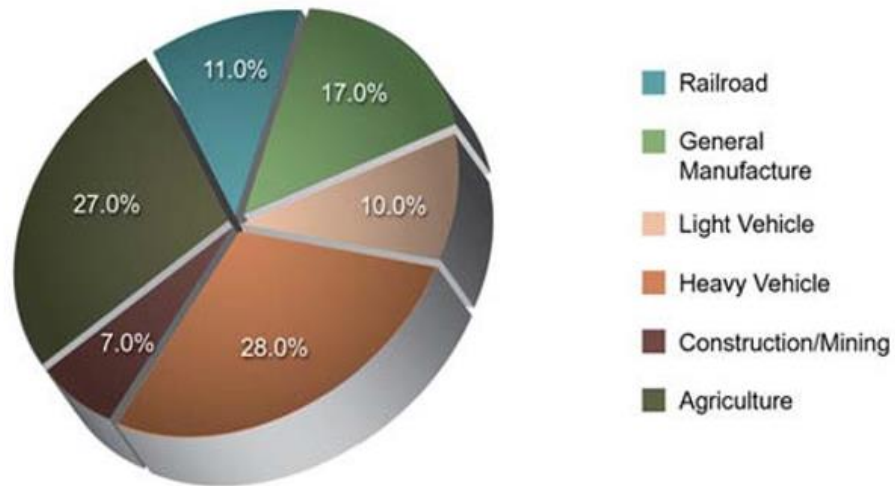


Figure 2.9-1 ADI - American market distribution, 2008 [67]

Some problems with machining can occur because of the substantial increase in strength and wear resistance of ADI [40]. Gear hobbing of ADI is not easy since tool failure appears in a short time [71]. Because of machining difficulties and inconsistent performance, ADI is hard to be used in high volume automotive applications [72]. Among many advantageous properties that make ADI appealing, there are also disadvantages like machining due to their hardness and strength [73].

CHAPTER 3

EXPERIMENTAL

3.1. Specimen Preparation

The material used in this study was first cast as a Y-blocks, having 4 different chemical compositions. From each Y-block at least 3 cylindrical specimens having 6-mm diameter were machined. Different alloying additions and heat treatment processes were conducted to observe how the processing parameters affect the final microstructure and mechanical properties of the castings. Castings' compositions and heat treatment processes are shown in Table 3. Lean alloy contains C, Si, Mn and all of the samples contain the same weight fraction of those elements.

Table 3.1-1 Compositions and heat treatment process details of present ADI castings

	T_{γ} and t_{γ}	T_{aus} and t_{aus}	Alloy Additions (Short Name)
ADI 1	900 – 950 °C 50 - 100 minutes	300 – 400 °C 75 - 100 minutes	Lean Alloy (Lean - Low T_{aus})
ADI 2	900 – 950 °C 50 - 100 minutes	350– 450 °C 100 - 125 minutes	Lean Alloy (Lean - High T_{aus})
ADI 3	900 – 950 °C 50 - 100 minutes	300 – 400 °C 75 - 100 minutes	Lean + Cu (Lean + Cu)
ADI 4	900 – 950 °C 50 - 100 minutes	300 – 400 °C 75 - 100 minutes	Lean + Cu + high Mo + low Ni (Lean + High Mo)
ADI 5	900 – 950 °C 50 - 100 minutes	300 – 400 °C 75 - 100 minutes	Lean + Cu + low Mo + high Ni (Lean + High Ni)

3.2. Heat Treatment and Mechanical Testing

Both heat treatment processes and mechanical tests were performed by using Gleeble 3500, shown in Figure 3.2.1 which is a fully integrated thermal and mechanical testing system. The reason of using the Gleeble 3500 for this study is it's capability of providing the versatility that is necessary to simulate many thermal-mechanical processes and ability of changing the control variables at any time and as often as required during the test.



Figure 3.2-1 The Gleeble 3500 System used for this study

Specimens to be analyzed in this study were heated to between 900 - 950°C with a heating rate of 50 °C/s and kept there for 50 - 100 minutes until a homogenous austenitic matrix was obtained. Austenitizing process was followed by austempering the specimens between 300 - 450°C for 75 - 125 minutes. Specimens were cooled from austenitizing temperature to austempering temperature with the cooling rate of 30°C/second. Heat treatment process was completed by quenching the specimens to room temperature with the rate of 10°C/second. During this thermal process cycle temperature was controlled by a K-type thermocouple.

Tensile tests were performed with a strain rate of 10^{-3} s^{-1} . HZT-071 contact type extensometer, as shown in Figure 3.2.2 was used to measure elongation and control strain rate during tensile test. Both the heat treatment processes and tensile tests were repeated 3 times to ensure repeatability using DSI-Gleeble 3500 thermomechanical simulator. All the tensile tests were performed at room temperature. The dimensions of the samples that are austempered and then tensile tested at Gleeble-3500 thermo-mechanical simulator are given in Figure 3.2.3

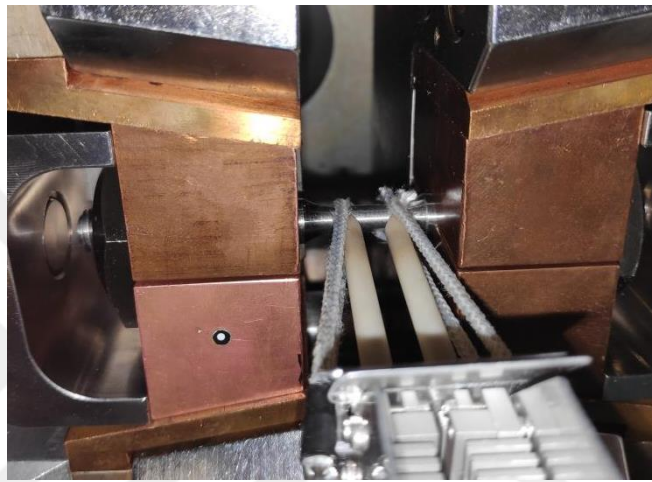


Figure 3.2-2 HZT-071 type extensometer used for strain rate and elongations measurements

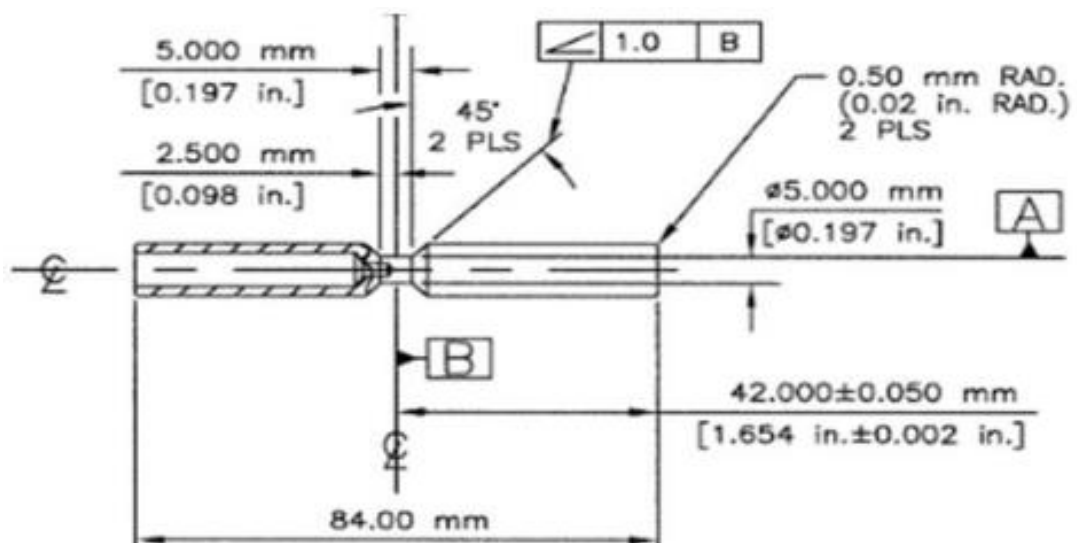


Figure 3.2-3 Technical drawing of Gleeble-3500 specimens used in this study

3.3. Microstructural Characterization

After heat treatment and mechanical testing procedures, all the specimens were subjected to metallographic preparation according to ASTM E03 [74]. Metallographic examination of the specimens started with sectioning using a precision cut-off machine (Struers Secotom-10). Grinding and polishing steps were performed with fully automatic Struers Tegramin-25 machines. Those steps were:

- 2 step grinding (320-500 grit) with SiC papers
- 3 step polishing (9μ - 3μ - 1μ) with diamond paste

From as-polished specimens of each casting, 30 images were taken at 50x magnification via Nikon Eclipse LV 150 optical microscope, under bright field illumination in order to characterize graphite particles. The nodularity, nodule count and nodule size of the specimens were determined according to ASTM E2567 [61] by using Clemex Vision-Pro software. The shape of graphite particles were evaluated using “maximum ferret diameter (MFD)”. This parameter can be defined as the maximum distance between pairs of parallel tangents to the projected outline of the particle. Schematic representation of MFD can be seen in Figure 3.3.1.

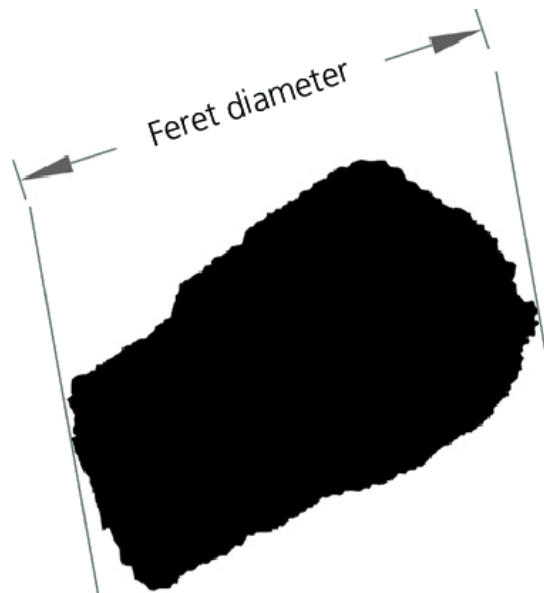


Figure 3.3-1 Schematic representation of Maximum Feret Diameter (MFD) [75]

The shape factor (SF) of graphite particles were then defined as:

$$\text{Shape Factor (SF)} = \frac{\text{Area of Graphite Particle}}{\pi(\text{MFD} / 2)^2} \quad (9)$$

For a perfect circle the SF should be 1, and it approaches to zero when the particle shape becomes losing its roundness. A particle is considered as graphite if its MFD is at least 10 μm (size criteria). A graphite is qualified as “spheroidal graphite (nodular graphite)” when its SF is at least 0.6 (SF criteria).

Afterwards, the specimens were polished with an additional final step using “oxide polishing suspension (OPS), for 5 minutes for electron back-scatter diffraction technique (EBSD). Later on, microstructural analysis continued with taking optical microscope and field-emission scanning electron microscope (FEG-SEM) images from specimen surfaces etched by nital solution to see details of acicular ferrite of ausferritic matrix.

Carl Zeiss Merlin – Field Emission Scanning Electron Microscope (SEM) was used to examine the microstructural properties of the specimens. SEM used in this study can be seen in Figure 3.3.1. The SEM was operated at an acceleration voltage of 15 kV and at a working distance of 8 - 10 mm. SEM micrographs of each specimen were taken from randomly selected positions at 1500X, 3000X and 5000X magnifications; using the secondary electron detector.

Electron back-scatter diffraction (EBSD) technique was employed to reveal the microstructural details of the ausferrite matrix of the ADI samples, including the grain size and phase fraction of the high-C austenite. For EBSD analysis, Zeiss Merlin field emission gun (FEG) scanning electron microscope (SEM), equipped with EDAX/TSL EBSD system and a Hikari EBSD camera was used. The accelerating voltage was 15 kV, beam current 6.0 nA and the working distance 13 mm; EBSD maps were measured on a hexagonal grid with a step size of 50 nm. EBSD camera was run at 100 frames s^{-1} , with 10 ms exposure time in 4×4 binning (160×120 pixels). During the post-processing of the raw EBSD data, firstly the

grain confidence index standardization (GCIS) method was used. The GICS method checks the confidence index (CI) of all points within a grain and then assigns the highest value measured to all points in that grain. Afterward, a minimum CI-filter of 0.1 was used to exclude only falsely indexed points with certainty. Note that, this clean-up procedure does not change the measured orientation of any point. The grains were then defined and reconstructed from sets of neighboring pixels having a misorientation less than 5° between each other.



Figure 3.3-2 Carl Zeiss: Merlin – Field Emission Scanning Electron Microscope

3.4. Hardness Measurements

Zwick ZHV10 micro hardness device was used to measure Vickers hardness values of the specimens. 1.96 N of load was applied to indent the as-polished surface of the specimens at a test speed of 25mm/min. For each specimen minimum 10 indentations were made at randomly selected locations, that are between nodular graphite particles. The size of indentations were measured by using an objective lens whose magnifying power is 20x.

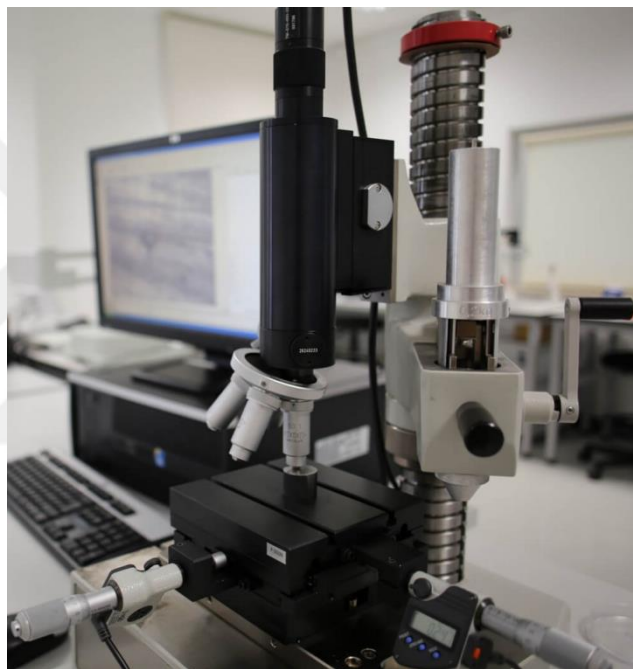


Figure 3.4-1 The Zwick/ZHV10 hardness tester

CHAPTER 4

RESULTS AND DISCUSSIONS

In this part, all of the results will be given under 3 main subsections:

(i) First; detailed nodularity analyses of the specimens were given under the title: *Nodularity Analyses*

(ii) Second; microstructural properties that were characterized by metallographic and microscopic techniques, image processing, and EBSD analyses were given under the title: *Microstructural Characterization*

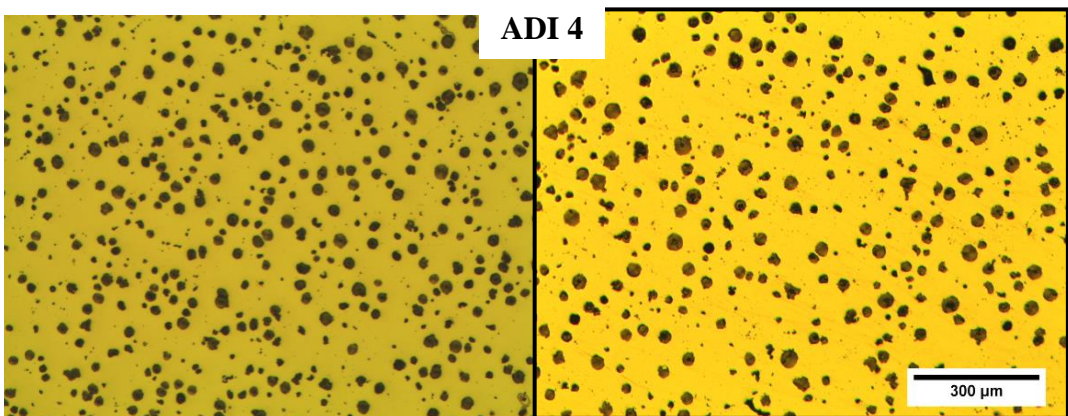
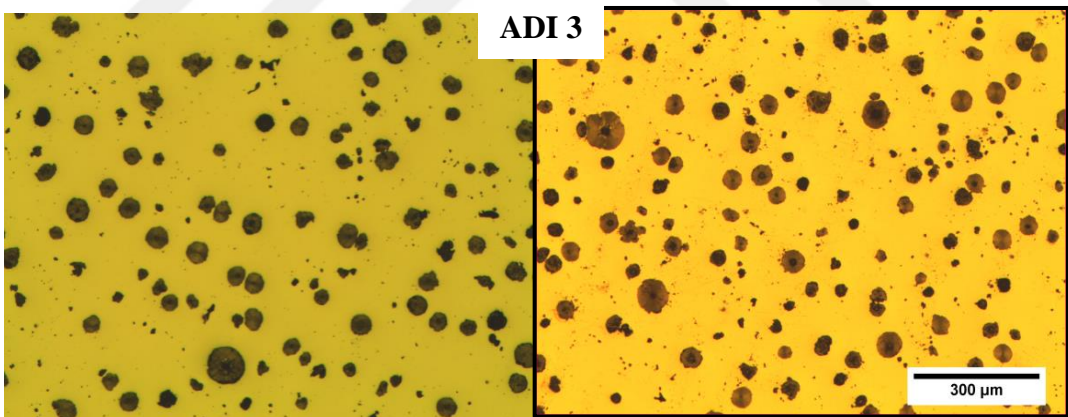
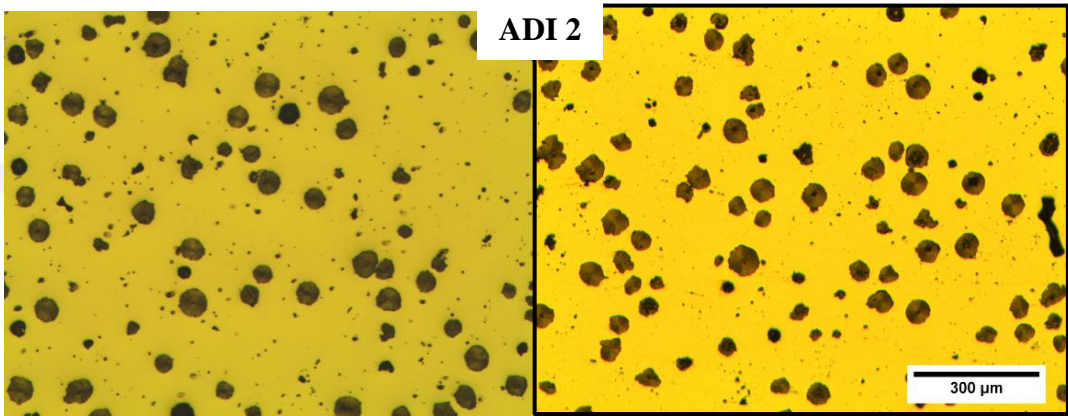
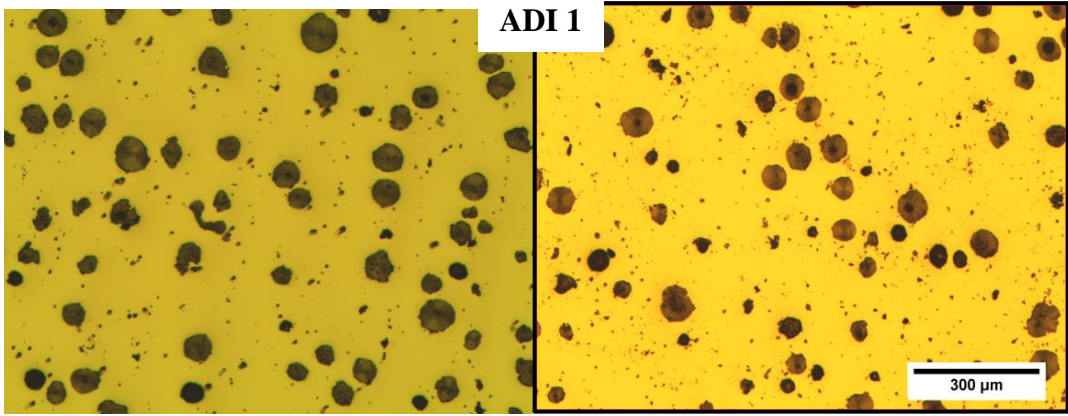
(iii) Third; the correlations between microstructural parameters and mechanical properties will be given under the title: *Correlation Between Microstructural Parameters and Mechanical Properties*

In addition, the reliability, representativeness and repeatability of EBSD-based measurements, specifically for determining retained austenite content will be discussed under the title: *Reliability and Representativeness of EBSD Technique*

4.1. Nodularity Analyses

Figure 4.1.1. shows the as-polished images of the ADI castings before and after austempering process taken by optical microscopy at 50x magnification. The micrographs indicate the size, shape and distribution of the spheroidal graphite.

Using the shape factor (SF), the percent nodularity of the ADI castings were compared. The “percent nodularity” can be defined by area, where the total area of spheroidal graphite particles (i.e. particles meeting the size and SF criteria) is divided by the area of graphite particles (i.e. particles meeting only size criteria). Comparison of the shape factor distributions of the specimens can be seen in Figure 4.1.2.



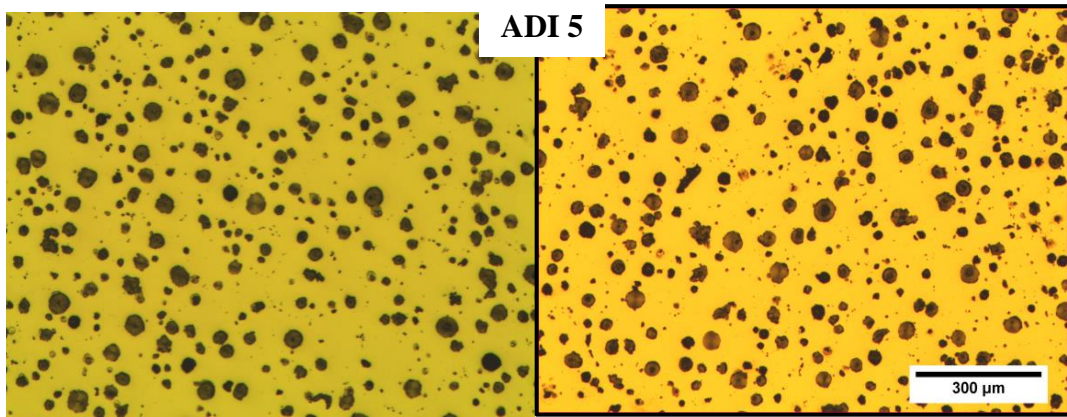


Figure 4.1-1 Optical micrographs of as-polished ADI castings before (left) and after (right) austempering heat treatment process

In the same manner, percent nodularity can be defined by number where total number of spheroidal graphite particles is divided by total number of graphite particles. Figure 4.1.3. compares both percent nodularity by area and number of the samples. Each alloy has almost the same nodularity; and all of the sample nodularity by area values are higher than 83%. The difference in nodularity by number is more noticeable. ADI 1 has the highest nodularity by area yet the lowest nodularity by number. Nodularities of ADI 1 and ADI 2 are nearly the same. Table 4.1-1 and Table 4.1-2 show the results of nodularity analysis of ADI samples according to ASTM E2567 [61] before and after austempering heat treatment process, respectively. Tables indicate that there is no drastic changes between results coming from before and after austempering process. The only noteworthy difference is ADI 3 samples's the nodule density and average nodule size; both of which shows a decrease after austempering treatment. The nodule fraction of ADI 1 also shows noticeable decrease. Those differences in ADI 1 and 3 can be attributed to the heterogeneity of the as-cast structures. It should be noted that the graphite shape factor distributions of those two samples (Fig 4.1.2) are broader than the rest of the tested samples, indicating heterogeneity.

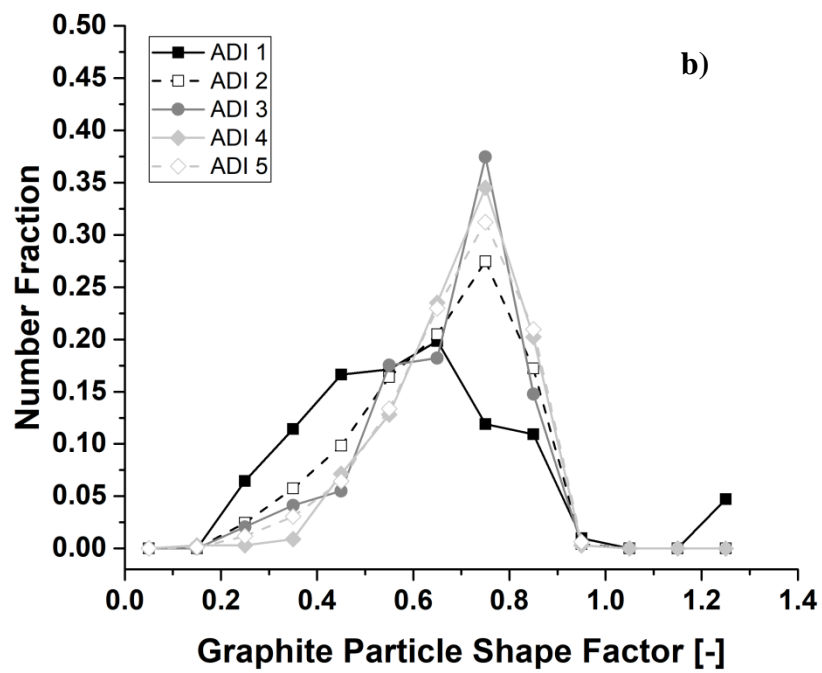
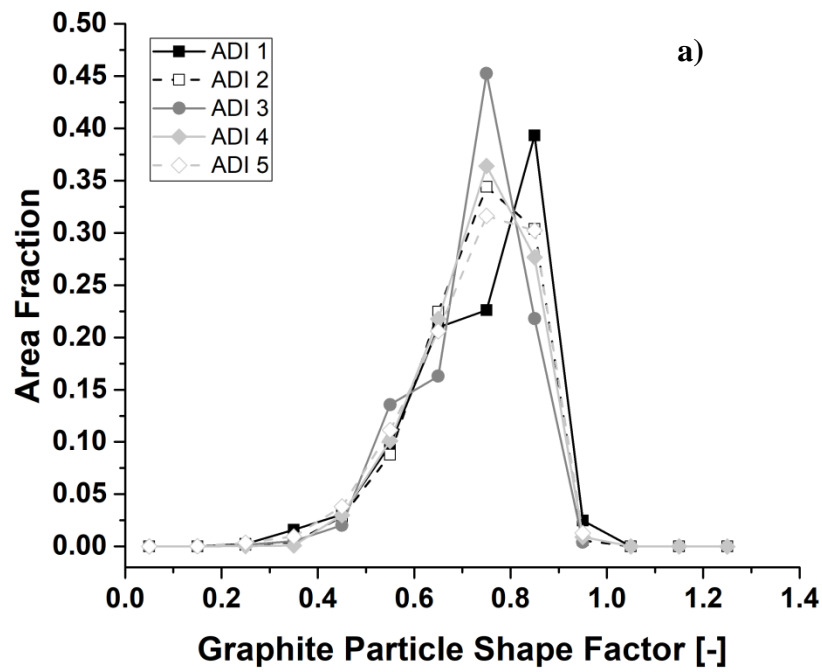


Figure 4.1-2 Comparison of a) Area and b) number fraction of graphite particles' shape factors

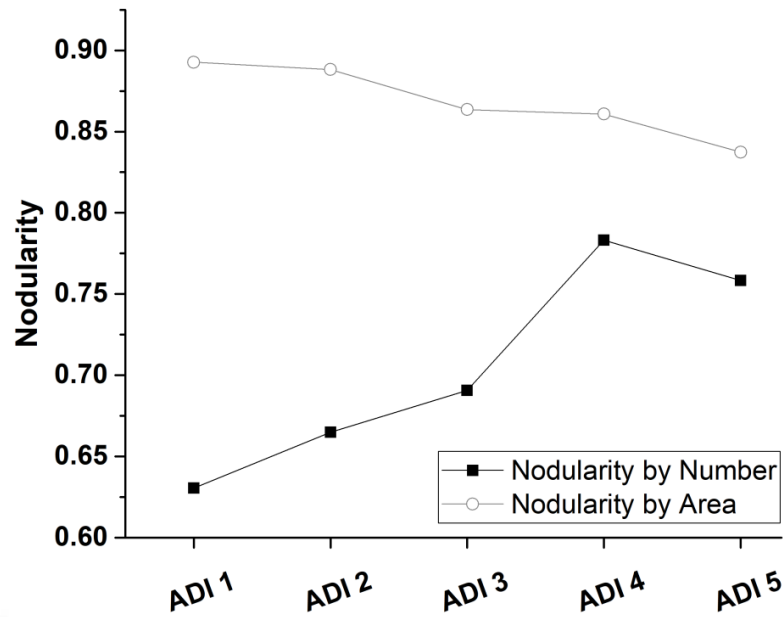


Figure 4.1-3 Nodularity by number and nodularity by area values of ADI castings

Table 4.1-1 Nodularity analyses of ADI samples before austempering heat treatment process

Before Heat Treatment	ADI 1	ADI 2	ADI 3	ADI 4	ADI 5
	Lean - Low T_{aus}	Lean - High T_{aus}	Lean + Cu	Lean + High Mo	Lean + High Ni
Nodularity by Area	89.33%	89.16%	82.22%	81.24%	84.40%
Avg. size of Nodular G-particles (μm) (Nod-s)	49.59	41.01	40.85	25.23	28.20
Nodule density (nodules/ mm^2)	59.93	78.34	85.63	216.73	168.78
Avg. shape factor	0.63	0.65	0.69	0.69	0.67
Nodule area fraction (V_{nodule})	10.34%	10.02%	10.18%	9.22%	9.22%
G-particle area fraction	11.55%	11.23%	10.98%	10.66%	10.90%

Table 4.1-2 Nodularity analyses of ADI samples after austempering heat treatment process

After Heat Treatment	ADI 1	ADI 2	ADI 3	ADI 4	ADI 5
	Lean - Low T_{aus}	Lean - High T_{aus}	Lean + Cu	Lean + High Mo	Lean + High Ni
Nodularity by Area	89.27%	88.82%	86.36%	86.08%	83.74%
Avg. size of Nodular G-particles (μm) (Nod-s)	47.47	41.07	35.31	27.45	27.91
Nodule density (nodules/ mm^2)	49.57	72.89	73.95	207.83	176.40
Avg. shape factor	0.62	0.63	0.64	0.67	0.67
Nodule area fraction (V_{nodule})	7.17%	9.06%	6.38%	10.26%	9.46%
G-particle area fraction	8.65%	10.18%	7.40%	11.95%	11.31%

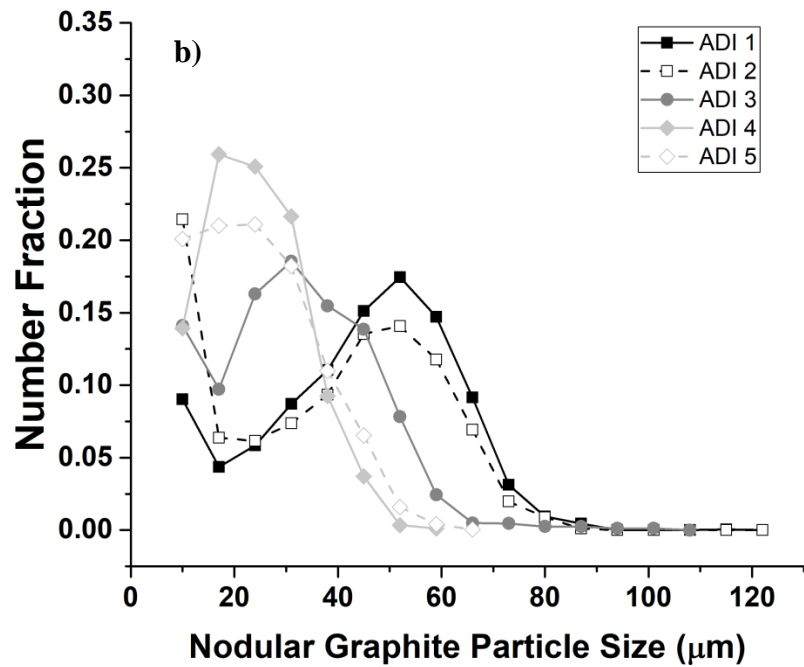
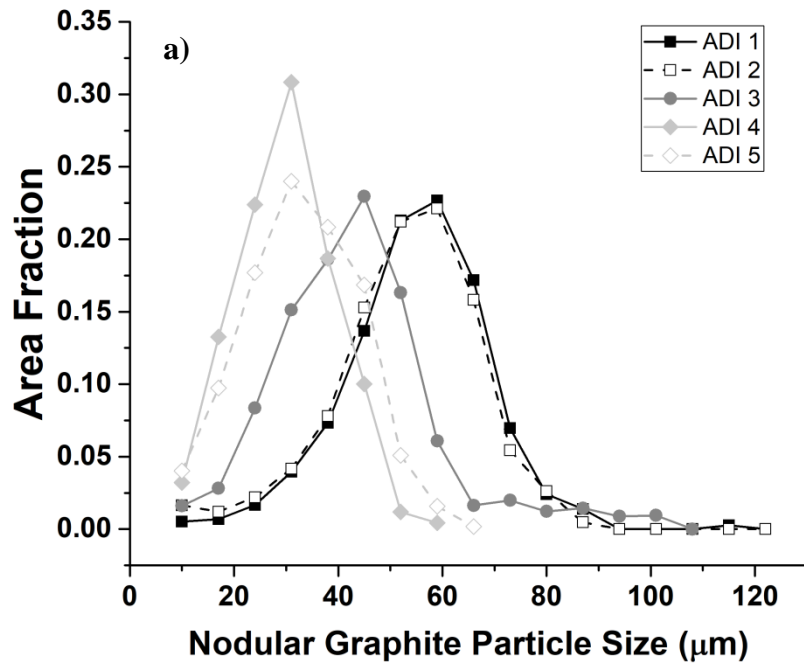


Figure 4.1-4 Comparison of size distribution of nodular graphite particles with respect to a) area and b) number fractions

Figure 4.1.4. shows the area and number fractions of nodular graphite particles. Average size of the nodular graphite particles is the largest in ADI 1 and smallest in ADI 4 and ADI 5.

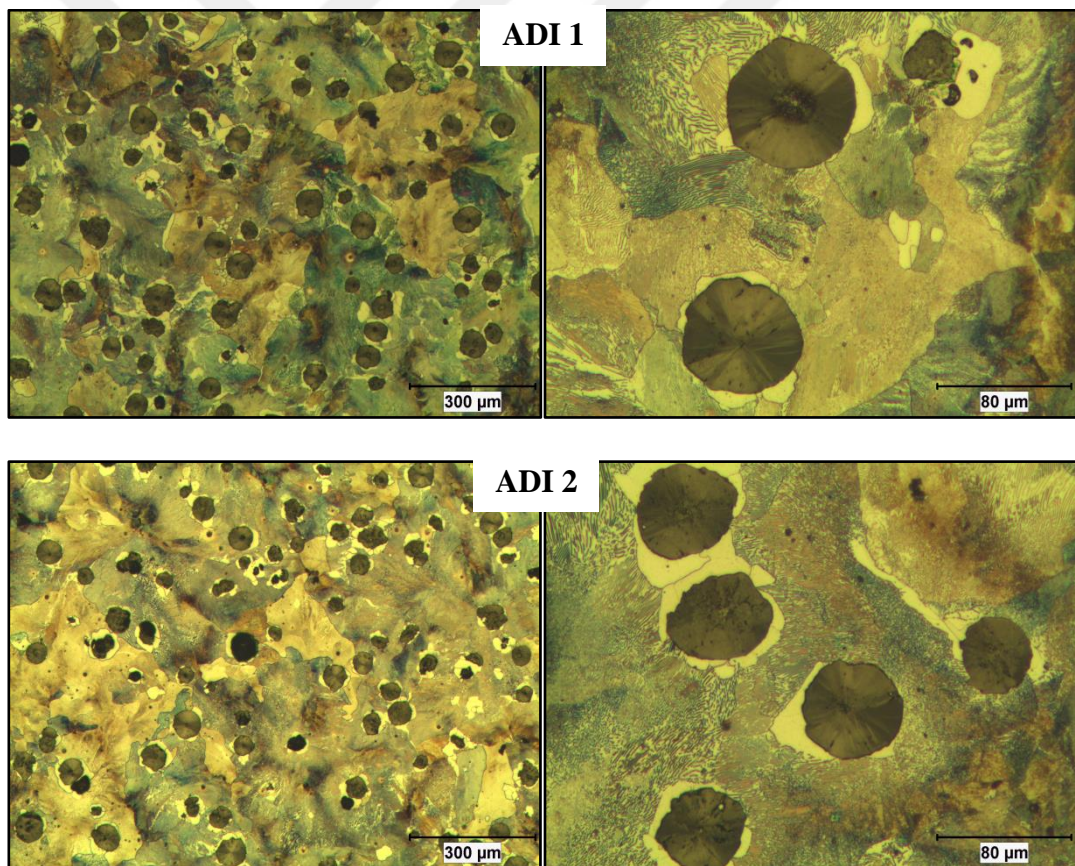
From Table 4.1-3, it can be seen that, alloys with additions of Cu, Mo and Ni have larger nodule count per mm^2 and smaller Ret- γ fraction than ADI 1 and ADI 3 alloys. Liu and Elliot show that increasing the nodule count accelerates the Stage I reaction and causes production of a finer, more uniform ausferrite structure [6]. The present study doesn't match with the Liu and Elliot's work. Although ret- γ fraction decreases with increasing nodule density, specimens with higher nodule count don't have finer matrix. ADI 3 alloy has 73.95 nodules per mm^2 and ADI 5 alloy has 176.4 nodules per mm^2 . However, both of the alloys have nearly the same acicular ferrite and retained austenite grain sizes. The same condition also applies to ADI 2 and ADI 4 castings. ADI 4 alloy has nearly three times more nodules per mm^2 square yet both alloys have similar grain sizes. The present results indicate that alloying additions and heat treatment parameters have larger impact on matrix structure than the nodularity of the castings.

Table 4.1-3 Comparison of microstructural parameters and nodularity analyses of ADI Samples

	ADI 1	ADI 2	ADI 3	ADI 4	ADI 5
	Lean - Low T_{aus}	Lean - High T_{aus}	Lean + Cu	Lean + High Mo	Lean + High Ni
Nodularity by Area	89.27%	88.82%	86.36%	86.08%	83.74%
Avg. size of Nodular G-particles (μm) (Nod-s)	47.47	41.07	35.31	27.45	27.91
Nodule density (nodules/ mm^2)	49.57	72.89	73.95	207.83	176.40
Avg. shape factor	0.62	0.63	0.64	0.67	0.67
Nodule area fraction (V_{nodule})	7.17%	9.06%	6.38%	10.26%	9.46%
G-particle area fraction	8.65%	10.18%	7.40%	11.95%	11.31%
Ret- γ fraction (V_{γ})	41.1%	32.4%	32.5%	22.3%	20.5%
Ret- γ grain size (γ -GS)	1.74	1.18	0.85	1.42	0.79
α -phase fraction (V_{α})	58.9%	67.6%	67.5%	77.7%	79.5%
α -phase grain size (α -GS)	2.62	3.38	2.78	3.07	2.95

4.2. Microstructural Properties

A multiscale microstructure analysis is required to fully understand the microstructure of ADI and then correlate the microstructure to mechanical properties. In the present case the size, shape, fraction and also the nodularity of graphite particles as well as the matrix microstructure influences the mechanical properties. A simple optical microscope (OM) image of as-polished ADI is usually enough to characterize the graphite particles, since their average size is in the range of 20 – 50 μm . However, the details of ausferrite matrix cannot be resolved with OM. Figures 4.2.1 and 4.2.2. shows optical microscopy images of ADI samples before and after austempering process, respectively.



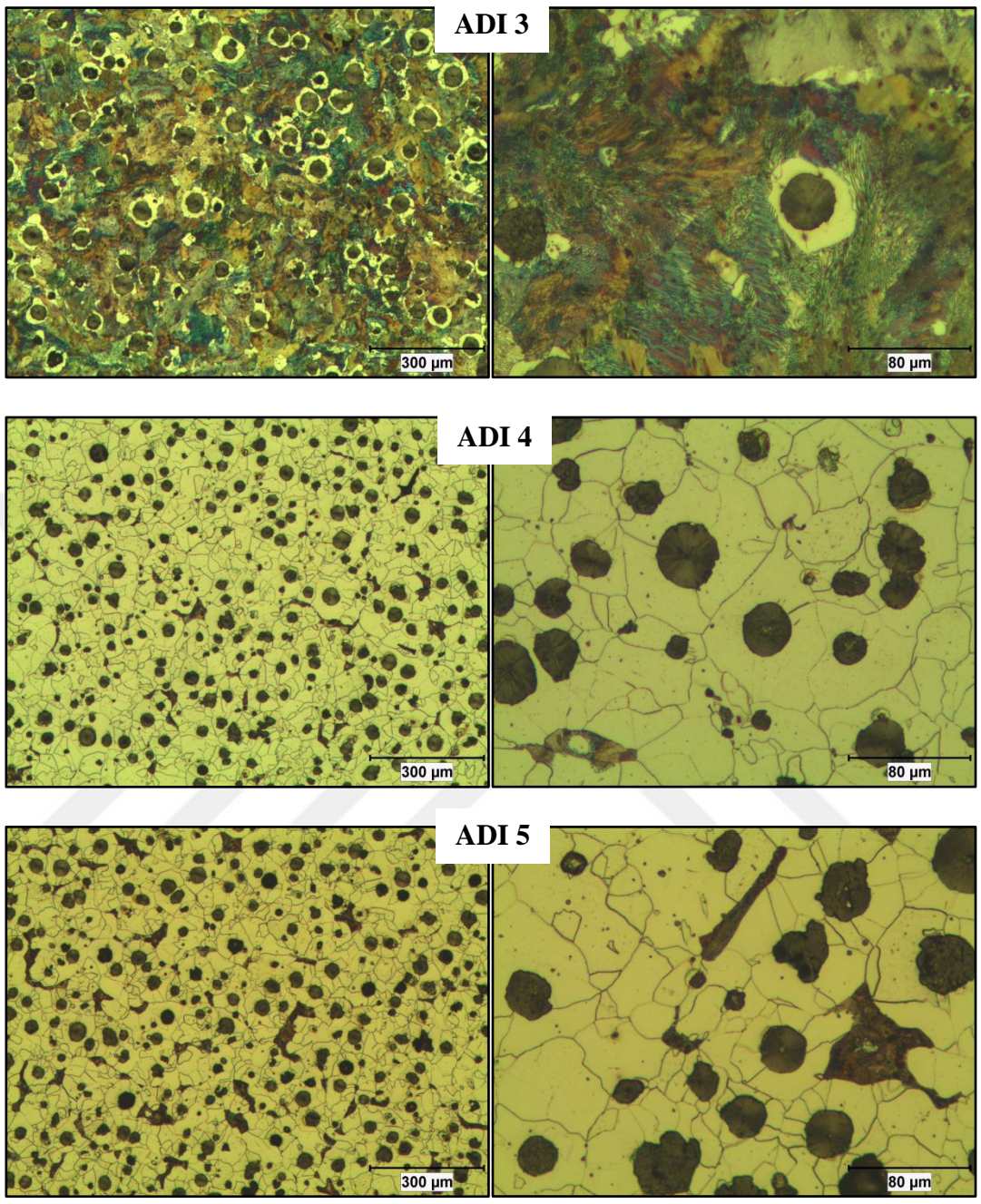
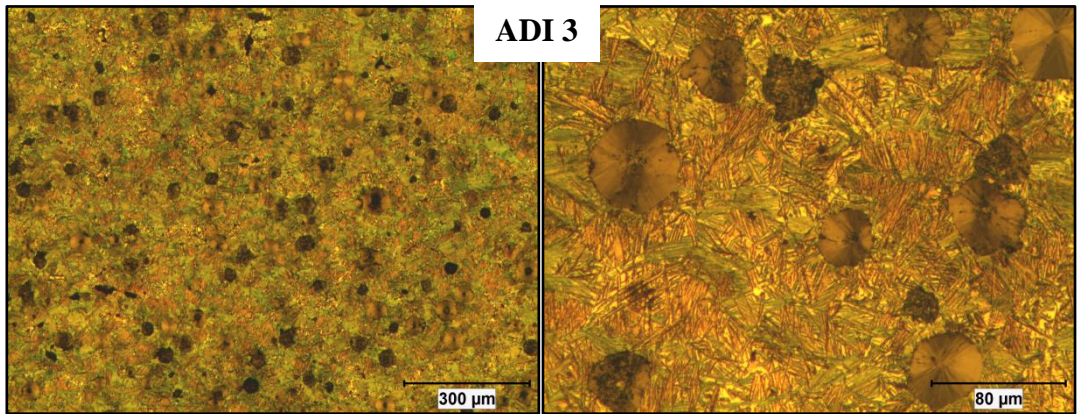
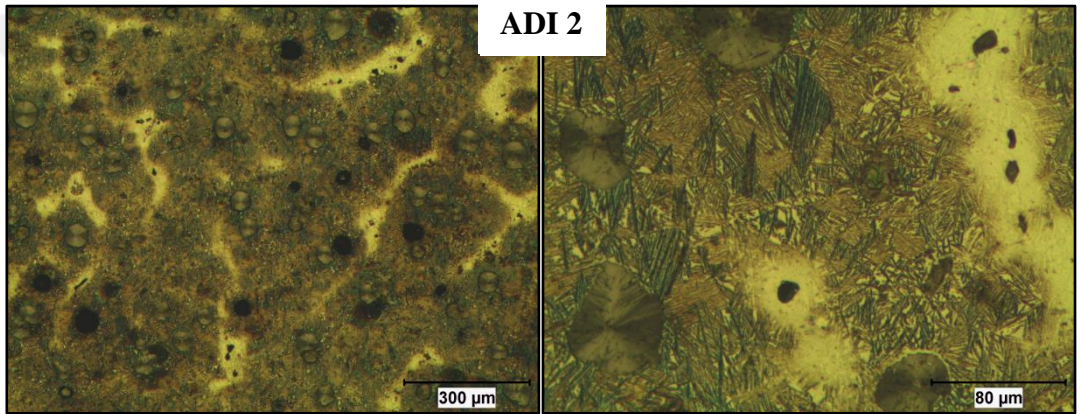
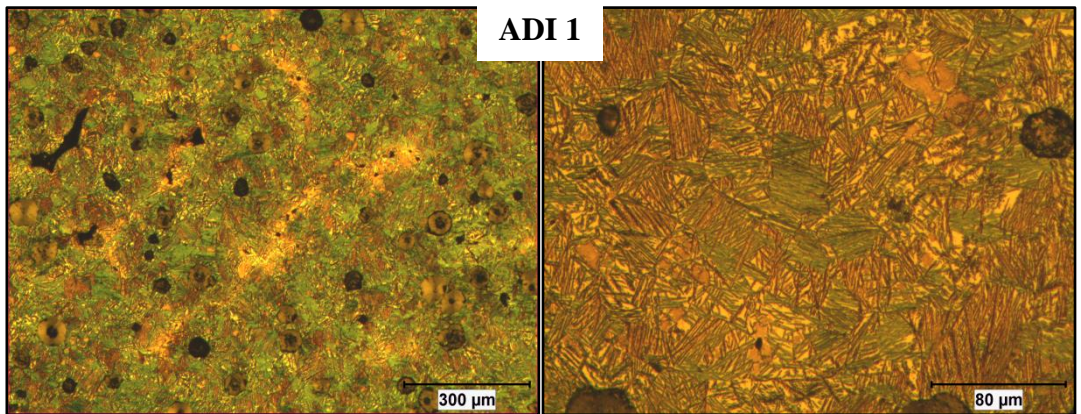


Figure 4.2-1 Optical micrographs of microstructures of ADI before austempering heat treatment process



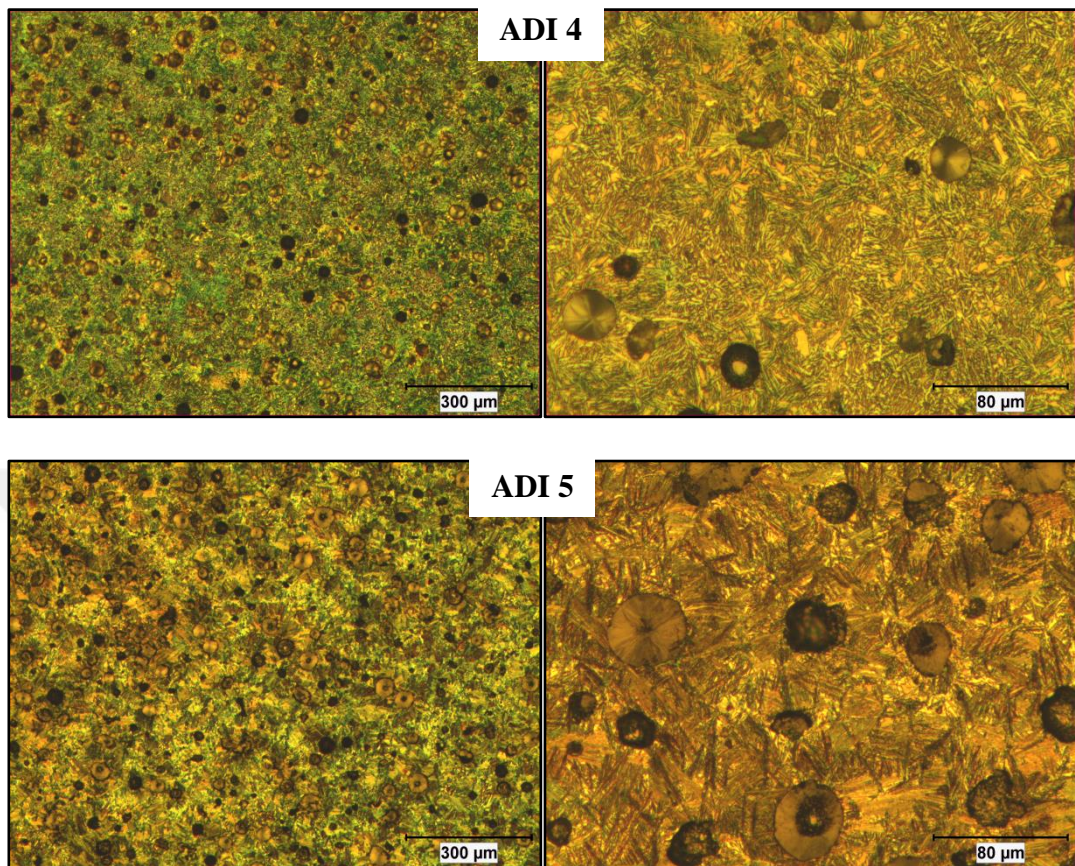


Figure 4.2-2 Optical micrographs of ADI samples after austempering process

The details of the acicular ferrite of ausferritic matrix can be resolved with field-emission scanning electron microscope (FEG-SEM). Moreover, in order to resolve the carbon enriched austenite regions of the ausferritic matrix, electron back-scatter diffraction technique (EBSD) should be employed [76].

Structure of acicular ferrite and retained austenite can be observed in OM images but without much detail. SEM images of samples as shown in Figure 4.2.3. reveal more detail about the structure as expected. Especially to reveal the martensite presence and separate it from the acicular ferrite structure, SEM images at high magnifications higher than 5000X are required. Two types of retained austenite are observed in the SEM images; i) film type γ present in between acicular-ferrite platelets; and ii) block type γ present around prior austenite grain (boundaries) and

those type-ii γ are the ones that are not transformed during austempering. Block type is coarser i.e. it has a larger grain size than the film type γ . Both types of those retained austenite can be found in each of the studied ADI alloys. However, their fractions and distributions are different in each alloy. This difference influences the average grain size and grain size distributions of austenite, which has been determined via EBSD analysis and will be given in detail further in this current Chapter. It should also be noted that ADI 1 has the highest γ -fraction and most of its γ are block type.

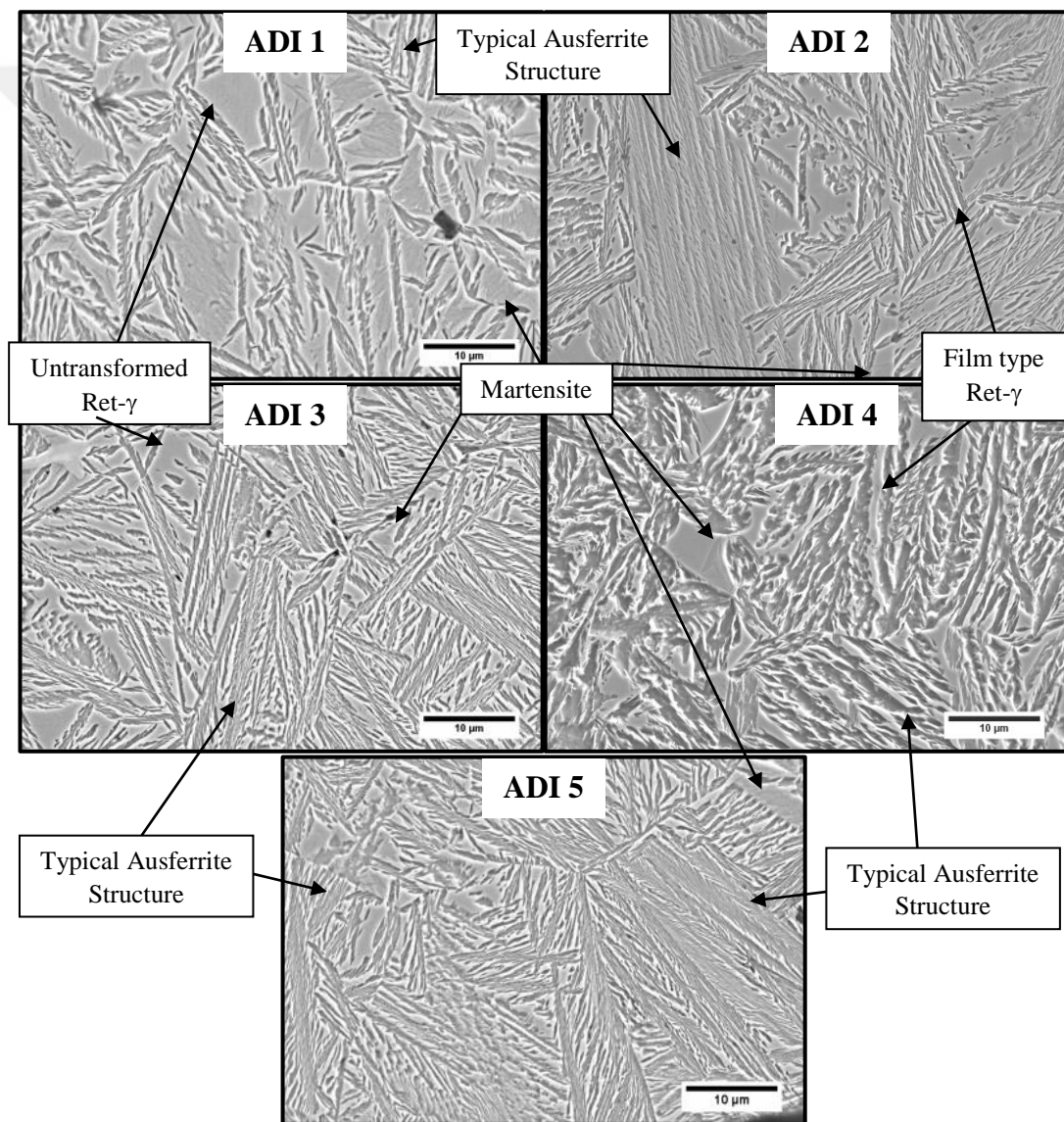


Figure 4.2-3 SEM micrographs ADI sample taken at 5000X

SEM images also reveal martensite regions in each alloys matrix, along with retained austenite and ausferrite; as shown in Figure 4.2.3. Moreover, Table 4.2-1 shows that, the ADI 1 has the highest hardness but lowest ductility. The strength of the ADI 1 is mainly coming from the presence of coarse martensitic regions as can be seen in SEM image of ADI 1. Martensite regions are coarser in ADI 1 than any alloy in this study. Martensite has higher strength and hardness whereas it lowers ductility significantly. It is clear that Stage I reaction wasn't completed at the end of the austempering process for ADI 1. Holding at the austempering temperature for a duration shorter than needed causes incomplete carbon enrichment of the austenite, which reduces its stability. This instable austenite, then transforms to martensite upon cooling to room temperature. ADI 2, which has the same composition with ADI 1, was austempered at a higher temperature and for a longer time than ADI 1. For ADI 2 the carbon diffusion rate is higher and there is enough time for carbon to stabilise the austenite. In the end, SEM images of ADI 2 also shows martensite regions but they are smaller and fewer. Those differences in microsturcture enhances the mechanical properties. ADI 2 exhibit better elongation, hardness and tensile strength than ADI 1; although both have the same composition. Table 4.2-1 also indicates that ADI 3 shows the second best mechanical properties after ADI 5

Table 4.2-1 Mechanical properties of ADI samples

Mechanical Properties	ADI 1	ADI 2	ADI 3	ADI 4	ADI 5
	Lean - Low T _{aus}	Lean - High T _{aus}	Lean + Cu	Lean + High Mo	Lean + High Ni
Hardness (HV 0.2)	462 ± 83	478 ± 39	458 ± 82	375 ± 55	437 ± 93
UTS (MPa)	1004.0 ± 28.1	1022.6 ± 23.4	1158.0 ± 4.3	1080.6 ± 30.5	1182 ± 14.7
Yield Strength (MPa)	732.1	718.9	830.1	846.2	902.37
Total Elongation	4.2 ± 0.8	6.65 ± 1.16	9.0 ± 2.2	5.04 ± 1.21	10.5 ± 0.01

EBSD technique was employed to resolve carbon enriched austenite regions of the matrix of the specimens. Figures 4.2.4., 4.2.5. and 4.2.6. represent the EBSD phase maps, inverse pole figure with respect to normal direction (IPF-ND) maps of FCC-indexed partition and BCC-indexed partition of ADI samples. ND is normal to the cross-section of Y-blocks and parallel to the tensile axis. The overlaid green regions on the phase maps show the retained austenite regions. BCC-indexed partition involves ferrite, bainite, martensite and acicular ferrite in ausferrite structure. These maps reveal that all of the sample's microstructures are composed of mostly acicular ferrite.

Figure 4.2.7. indicates that both ausferrite and retained austenite become finer after increasing alloying elements. Alloys with finer matrix phases exhibit higher elongation, tensile and yield strength. Both ADI 1 and ADI 5 castings have the finest ausferrite microstructures among castings in this study. These castings surpass both ADI 1 and ADI 2 in elongation, yield strength and tensile strength with very close hardness values.

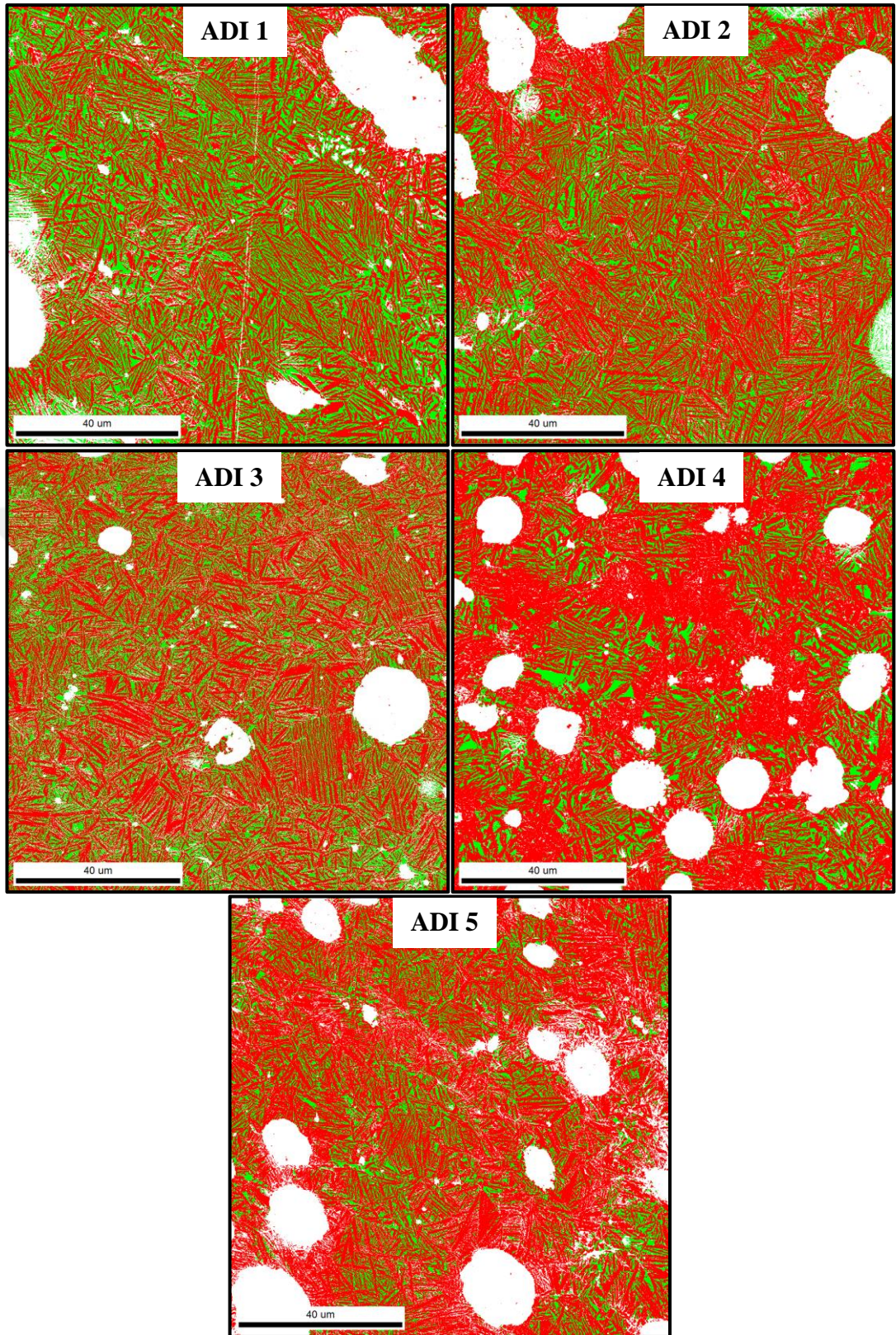


Figure 4.2-4 EBSD phase maps of ADI castings. Large white areas represent nodular graphite particles; green areas represent retained austenite structure; red areas represent ferrite structure

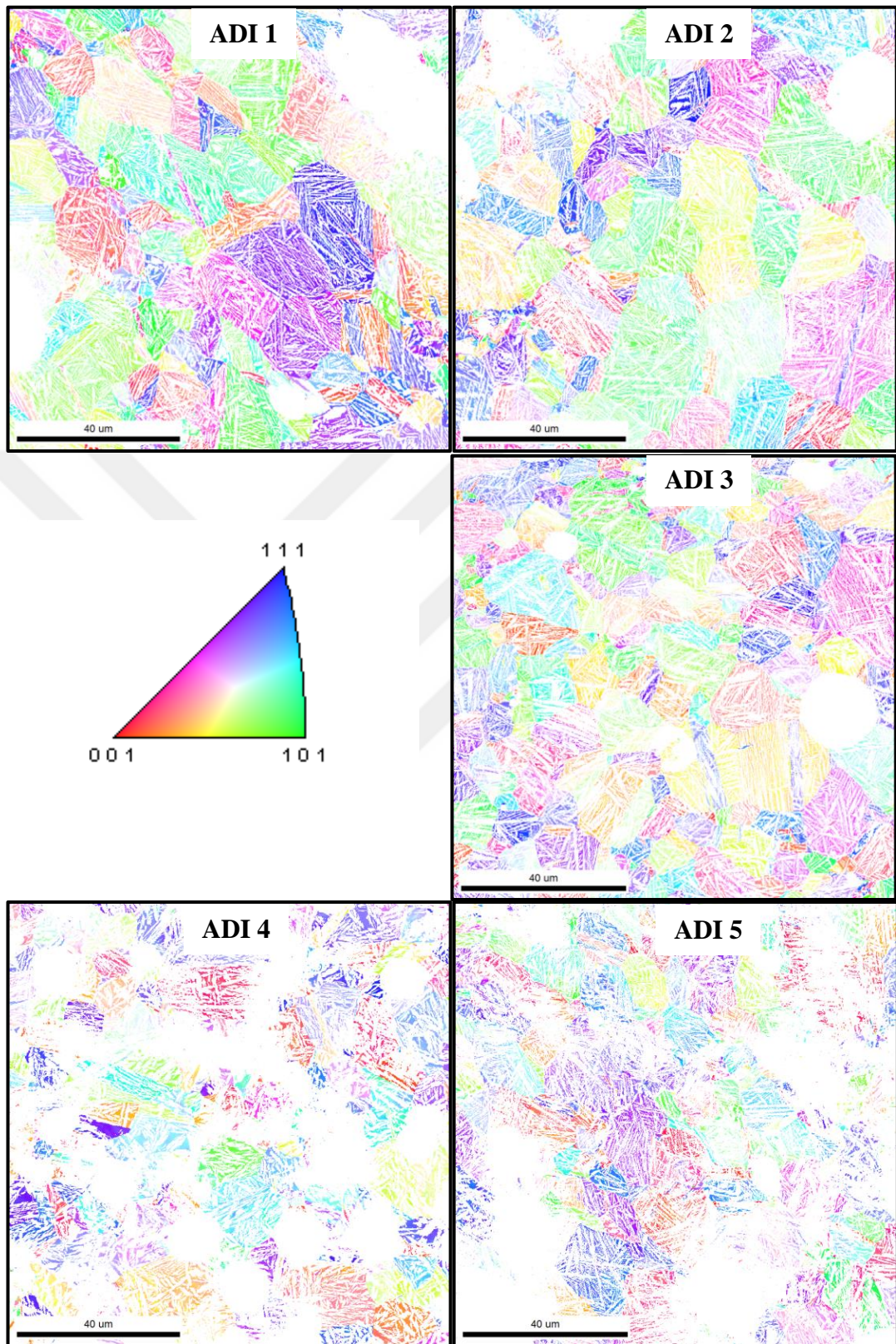


Figure 4.2-5 Inverse pole figure with respect to normal direction (IPF-ND) maps of FCC-indexed partition of ADI castings

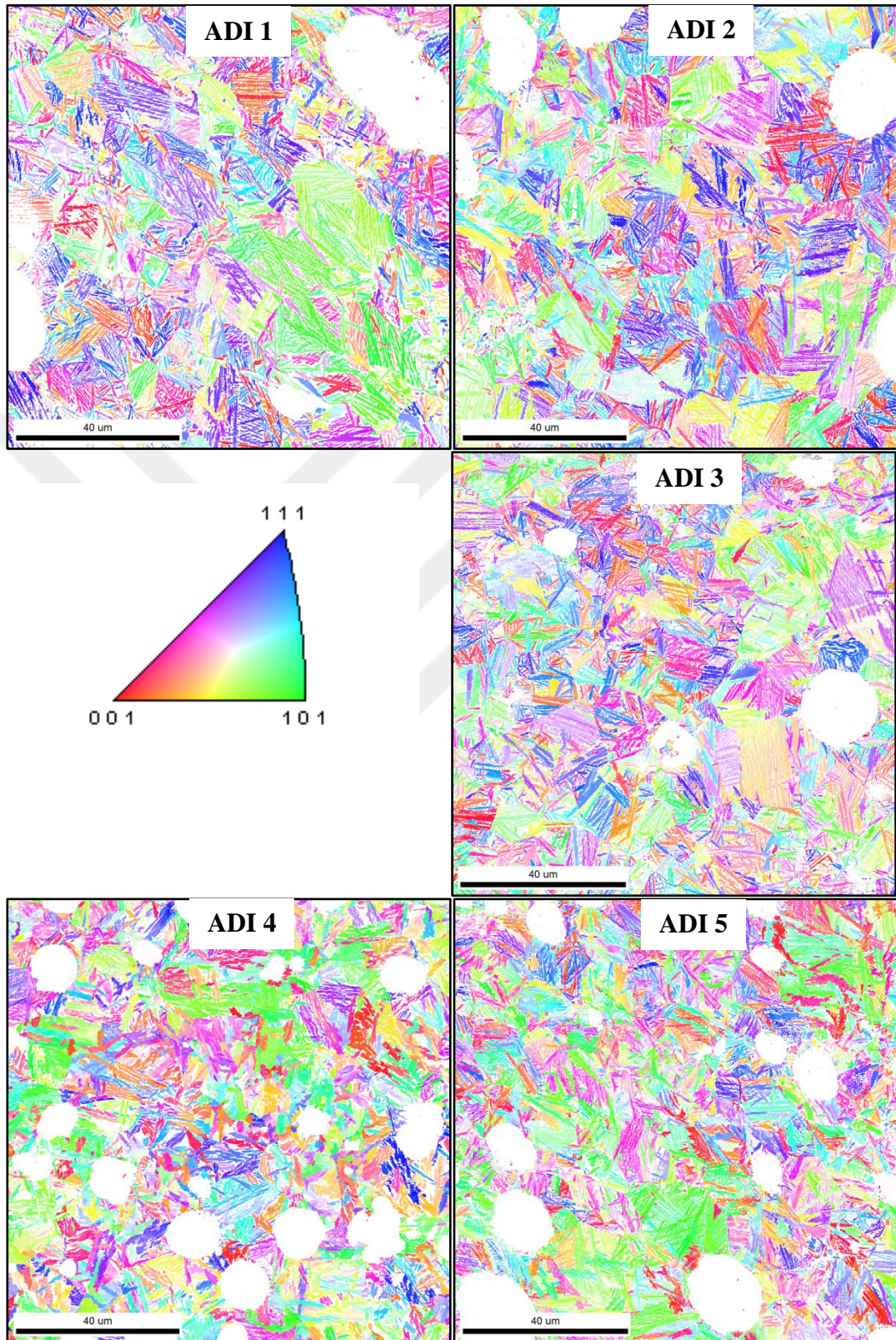


Figure 4.2-6 Inverse pole figure with respect to normal direction (IPF-ND) maps of BCC-indexed partition of ADI castings

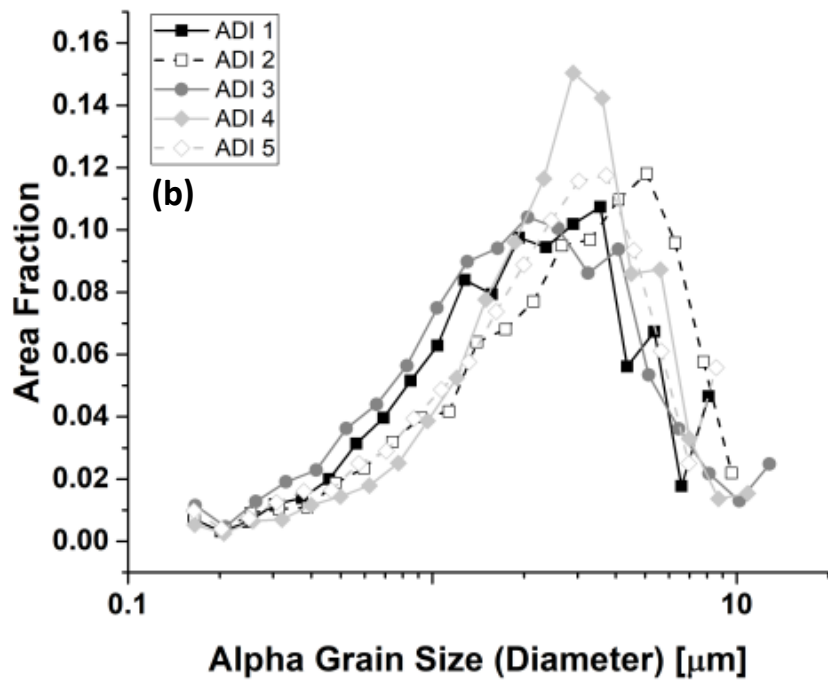
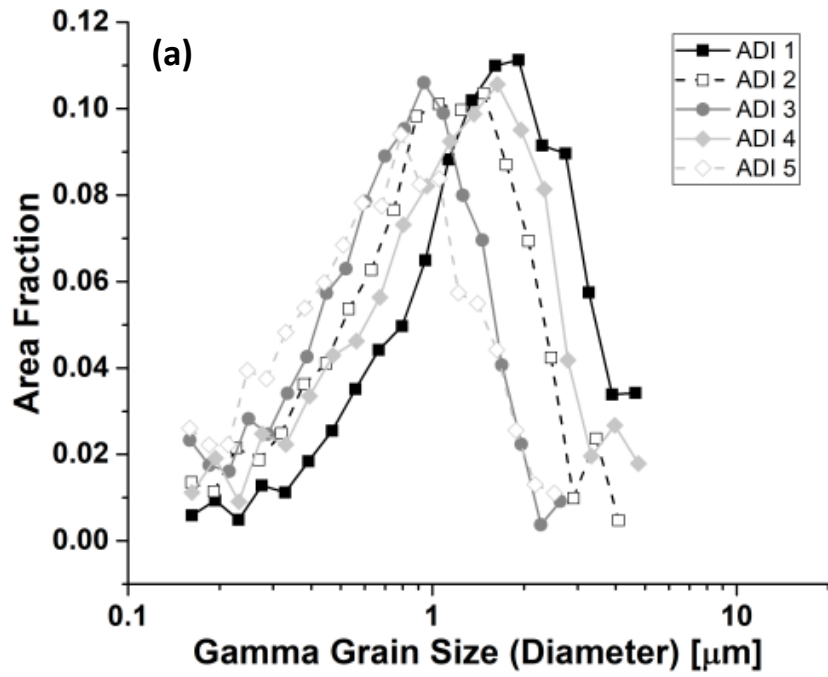


Figure 4.2.7 Area fraction comparisons of a) gamma and b) alpha grain sizes

It should be noted that the results of the present study are identical, if not better than previously reported results of similar ADI alloys. Eric et al. (2004) [33] and Shelton et al. [19] studied on alloys identical to ADI 4 and ADI 5 presented in this study. Shelton et al. [19] reported 650-780 MPa UTS values. In the present study those strength levels are reached with a cheaper, virtually un-alloyed ADI 1. The present ADI 5 alloy has higher strength and ductility compared to Shelton et al's [19]. On the other hand, the study of Eric et al.[29] reported higher yield and tensile strength, whereas much lower ductility. Similarly, Swain et al. [20] work indicates UTS and YS values nearly the same as present ADI 5 alloy but the present alloy has almost 3 times higher ductility. The present ADI 3 alloy has lower alloying but also exhibits better strength compared to Chinella et al. [31] study at identical ductility levels. The enhanced ductility of present alloys can be attributed to the higher retained austenite fraction, which is 10 to 15 times higher than the previously mentioned studies. Figure 4.2.8 compares the mechanical properties of ADI samples obtained from several different studies in literature to the results of the present study.

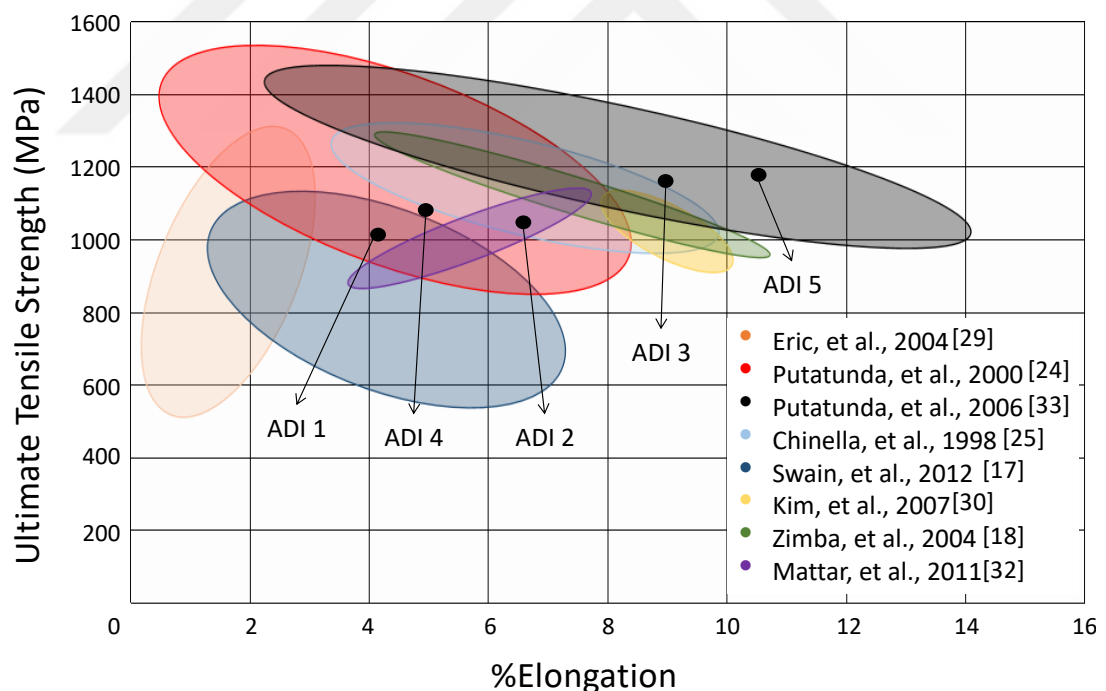


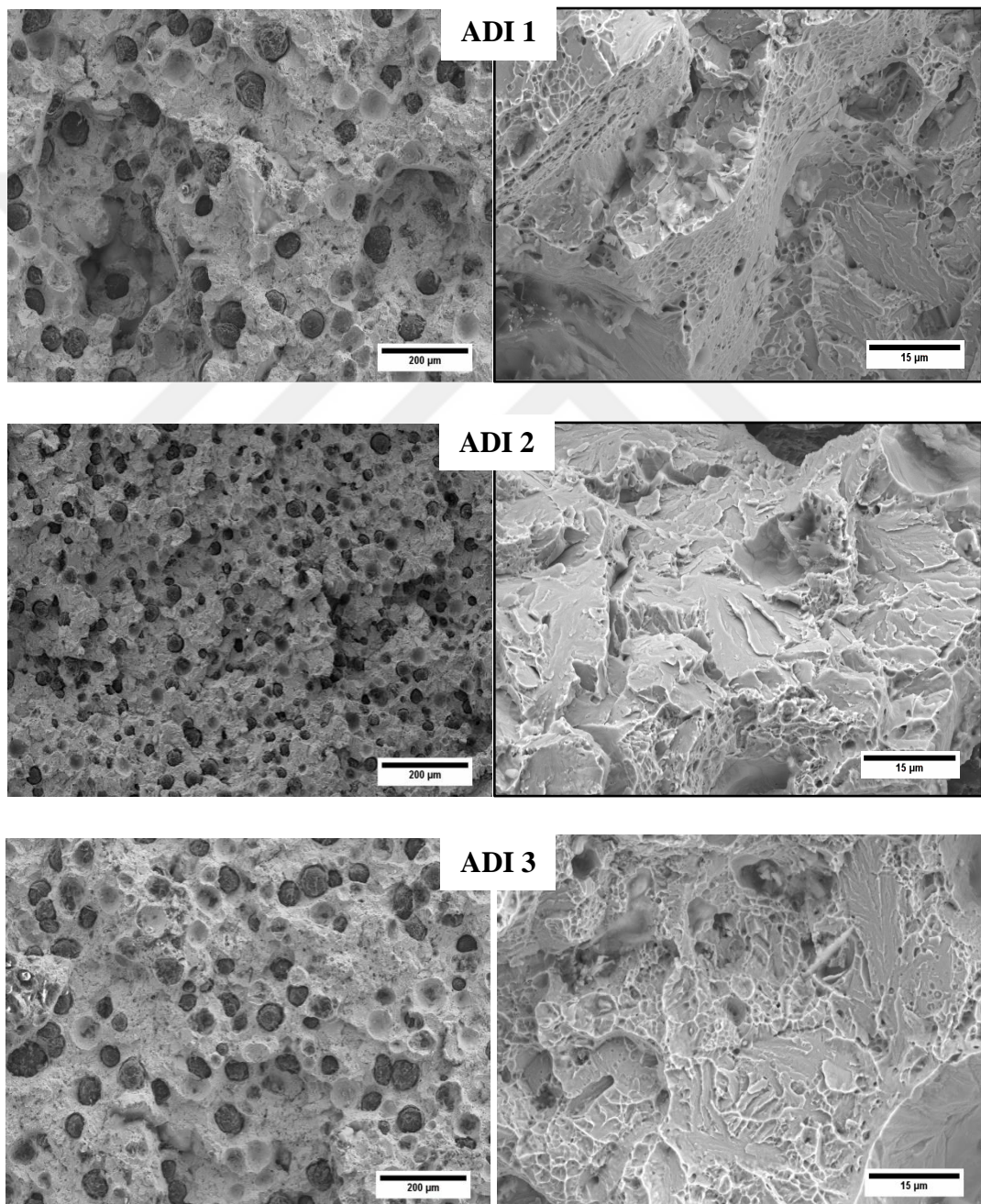
Figure 4.2.8 UTS vs. %Elongation comparison of several studies on ADI in literature and present study

Table 4.2-2 Comparison of microstructural parameters and mechanical properties of the ADI samples

Table of Results	ADI 1	ADI 2	ADI 3	ADI 4	ADI 5
	Lean - Low T_{aus}	Lean - High T_{aus}	Lean + Cu	Lean + High Mo	Lean + High Ni
Nodularity by Area	89.27%	88.82%	86.36%	86.08%	83.74%
Avg. size of Nodular G-particles (μm) (Nod-s)	47.47	41.07	35.31	27.45	27.91
Nodule density (nodules/mm²)	49.57	72.89	73.95	207.83	176.40
Avg. shape factor	0.62	0.63	0.64	0.67	0.67
Nodule area fraction (V_{nodule})	7.17%	9.06%	6.38%	10.26%	9.46%
G-particle area fraction	8.65%	10.18%	7.40%	11.95%	11.31%
Ret-γ fraction (V_γ)	41.1%	32.4%	32.5%	22.3%	20.5%
Ret-γ grain size (γ-GS)	1.74	1.18	0.85	1.42	0.79
α-phase fraction (V_α)	58.9%	67.6%	67.5%	77.7%	79.5%
α-phase grain size (α-GS)	2.62	3.38	2.78	3.07	2.95
Hardness (HV 0.2)	462 ± 83	478 ± 39	458 ± 82	375 ± 55	437 ± 93
UTS (MPa)	1004.0 ± 28.1	1022.6 ± 23.4	1158.0 ± 4.3	1080.6 ± 30.5	1182 ± 14.7
Yield Strength (MPa)	732.1	718.9	830.1	846.2	902.37
Total Elongation	4.2 ± 0.8	6.65 ± 1.16	9.0 ± 2.2	5.04 ± 1.21	10.5 ± 0.01

Finally; Table 4.2-2 shows that the most important factor that determines the mechanical properties is the matrix structure of ADI. The ADI 1 has the lowest elongation, tensile and yield strength; whereas it has the highest nodularity and ADI 5 has the highest elongation, tensile and yield strength; whereas it has the lowest nodularity. But as mentioned above and can be seen in table, nodularity values of all specimens are very close to each other. It seems small differences in nodularity values do not have significant effect on the matrix structure and not correlate with the mechanical properties.

The fracture surfaces of the specimens are shown in Figure 4.2.9. which reveals that all specimens have both brittle and ductile fracture zones indicating a mixed mode of fracture. The presence of martensite, specifically in the ADI 1 promotes brittle fracture, whereas specimens with finer ausferrite matrix exhibit more ductile behavior. The results of this fractographic examination agree well with the ductility (percent elongation) values listed in Table 4.2-2.



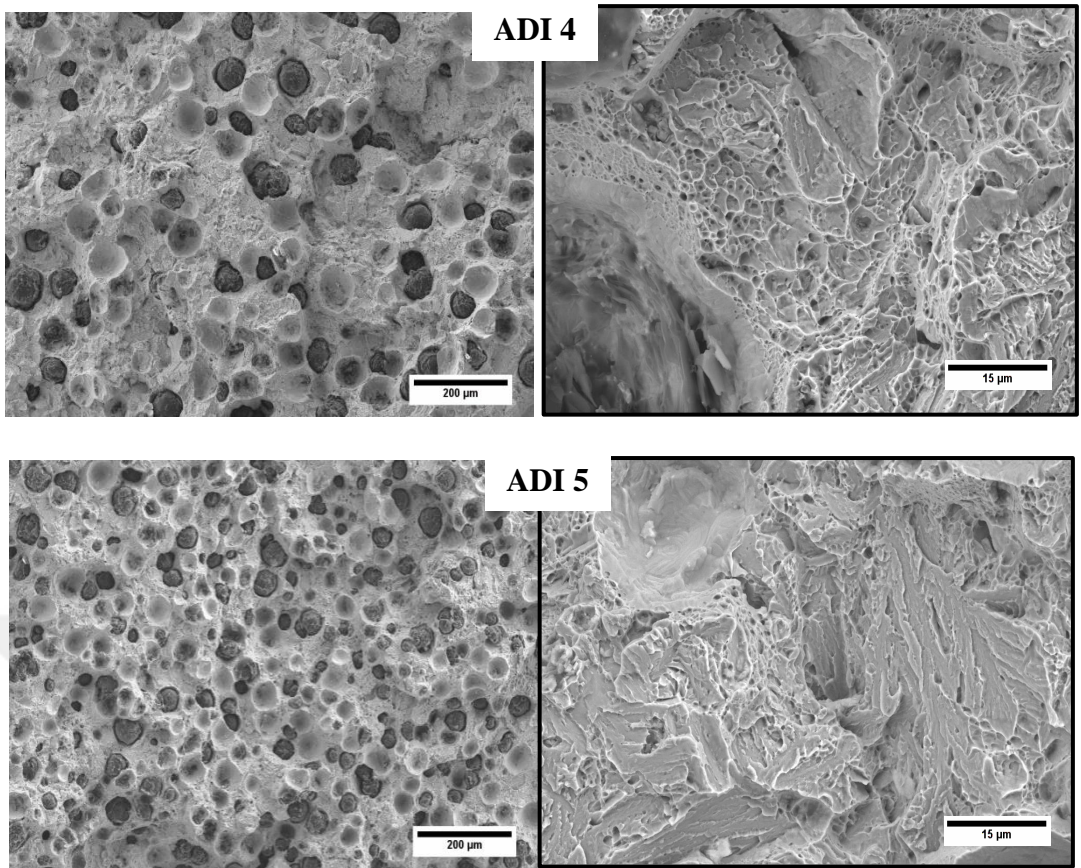


Figure 4.2-7 SEM images of fracture surfaces of ADI samples taken at 200x (left) and 3500x (right)

4.3. Reliability and Representativeness of EBSD Technique

The electron back-scatter diffraction (EBSD) technique is a convenient way to reveal the multi-phase nature of materials in a quantitative manner and to distinguish the phases. However, statistical reliability of EBSD is questioned since its interaction volume is rather small when compared to XRD. Because of that, especially for materials which have heterogenous microstructure EBSD results could be inconsistent [77].

For the present case of ADI, the microstructure is heterogeneous since it is first produced by a conventional casting process. Graphite floatation or alloy segregation, just to name a very possible problems, would definitely cause a difference between center and near the surface microstructures of castings.

In addition to that, artifacts caused by specimen preparation can also lead to errors. During grinding and mechanical polishing steps of metallographic specimen preparation, retained austenite can transform into martensite. Moreover, retained austenite can also transform during the hot-mounting process. Because of the alloying additions to enhance austemperability, martensite start (M_s) temperature of the specimens drop to temperatures lower than 200 °C. Since typical hot mounting temperatures are around 180 °C, microstructure of the specimen may change (i.e. austenite can transform into martensite) during cooling of the hot-mount that the specimen has been recently embedded into.

All of the above mentioned aspects can cause variations and errors in the measurement of retained austenite content via EBSD. In order to check the representativeness of the EBSD technique, repeatative measurements were performed. Moreover, in order to check the influence of hot mounting, another set of ADI 1 and 5 samples were prepared using cold-mounting. Figures 4.3.1 and 4.3.2 show the comparison of phase fractions of acicular ferrite and high carbon stable retain austenite. Figures 4.3.3 and 4.3.4 shows all of the phase maps taken for ADI 1 and ADI 5, respectively. The reason of selecting this samples is because ADI 1 has the lowest and ADI 5 has the highest amount of alloying additions.

EBSD results obtained from 4 different randomly selected areas are nearly identical. Also the results of specimens prepared by hot mounting and cold mounting show very little differences in austenite fractions. It should also be noted that the Figure(s) 4.3.3 and 4.3.4 indicate that retained austenite grains are not distributed homogeneously over the measured area. Nevertheless, an EBSD measurement over 100 x 100 micron sized area gives consistent, representative and repeatable retained austenite fraction values.

The results of ADI 5 specimen, given in Fig 4.3.4 shows EBSD results of 3 hot and 2 cold mounted specimens, all of which gives almost the same retained austenite fraction. This indicates that EBSD gives repeatable retained austenite fractions, i.e. high precision measurements. However, the technique might have a systematic error causing its accuracy to be low. In order to understand the accuracy of EBSD measurements, one of the ADI-5 specimen's retained austenite fraction was measured via X-ray diffraction (XRD). XRD technique is more commonly used in earlier studies and considered to be a *standard technique*. Retained austenite fractions obtained via EBSD are compared to the XRD-based results in Fig 4.3.3. EBSD and XRD based retained austenite fractions are almost the same, the differences between these two are lower than the variation in the sample itself. Therefore, it is concluded that EBSD-based results of the present study are as reliable and accurate as XRD-based results.

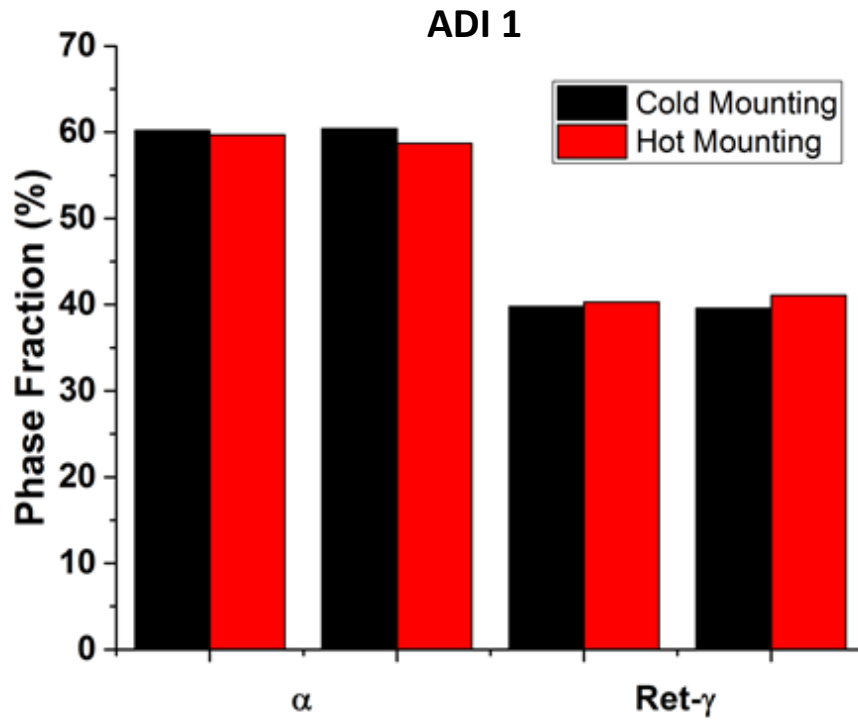


Figure 4.3-1 Comparison of effect of hot mounting and cold mounting to the alpha and gamma phase fractions on ADI 1

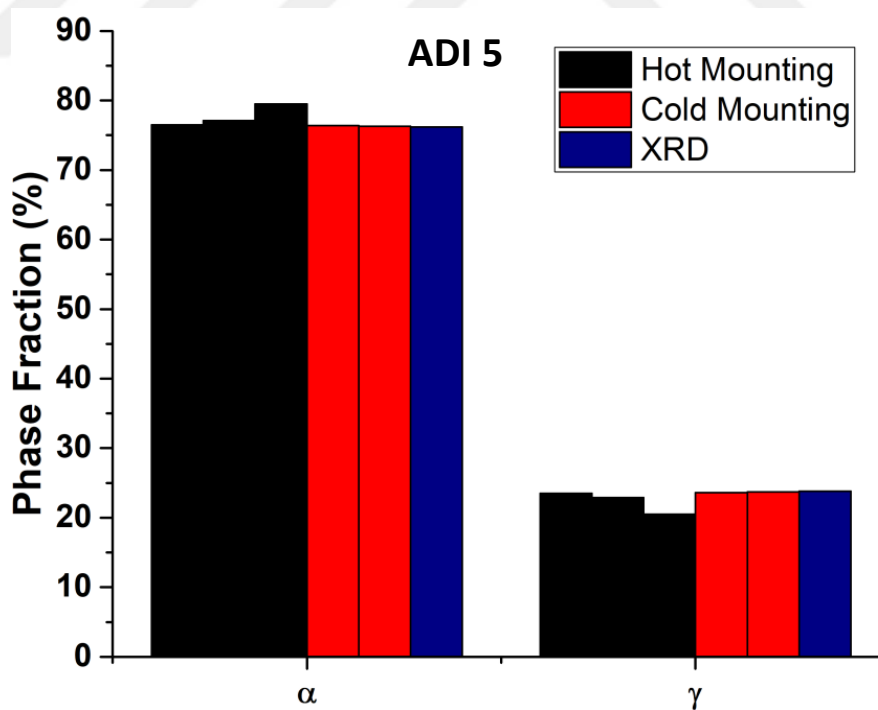


Figure 4.3-2 Comparison of EBSD and XRD results of alpha and gamma phase fractions on ADI 5

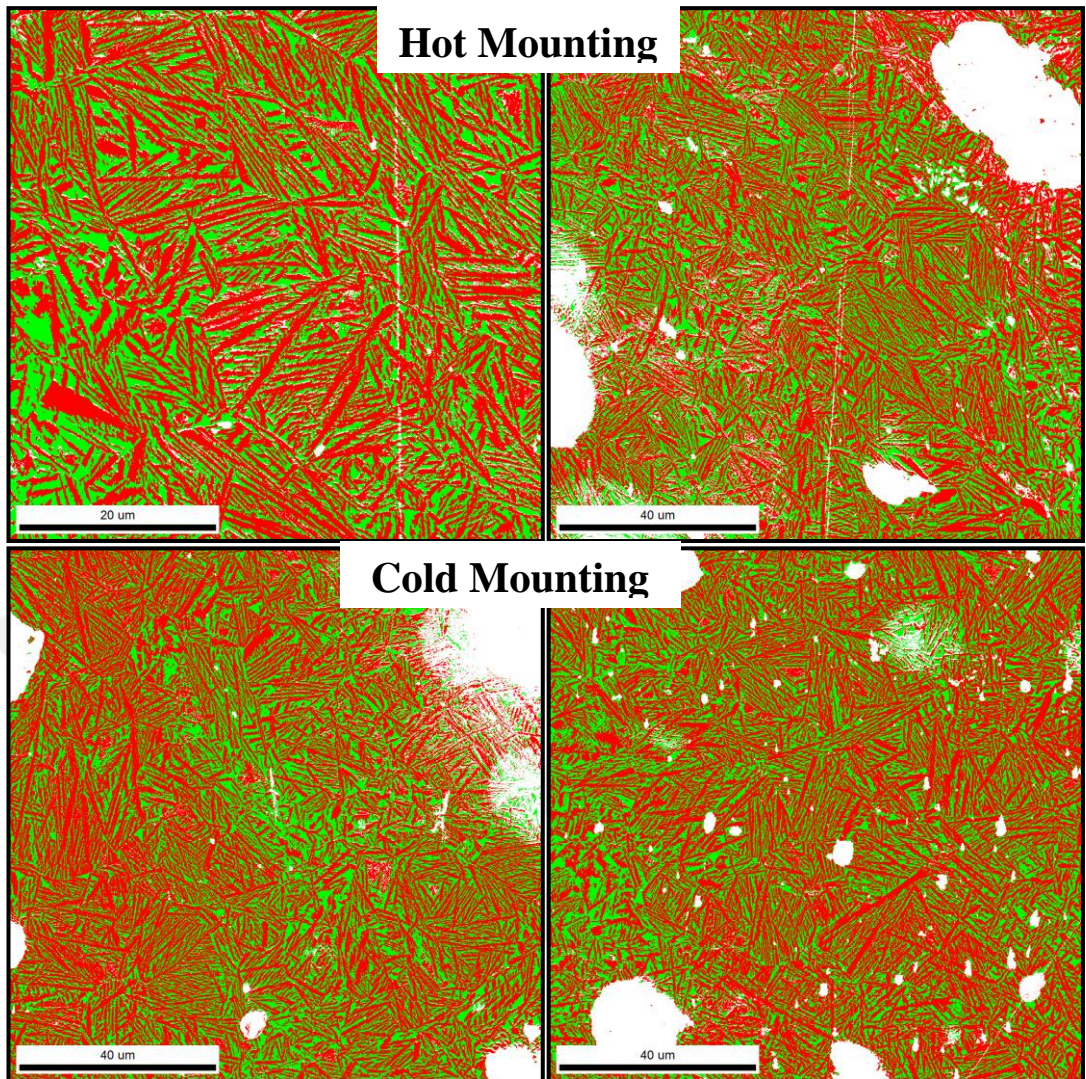


Figure 4.3-3 EBSD phase maps of the ADI 1 (Lean Alloy)

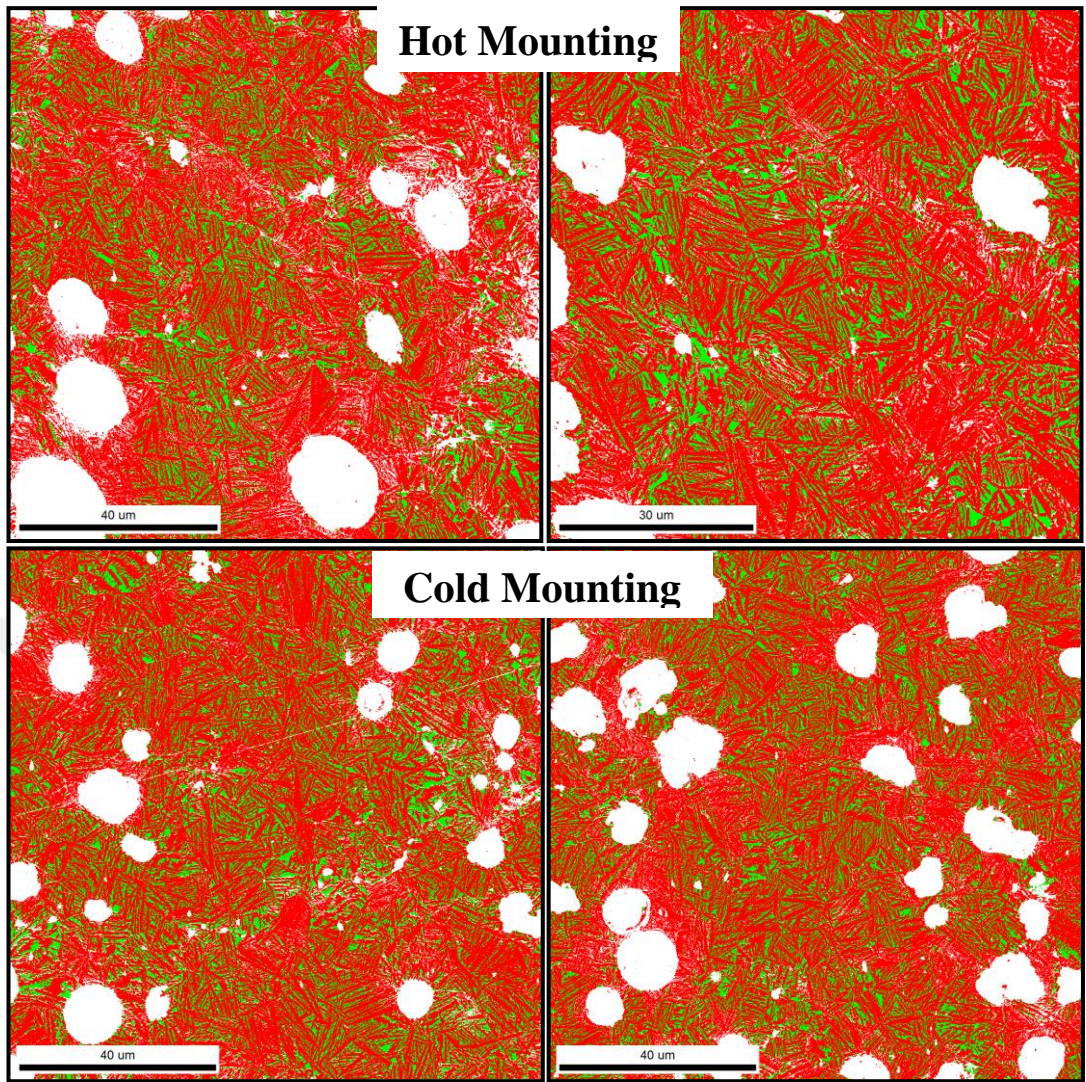


Figure 4.3-4 EBSD phase maps of the ADI 5 (Lean + High Ni)

4.4. Correlation between Microstructural Parameters and Mechanical Properties

The influence of alloying and austempering treatment parameters on mechanical properties have been explained in section 4.2. Moreover, a detailed analysis of volume fraction, size and morphology of graphite particles has also been presented in section 4.1. In this section the correlations between those microstructural parameters and mechanical properties will be presented. Moreover, the correlations in-between microstructural parameters will also be discussed. These correlations are quantified by calculating the “Pearson Correlation Coefficient (PCC)”.

In statistics, the “Pearson Correlation Coefficient” is a measure of the linear correlation between two variables with the indication of strength and direction of the relationships. Result of the correlation has a value between +1 and -1, where 1 is total positive linear correlation, 0 is no linear correlation, and -1 is total negative linear correlation [78]. The PCC is calculated by the following equation:

$$\text{Correl}(X, Y) = \frac{\sum(x-\bar{x})(y-\bar{y})}{\sqrt{\sum(x-\bar{x})^2 \sum(y-\bar{y})^2}} \quad (10)$$

Here x and y are the each results and \bar{x} and \bar{y} are the mean values of the results of properties that to be correlated.

Using **equation-10** the PCC between all of the values listed in Table 4.2-2 has been calculated and shown in Table 4.4-1. This table shows correlations in-between microstructural parameters, in-between mechanical properties and also between microstructural parameters and mechanical properties.

Table 4.2-2 shows that some of the microstructural parameters are directly related to each other; in other words those parameters are not independent. Those parameters have been highlighted in Table 4.2-2.

Nodule density and nodule size, both have a negative correlation with **nodularity by area** which means as nodularity by area increases, nodule size and nodule density decreases. The correlations between nodule size, nodule density and nodularity by area values have been shown also in Figure 4.4-1. A relationship between nodule size and nodule density is simple since number of nodular graphites per mm^2 increases

with the decreasing nodule size. ADI 4 and ADI 5 which have nickel and molybdenum as alloying elements, have the worst nodularity by area values. On the other hand those 2 samples have the smallest nodule size and the largest nodule density. Although, ADI 4 and ADI 5 samples have smaller nodularity by area values than ADI 1, ADI 2 and ADI 3 samples, the results are very close to each other. Results indicate that, high alloying additions seems to have a stronger effect on nodule size and density rather than the nodularity values. It should also be noted that the nodularity by area values of the present ADI samples are very high, all values are above 83% and the difference between those values are lower than 6%. Therefore, the high correlation between nodularity and nodule size ($PCC = -0.8985$); and also between nodularity and nodule density ($PCC = -0.7578$) could be specific only to the present set of samples. To understand those correlations better, another set of samples that have a wider range of “nodularity by area” values should be studied. Moreover, foundary practices, process parameters during production of as-cast Y-blocks determine the nodule count and nodularity values. Lower pouring temperature, higher cooling rate or differences in inoculation and Mg-treatment may be the reason of high nodule count of ADI 4 and ADI 5 [79].

The volume fraction of alpha and gamma phases are inversely proportional; since their total fraction is equal to the the volume fraction of the matrix. Moreover, there is a moderate correlation ($PCC = 0.6790$) between volume fraction of alpha phases and volume fraction of graphite nodules; an excellent correlation between nodularity by area and volume fraction of alpha phases ($PCC = 0.9085$) Those relations can be attributed to the proportion of alloying elements, whose influence has been mentioned previously.

Table 4.4-1 Correlation between microstructural parameters and mechanical properties

	$1/\sqrt{(\alpha-GS)}$	$1/\sqrt{(\gamma-GS)}$	V_{α}	V_{γ}	V_{nodule}	$1/\sqrt{(Nod-s)}$	Nodule density	Nodularity (by Area)	Yield Strength	UTS	Total elongation	Hardness
$1/\sqrt{(\alpha-GS)}$	1											
$1/\sqrt{(\gamma-GS)}$	-0,1456	1										
V_{α}	-0,4353	0,5822	1									
V_{γ}	0,5124	-0,4816	-0,9890	1								
V_{nodule}	-0,7028	-0,0728	0,6790	-0,7799	1							
$1/\sqrt{(Nod-s)}$	-0,2979	0,4753	0,9753	-0,9604	0,6415	1						
Nodule density	-0,3354	0,1965	0,9047	-0,9338	0,8080	0,9460	1					
Nodularity (by Area)	0,0790	-0,7412	-0,9085	0,8489	-0,3700	-0,8985	-0,7578	1				
Yield Strength	0,0434	0,6587	0,8744	-0,8092	0,3172	0,9047	0,7725	-0,9833	1			
UTS	0,0617	0,8996	0,7311	-0,6249	0,0081	0,7112	0,4650	-0,9160	0,9006	1		
Total elongation	-0,1304	0,9915	0,5752	-0,4811	-0,0458	0,4582	0,1976	-0,7483	0,6563	0,8833	1	
Hardness	0,0878	0,1507	-0,6438	0,6741	-0,6232	-0,7783	-0,8774	0,4937	-0,5878	-0,2267	0,1814	1

correlations in-between microstructural parameters
 correlations between microstructural parameters and mechanical properties
 correlations in-between mechanical properties

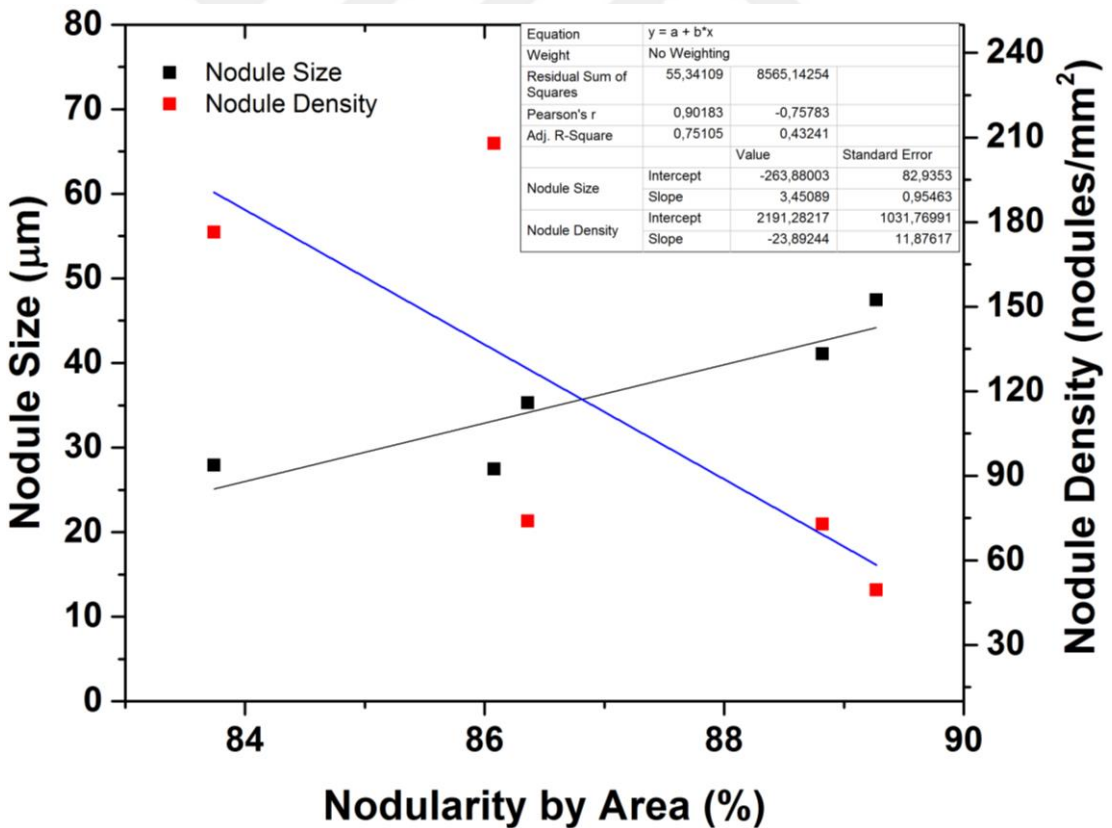


Figure 4.4-1 Correlation between nodularity by area and nodule density and nodule size

Regarding the correlations in-between mechanical properties; there is a positive correlation between strength (both yield and UTS) and ductility (%elongation) values. This means, improving strength improves ductility as well; for the present set of ADI samples. In more conventional ferrous alloys, strength and ductility are inversely proportional. This indicates a very important aspect of ADI, its strengthening mechanism does not decrease the ductility. Only grain refinement and TRIP effect can improve strength without sacrificing ductility. More detailed analysis of a set of samples deformed to varying strain levels or in-situ measurement of retained austenite during deformation can be utilized to prove the presence of TRIP effect.

Figures 4.4.2. and 4.4.3 show that there is Hall-Petch like relation between grain size of retained austenite and yield strength, UTS and total elongation. As mentioned above decreasing the grain size of retained austenite improves both strength and ductility, in accordance with the Hall-Petch relation. Finer austenite grains are mostly film type- γ (Figure 4.2.5) found between platelet like ferritic structure. Coarser austenite grains are mostly parent austenite grains that are not transformed during the austempering treatment. Samples with higher alloying additions have finer austenite grains. This can be attributed to prior austenite grain size and ausferrite transformation kinetics. IPF-ND maps (Fig 4.2.5 and 4.2.6) also shows the prior austenite structure, ausferrite regions originating from the same parent austenite are seen in same colour, indicating a variant selection mechanism. Since samples with higher alloy additions (ADI 3, 4 and 5) have finer parent austenite structure, their product ausferritic structure, specifically the high-C retained austenite regions are also finer. Moreover, during austempering formation of platelet like ferritic regions pumps carbon into the remaining parent austenite. When the parent austenite is finer, it can be stabilized better with C-enrichment, since lesser diffusion distances are needed. On the other hand, when parent austenite grain is coarser, longer diffusion distances are needed. When all of the alloys are austempered at the same time-temperature combination; the coarser parent austenite grains would then have less C; which in turn reduce their stability. Because of this size effect, longer diffusion distances are required for complete austempering of ADI 1 and ADI 2 alloys. Therefore, those alloys contain more block-type untransformed austenite, which has a lower stability.

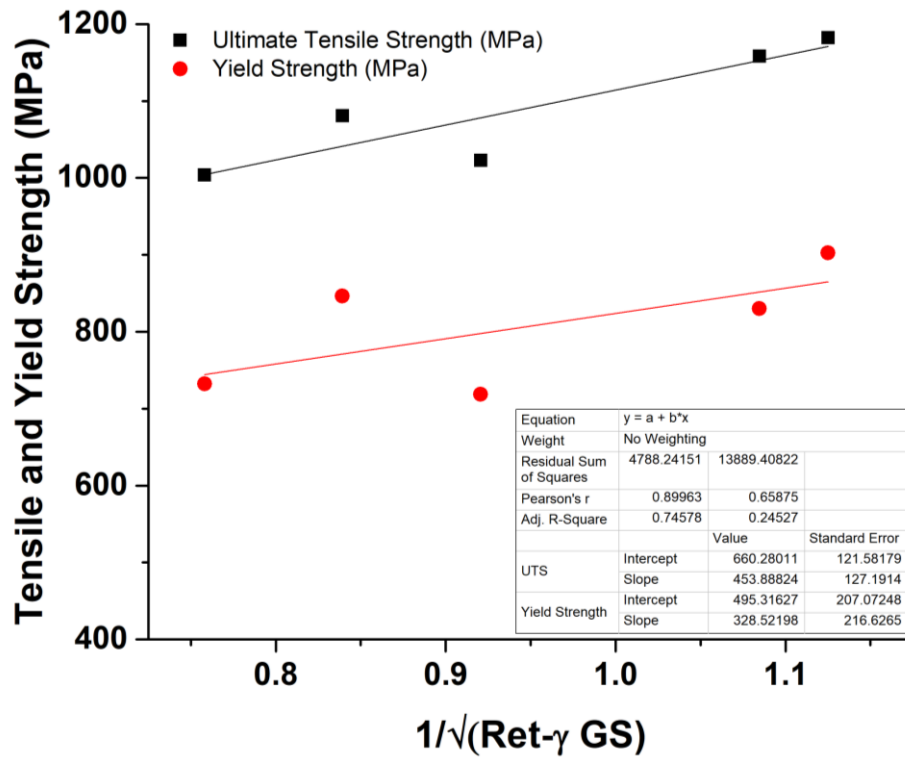


Figure 4.4-2 Correlation between retained austenite grain size and yield strength and UTS

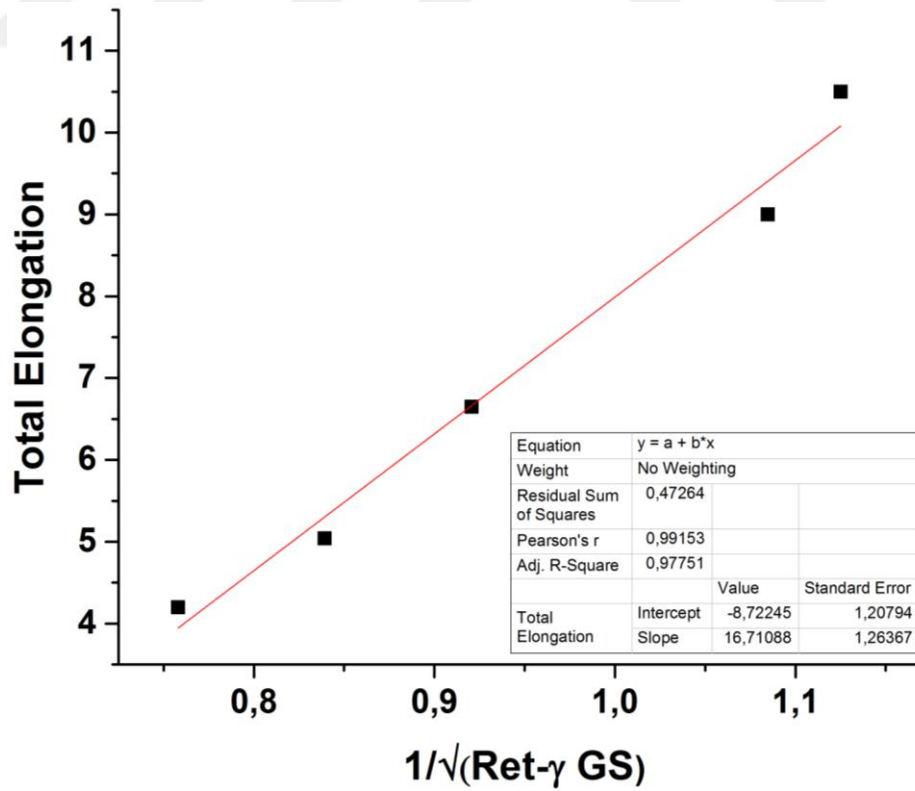


Figure 4.4-3 Correlation between retained austenite grain size and total elongation

Table 4.4-1 also shows that volume fraction of retained austenite also have a negative correlation with yield strength, UTS and total elongation. This is another implication of aforementioned TRIP effect.

The “Pearson Correlation Coefficient between austenite grain size and mechanical properties reach up to a value of 0.9915, for the case of total elongation. On the other hand the PCC values between grain size of acicular ferrite and mechanical properties are very low (between 0.0434 to 0.1304); meaning those parameters are unrelated. The acicular ferritic structure of the present ADI samples have almost the same size, the differences in average grain size are lower than 0.7 μm . This indicates that regardless of alloying, the acicular ferritic structure in present ADI samples have very similar grain sizes

Other notable relationships that draw attention is the ones between yield strength, nodule size and ferrite volume fraction in the Table 4.4-1. As mentioned above, like volume fraction of retained austenite yield strength is highly dependent on volume fraction of acicular ferrites. In addition to that volume fraction of acicular ferrite seems highly dependent on nodule size. The reason behind this relationship is decreasing nodule size increases nodule count and causes production of a finer, more uniform ausferrite structure [6]. This means retained austenite in structure transforms into acicular ferrite platelets and increase in volume fraction of ferrite is observed. Finer ausferritic structure leads to better yield strength values. Relationships of yield strength/nodule size and alpha phase fraction/nodule size can be seen in Figures 4.4.4 and 4.4.5, respectively.

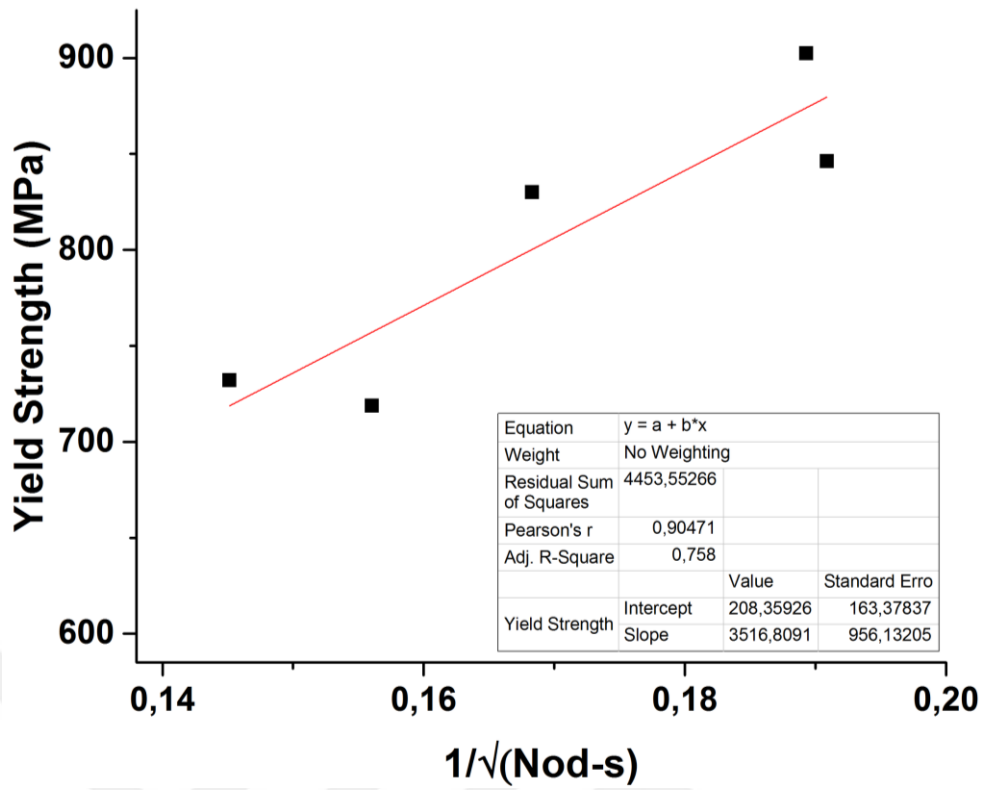


Figure 4.4-4 Correlation between nodule size and yield strength

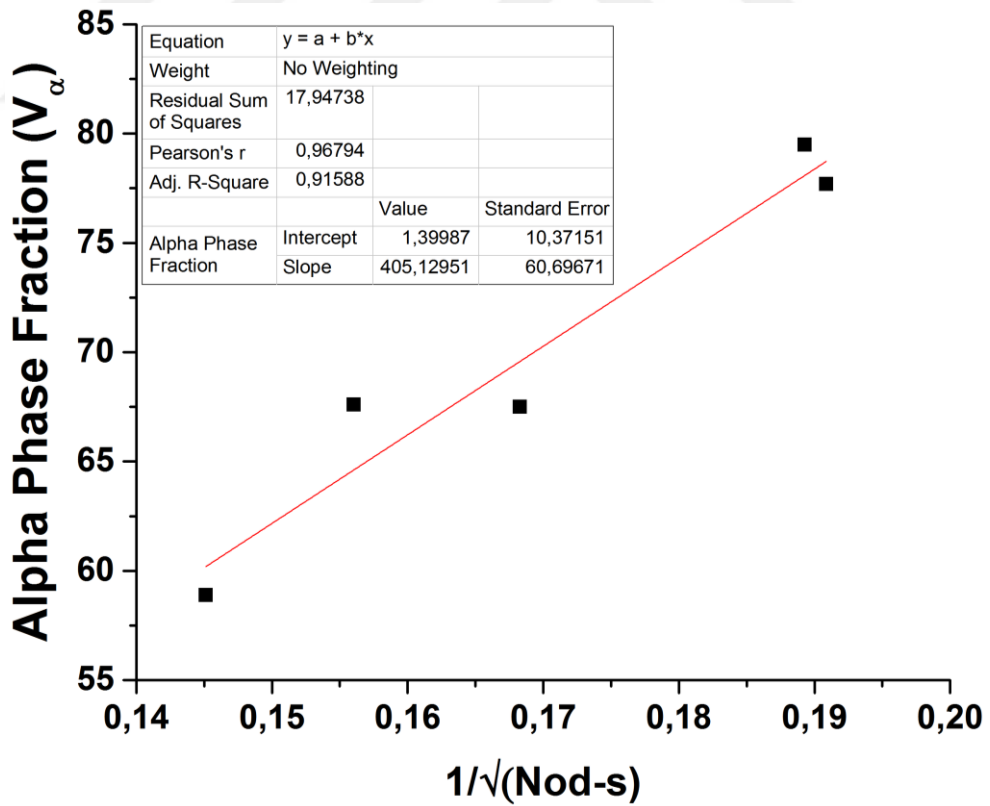


Figure 4.4-5 Correlation between nodule size and alpha phase fraction

To summarize, the volume fraction and grain size of retained austenite, as well as the size of graphite particles influence the strength and ductility of the present ADI samples. For the present set of samples the nodule density, volume fraction of nodules and nodularity values are not independent microstructural variables; those parameters are also correlated to the size of graphite particles.

It should also be noted that the here presented PCC values are valid only for the present set of samples. For the present set, the differences between nodularity and alpha grain size values are not significant. In order to understand and quantify the influence of nodularity, another set of specimens having a wider range of graphite nodularity should be studied. Nevertheless, the present study shows the importance of retained austenite grain size on mechanical properties.

CHAPTER 5

CONCLUSIONS

A multi-scale microstructure analysis has been performed on Austempered Ductile Iron (ADI) samples having various different compositions and austempering conditions. Afterwards, the microstructural parameters including the size and morphology of graphite particles as well as the matrix microstructure has been correlated to the mechanical properties. The following conclusions were drawn:

- Nodularity (by area), nodule density and nodule size are not independent properties; due to the casting process. For the present case, nodule size influences yield strength and UTS; whereas nodularity of graphite particles has no significant influence on mechanical properties beyond 83%. Copper, nickel and molybdenum additions refine the graphite particles, increase the nodule count and hence improve strength and ductility. For alloys having identical matrix hardness (difference < 10%), refining the nodular graphite particles by 20.5% improves the strength 2.1% only.
- Austempering treatment does not change the size or nodularity values of the samples.
- The matrix microstructure plays a more important role for determining mechanical properties. Fineness of acicular ausferritic structure, particularly the grain size of retained austenite have almost a perfect (up to 0.99 PCC) Petch-like correlation with yield strength, UTS and elongation.
- Alloying additions as well as austempering temperature influence the fineness of the microstructure. Lean alloy with higher austempering temperature has the coarsest acicular alpha structure. Lean alloy also has the coarsest austenite structure. For the lean alloy; Cu addition rather than increasing austempering temperature has more significant effect on mechanical properties of ADI. For

the samples with higher alloying additions; Ni addition has the most significant influence on the strength, ductility and hardness of the ADI

- The higher the alloy content, the finer the austenite structure. EBSD measurements reveal two types of austenite: i) film type between acicular ferrite and ii) blocky type around prior austenite grains. This room temperature microstructure is a transformation product of a prior austenitic structure, which forms during the austenitization step of austempering treatment. Prior austenite grains that are not transformed into ausferrite during austempering gives rise to blocky type; and hence increases the average grain size. Those large austenite grains are not stabilized well with carbon; due to the limited diffusion distances at austempering temperatures. Increasing alloying additions also refine the prior austenite grain structure (PAGS). Increasing T_{aus} also coarsens PAGS, although its effect is less significant than alloying additions.
- EBSD investigations reveal that acicular ferrite grains originating from the same parent- γ have almost the same orientation, indicating a variant selection mechanism for the formation of ausferritic structure. In addition, there is no significant difference between the grain size of acicular ferrite grains of the present set of ADI samples.
- For the present set of ADI samples, the ones with higher strength also exhibit higher ductility. This indicates a very important aspect of ADI, its strengthening mechanism(s) do(es) not decrease ductility. Therefore; the strengthening of ADI can be attributed to refinement of its microstructure and also to the TRIP effect. Moreover; retained austenite fraction (after tensile testing) correlates to yield strength, UTS and ductility negatively; which is another implication of TRIP effect. Nevertheless, additional experiments should be performed to prove the presence of this effect.

The present study shows that, even in conventional materials such as ADI, a multi-scale approach is required to fully understand and correlate the mechanical properties resulting from the aforementioned specific microstructure. The influence of Cu, Ni and Mo additions on mechanical properties has been shown. The combined effect of size, fraction and morphology of nodular graphite particles as well as the size, fraction of matrix phases on mechanical properties have been shown, for the first time. The calculated Pearson Correlation Coefficients (PCC) show that the most important microstructural parameters on strength and ductility of present set of ADI samples are size of graphite particles, volume fraction and grain size of retained austenite. It should be noted that some microstructural parameters of the present set are not independent and the here shown PCC values are only valid for the present set of samples. Nevertheless these results should provide a useful basis for further development and improvement of “austempered ductile irons”.

For future studies, another set of ADI samples having a wider range of graphite nodularity should be studied in order to quantify the influence of graphite nodularity on mechanical properties. After identifying the independent microstructural parameters a multi-linear regression analysis can be performed to quantify the relative importance of each microstructural parameter. Furthermore, monitoring the change in retained austenite fraction during deformation, preferably by in-situ tests can also prove the presence of TRIP effect directly.

REFERENCES

- [1] B. Cetin, H. Meco, K. Davut, E. Arslan, and M. C. Uzun, "Microstructural Analysis of Austempered Ductile Iron Castings," *Hittite J. Sci. Eng.*, vol. 3, no. 1, pp. 29–34, 2016.
- [2] J. R. Keough, K. L. Hayrynen, and G. L. Pioszak, "Designing with Austempered Ductile Iron (ADI)," *Trans. Am. Foundry Soc.*, vol. 118, no. 10–129, pp. 503–517, 2010.
- [3] "ASTM A536-84(2019)e1, Standard Specification for Ductile Iron Castings," West Conshohocken, PA, 2019.
- [4] "ASTM A897 / A897M-16, Standard Specification for Austempered Ductile Iron Castings," West Conshohocken, PA, 2016.
- [5] R. A. Harding, "The production , properties and automotive applications of austempered ductile iron," *Kov. Mater.*, vol. 45, no. 1, pp. 1–16, 2007.
- [6] J. Liu and R. Elliott, "The influence of cast structure on the austempering of ductile iron. Part 3. the role of nodule count on the kinetics, microstructure and mechanical properties of austempered Mn alloyed ductile iron," *Int. J. Cast Met. Res.*, vol. 12, no. 3, pp. 189–195, 1999.
- [7] R. C. Voigt, "Austempered Ductile Iron—Processing and Properties," *Cast Met.*, vol. 2, no. 2, pp. 71–93, 1989.
- [8] K. L. Hayrynen, "The Production of Austempered Ductile Iron (ADI)," *World Conf. ADI*, 2002.
- [9] J. S. Santner and G. M. Goodrich, "Engineering Casting Solution," *Cast. Source Dir.*, pp. 17–22, 2006.
- [10] A. G. Fuller, "Austempered Ductile Irons- Present Applicationst," *Mater. Des.*, vol. 6, no. 3, pp. 127–130, 1985.
- [11] P. A. Blackmore, "The Effects of Metallurgical Process Variables on the Properties of Austempered Ductile Irons," *J. Heat Treat.*, vol. 3, no. 4, pp.

310–325, 1984.

- [12] A. Nofal, “Advances in the Metallurgy and Applications of ADI,” *J. Metall. Eng.*, vol. 2, no. 1, pp. 1–18, 2013.
- [13] E. S. Davenport and E. C. Bain, “Transformation of Austenite at Constant Subcritical Temperatures,” in *Transformation of Austenite at Constant Subcritical Temperatures*, 1930, vol. 1.
- [14] K. L. Hayrynen and J. R. Keough, “Austempered Ductile Iron-The State of the Industry in 2003,” in *2003 Keith D. Mills Symposium on Ductile Iron*, 2003.
- [15] M. Johansson, A. Vesanen, and H. Retting, “Austenitisch-bainitisches Gusseisen mit Kugelgraphit fuer Getriebe,” *Tech. Rupperswil*, vol. 29, no. 1, pp. 51–55, 1980.
- [16] Z. Yicheng, “Hypoid Pinion and Ring Gears of Bainitic Nodular Iron with Shell-Moulded Cast Teeth,” *Giesseri*, vol. 68, no. 8, pp. 206–216, 1980.
- [17] S. K. Putatunda, S. Kesani, R. Tackett, and G. Lawes, “Development of austenite free ADI (austempered ductile cast iron),” *Mater. Sci. Eng. A*, vol. 435–436, pp. 112–122, 2006.
- [18] A. Refaey and N. Fatahalla, “Effect of microstructure on properties of ADI and low alloyed ductile iron,” *J. Mater. Sci.*, vol. 38, no. 2, pp. 351–362, 2003.
- [19] P. W. Shelton and A. A. Bonner, “The effect of copper additions to the mechanical properties of austempered ductile iron (ADI),” *J. Mater. Process. Technol.*, vol. 173, no. 3, pp. 269–274, 2006.
- [20] S. K. Swain and S. Sen, “Effect of austempering variables on the mechanical properties of spheroidal graphite iron,” *Int. J. Curr. Res.*, vol. 4, no. 6, pp. 72–76, 2012.
- [21] J. Zimba, D. J. Simbi, and E. Navara, “Austempered ductile iron: An alternative material for earth moving components,” *Cem. Concr. Compos.*, vol. 25, no. 6, pp. 643–649, 2003.
- [22] S. Yazdani and R. Elliott, “Influence of molybdenum on austempering behaviour of ductile iron. Part 1 - Austempering kinetics and mechanical

- properties of ductile iron containing 0.13%Mo,” *Mater. Sci. Technol.*, vol. 15, no. 5, 1999.
- [23] J. Yang and S. K. Putatunda, “Improvement in strength and toughness of austempered ductile cast iron by a novel two-step austempering process,” *Mater. Des.*, vol. 25, no. 3, pp. 219–230, 2004.
- [24] J. ARanzabal, I. Gutierrez, J. M. Rodriguez-Ibabe, and J. J. Urcola, “Influence of the amount and morphology of retained austenite on the mechanical properties of an austempered ductile iron,” *Metall. Mater. Trans. A*, vol. 28, no. 5, pp. 1143–1156, 1997.
- [25] R. C. Voigt and C. R. Loper, “Austempered Ductile Iron Process Control and Quality Assurance,” *J. Heat Treat.*, vol. 3, no. 4, pp. 291–309, 1984.
- [26] D. S. Padan, “Microalloying in Austempered Ductile Iron (ADI),” *Trans. Am. Foundry Soc.*, vol. 120, no. 12–019, pp. 277–288, 2012.
- [27] S. K. Putatunda, “Development of austempered ductile cast iron (ADI) with simultaneous high yield strength and fracture toughness by a novel two-step austempering process,” *Mater. Sci. Eng. A*, vol. 315, no. 1–2, pp. 70–80, 2001.
- [28] S. K. Putatunda, “Influence of austempering temperature on fracture toughness of a low manganese austempered ductile iron (ADI),” *Mater. Manuf. Process.*, vol. 16, no. 2, pp. 245–263, 2001.
- [29] G. Cooper, A. Roebuck, H. Bayati, and R. Elliott, “The influence of nodule count on the austempering kinetics of a Mn-Cu ductile iron,” *Int. J. Cast Met. Res.*, vol. 11, no. 4, pp. 227–235, 1999.
- [30] J. Aranzabal, I. Gutierrez, J. M. Rodriguez-Ibabe, and J. J. Urcola, “Influence of Heat treatments on microstructure of austempered ductile iron,” *Mater. Sci. Technol.*, vol. 8, pp. 263–273, 1992.
- [31] J. F. Chinella, B. Pothier, and M. G. H. Wells, “Processing, mechanical properties, and ballistic impact effects of austempered ductile iron,” *Am. Soc. Mech. Eng. Press. Vessel. Pip. Div. PVP*, vol. 351, no. August, pp. 285–296, 1997.

- [32] S. Dhanasekaran, A. Vadiraj, G. Balachandran, and M. Kamaraj, "Transactions of The Indian Institute of Metals Mechanical behaviour of an austempered ductile iron," *October*, vol. 63, no. 5, pp. 779–785, 2010.
- [33] O. Eric, M. Jovanovic, L. Sidjanin, and D. Rajnovic, "Microstructure and mechanical properties of CuNiMo austempered ductile iron," *J. Min. Metall. Sect. B Metall.*, vol. 40, no. 1, pp. 11–19, 2004.
- [34] Y. J. Kim, H. Shin, H. Park, and J. D. Lim, "Investigation into mechanical properties of austempered ductile cast iron (ADI) in accordance with austempering temperature," *Mater. Lett.*, vol. 62, no. 3, pp. 357–360, 2008.
- [35] M. Leonavičius, A. Krenevičius, and M. Šukšta, "The investigation and peculiarities of calculation of transport machine elements made of austempered ductile iron," *Transport*, vol. 4142, no. April, pp. 162–167, 2017.
- [36] A. R. Mattar, S. C. Heck, A. L. Neto, F. A. P. Fernandes, G. E. Totten, and L. C. Casteletti, "Influence of alloying elements Cu, Ni and Mo on mechanical properties and austemperability of austempered ductile iron," *Int. Heat Treat. Surf. Eng.*, vol. 5, no. 2, pp. 78–82, 2011.
- [37] B. Wang, G. Barber, X. Sun, M. Shaw, and P. Seaton, "Characteristics of the Transformation of Retained Austenite in Tempered Austempered Ductile Iron," *J. Mater. Eng. Perform.*, no. Ref 18, 2017.
- [38] Y.-C. Peng, H.-J. Jin, J.-H. Liu, and G.-L. Li, "Effect of boron on the microstructure and mechanical properties of carbidic austempered ductile iron," *Mater. Sci. Eng. A*, vol. 529, pp. 321–325, 2011.
- [39] C.-H. Hsu and T.-L. Chuang, "Influence of stepped austempering process on the fracture toughness of austempered ductile iron," *Metall. Mater. Trans. A*, vol. 32, no. 10, pp. 2509–2514, 2001.
- [40] M. C. Cakir, A. Bayram, Y. Isik, and B. Salar, "The effects of austempering temperature and time onto the machinability of austempered ductile iron," *Mater. Sci. Eng. A*, vol. 407, no. 1–2, pp. 147–153, 2005.
- [41] A. R. Ghaderi, M. Nili Ahmadabadi, and H. M. Ghasemi, "Effect of graphite morphologies on the tribological behavior of austempered cast iron," *Wear*,

- vol. 255, no. 1–6, pp. 410–416, 2003.
- [42] S. Detwal and D. R., “Properties of Austempered Ductile Iron,” *Met. Mater. Eng.*, vol. 22, no. 1, pp. 25–29, 2016.
- [43] S. Sharma and R. Gupta, “Effect of Austempering Temperature and Time on the Wear Characteristics of Austempered Ductile Iron (ADI),” *Int. J. Eng. Res. Gen. Sci.*, vol. 3, no. 1, pp. 986–990, 2015.
- [44] E. Guzik, M. Sokolnicki, M. Ronduda, and A. Nowak, “Prediction of Microstructure in ADI Castings,” *Arch. Met. Mater.*, vol. 61, no. 4, pp. 2159–2164, 2016.
- [45] B. Bosnjak, B. Radulovic, and V. Asanovic, “Influence of Microalloying and Heat Treatment on the Kinetics of Bainitic Reaction in Austempered Ductile Iron,” *J. Mater. Eng. Perform.*, vol. 10, no. April, pp. 203–211, 2001.
- [46] O. Eric, D. Rajnovic, S. Zec, L. Sidjanin, and M. T. Jovanovic, “Microstructure and fracture of alloyed austempered ductile iron,” *Mater. Charact.*, vol. 57, no. 4–5, pp. 211–217, 2006.
- [47] B. Voigt, “Machinability of Cast Irons : From Grey Irons to Austempered Ductile Irons,” in *World Conference on ADI*, 2016.
- [48] L. Meier, M. Hofmann, P. Saal, W. Volk, and H. Hoffmann, “ScienceDirect In-situ measurement of phase transformation kinetics in austempered ductile iron,” *Mater. Charact.*, vol. 85, pp. 124–133, 2013.
- [49] P. Saal *et al.*, “In Situ Study of the Influence of Nickel on the Phase Transformation Kinetics in Austempered Ductile Iron,” *Metall. Mater. Trans. A*.
- [50] K. B. Rundman, D. J. Moore, K. L. Hayrynen, W. J. Dubensky, and T. N. Rouns, “The Microstructure and Mechanical Properties of Austempered Ductile Iron,” *J. Heat Treat.*, vol. 5, no. 2, pp. 1–17, 1988.
- [51] D. J. Moore, T. N. Rouns, and K. B. Rundman, “The effect of heat treatment, mechanical deformation, and alloying element additions on the rate of bainite formation in austempered ductile irons,” *J. Heat Treat.*, vol. 4, no. 1, pp. 7–24,

1985.

- [52] M. Pellizzari *et al.*, “Austempering kinetics of a ductile iron,” *Metall. Ital.*, vol. 107, no. 11–12, pp. 13–18, 2015.
- [53] A. Kowalski, B. Mrzyglod, I. Olejarczyk-Wozenska, T. Gietka, and M. Glowacki, “Characteristics of ADI ductile cast iron with single addition of 1.56% Ni,” *Arch. Metall. Mater.*, vol. 62, pp. 2273–2280, 2017.
- [54] A. Kowalski, K. Regulski, and G. Gumienny, “Optymalizacja dodatków Ni i Cu w żeliwie ADI z uwzględnieniem szybkości stygnięcia odlewu
Optimization of Ni and Cu additions in ADI cast iron in respect of cast cooling rate,” *Trans. Foundry Res. Inst.*, vol. 57, no. 2, pp. 85–94, 2017.
- [55] B. V Kovacs Sr, “Austempered Ductile Iron: Fact and Fiction,” *Mod. Cast.*, vol. 80, no. 3, pp. 38–41, 1990.
- [56] V. Kılıçlı, “Küresel Grafitli Dökme Demirlerde Kısmi Östenitleme ve Östemperleme Isıl İşleminin Mikroyapı ve Mekanik Özelliklere Etkisi,” Gazi Üniversitesi, 2004.
- [57] T. Tun and K. T. Lwin, “Optimizing the microstructure and mechanical properties of austempered ductile iron for automobile differential gear,” *J. Met. Mater. Miner.*, vol. 18, no. 2, pp. 199–205, 2008.
- [58] S. Yazdani and R. Elliott, “Influence of molybdenum on austempering behaviour of ductile iron Part 3 – Austempering kinetics, mechanical properties, and hardenability of ductile iron containing 0.25%Mo,” *Mater. Sci. Technol.*, vol. 15, no. 8, pp. 885–895, 1999.
- [59] S. Yazdani and R. Elliott, “Influence of molybdenum on austempering behaviour of ductile iron. Part 2 - Influence of austenitising temperature on austempering kinetics, mechanical properties, and hardenability of ductile iron containing 0.13%Mo,” *Mater. Sci. Technol.*, vol. 15, no. 5, pp. 541–546, 1999.
- [60] S. Yazdani and R. Elliott, “Influence of molybdenum on austempering behaviour of ductile iron Part 4 – Austempering behaviour of ductile iron containing 0.45%Mo,” *Mater. Sci. Technol.*, vol. 15, no. 8, pp. 896–902, 1999.

- [61] ASTM E2567, "Standard Test Method for Determining Nodularity And Nodule Count In Ductile Iron," West Conshohocken, PA, 2014.
- [62] C. M. Ecob, "A Review of Common Metallurgical Defects in Ductile Cast Iron," 2005.
- [63] J. R. Keough, "Austempered Ductile Iron (ADI) – A Green Alternative," *Trans. Am. Foundry Soc.*, vol. 119, no. 11–126, pp. 591–599, 2011.
- [64] P. Skoczylas, A. Krzynksa, and M. Kaczorowski, "The comparative studies of ADI versus Hadfield cast steel wear resistance," *Arch. Foundry Eng.*, vol. 11, no. 2, pp. 123–126, 2011.
- [65] G. Vidyathee and K. K. Singh, "Thin Wall Austempered Ductile Iron: A Best Replaceable Material To Steel And Aluminum," *Int. J. Mech. Eng. Robot. Res.*, vol. 3, no. 3, pp. 465–473, 2014.
- [66] E. Fraś, M. Górny, and H. Lopez, "Thin Wall Ductile Iron Castings as Substitutes for Aluminium Alloy Castings," *Arch. Metall. Mater.*, vol. 59, no. 2, pp. 459–465, Jun. 2014.
- [67] A. Polishetty, "Machinability and microstructural studies on phase transformations in Austempered Ductile Iron," Auckland University of Technology, 2011.
- [68] K. Brandenburg, "Successfully Machining Austempered Ductile Iron (ADI)," *Manuf. Eng.*, no. October, 2001.
- [69] R. J. Warrick *et al.*, "Austempered Ductile Iron Castings for Chassis Applications," *SAE Tech. Pap. Ser.*, vol. 1, no. 724, 2000.
- [70] K. R. Brandenburg, J. Ravenscroft, and K. L. Hayrynen, "An ADI Crankshaft Designed for High Performance in TVR's Tuscan Speed Six Sports Car," *Soc. Automot. Eng.*, 2001.
- [71] H. MATSUOKA, Y. TSUDA, and H. ONO, "Fundamental Research on Hobbing of Austempered Ductile Iron Gear (Influence of Graphite Particle on Machinability)," *JSME International Journal Series C*, vol. 46, no. 3. pp. 1160–1170, 2004.

- [72] A. P. Druschitz and D. C. Fitzgerald, "MADI™: Introducing a New, Machinable, Austempered Ductile Iron," *SAE Tech. Pap. Ser.*, vol. 1, no. 724, 2003.
- [73] C. C. Wang, B. H. Yan, H. M. Chow, and Y. Suzuki, "Cutting austempered ductile iron using an EDM sinker," *J. Mater. Process. Technol.*, vol. 88, no. 1, pp. 83–89, 1999.
- [74] ASTM International, "ASTM E3-01, Standard Guide for Preparation of Metallographic Specimens," West Conshohocken, PA, 2001.
- [75] S. D. N. Lourenço, S. K. Woche, J. Bachmann, and Y. Saulick, "Wettability of crushed air-dried minerals," *Geotech. Lett.*, vol. 5, no. 3, pp. 173–177, 2015.
- [76] K. Davut, A. Yalçın, and B. Çetin, "Multiscale Microstructural Analysis of Austempered Ductile Iron," *Hittite J. Sci. Eng.*, vol. 3, no. 1, pp. 29–34, 2016.
- [77] K. Davut and S. Zaeferrer, "Statistical reliability of phase fraction determination based on electron backscatter diffraction (EBSD) investigations on the example of an Al-trip steel," *Metall. Mater. Trans. A Phys. Metall. Mater. Sci.*, vol. 41, no. 9, pp. 2187–2196, 2010.
- [78] K. Pearson, "Notes on regression and inheritance in the case of two parents," *Proc. R. Soc. London*, no. 58, pp. 204–242, 1895.
- [79] J. F. Wallace, P. Du, and H. Su, "The Influence of Foundry Variables on Nodule Count in Ductile Iron," *Ductile Iron Soc.*, no. 12, 1984.